The Heterogeneous Multiscale Method: A Review

Weinan E[1], Bjorn Engquist[2], Xiantao Li[3], Weiqing Ren[4], and Eric Vanden-Eijnden[5]

[1] Princeton University, Princeton, NJ 08544 weinan@princeton.edu
[2] University of Texas, Austin, TX 78712 engquist@math.utexas.edu
[3] University of Minnesota, Minneapolis, MN 55455 xli@ima.umn.edu
[4] Princeton University, Princeton, NJ 08544 weiqing@princeton.edu
[5] New York University, New York, NY 10012 eve2@courant.nyu.edu

Summary. This paper gives a systematic introduction to HMM, the heterogeneous multiscale method, including the fundamental design principles behind the HMM philosophy and the main obstacles that have to be overcome when using HMM for a particular problem. This is illustrated by examples from several application areas, including complex fluids, micro-fluidics, solids, interface problems, stochastic problems, and statistically self-similar problems. Emphasis is given to the technical tools, such as the various constrained molecular dynamics, that have been developed, in order to apply HMM to these problems. Examples of mathematical results on the error analysis of HMM are presented. The paper ends with a discussion on some of the problems that have to be solved in order to make HMM a more powerful tool.

Contents

The Heterogeneous Multiscale Method: A Review
Weinan E, Bjorn Engquist, Xiantao Li, Weiqing Ren, Eric Vanden-Eijnden 1
1 Introduction 5
1.1 Classical and new multiscale methods 6
1.2 Classification of multiscale problems 10
1.3 Sequential and concurrent coupling 11
2 The HMM framework 12
2.1 The structure of HMM 12
2.2 Type B examples 14
ODEs with multiple time scales 14
Elliptic equation with multiscale coefficients 17
Kinetic schemes 19
Large scale MD simulation of gas dynamics 21
2.3 A type A example: Coupled kinetic-hydrodynamic simulation of shock propagation 23
Comparison with domain decomposition methods 25
3 The heterogeneous multiscale finite element method 26
3.1 The macroscale solver 27
3.2 Estimating the stiffness matrix 27
3.3 Other multiscale finite element methods 30
4 Complex fluids and microfluidics 31
4.1 The macroscale and microscale models 32
4.2 Type B problems: Atomistic-based constitutive modeling 33
Macroscale solver 33
Estimating the stress 34
Constrained microscopic solver: Constant rate-of-strain MD . . . 35
Fluid dynamics of chain molecules 38
4.3 Type A problems: Modeling boundary conditions 39
Marangoni flows 40
Contact line dynamics 42

5 Dynamics of solids at finite temperature 47
5.1 Macroscopic and microscopic models 48
5.2 Type B problem: Atomistic-based constitutive modeling 49
Macroscale solver 49
Constrained microscale solver 50
Modeling thermal expansion using MD 52
5.3 Type A problem: Dealing with isolated defects 52
The relevant time scales 54
MD boundary conditions 54
Twin boundary dynamics in Ni-Al alloy 56
6 Interface problems 59
6.1 Macroscale solver: The level set method 61
6.2 Estimating the macroscale interface velocity 61
7 Stochastic ODEs with multiple time scales 63
8 Exploring statistical self-similarity: An example without scale separation 66
8.1 General strategy for data estimation 66
8.2 Transport on a percolation network at criticality 66
9 Error analysis 69
9.1 Error analysis of the HMM-FEM 70
9.2 Dynamic problems 73
ODEs with multiple time scales 74
The effect of the fast variable reinitialization 76
Stochastic ODEs with multiple time scales 77
Other examples 80
10 Limitations of HMM 81
11 Conclusions and new directions 83
11.1 General procedures and main features of HMM 83
11.2 New application areas 84
11.3 Algorithm development 84
11.4 Analytical issues 86
References 87

1 Introduction

The heterogeneous multiscale method, or HMM, proposed in [EE03a] is a general framework for designing multiscale methods for a wide variety of applications. The name "heterogeneous" was used to emphasize the "multi-physics" applications that it targets, namely that the models at different scales may be of very different nature, e.g. molecular dynamics at the microscale and continuum mechanics at the macroscale. Since its inception, there has been substantial progress on multiscale modeling using the philosophy of HMM. The HMM framework has proven to be very useful in guiding the design and analysis of multiscale methods, and in several applications, it helps to transform multiscale modeling from a somewhat ad hoc practice to a systematic technique with a solid foundation. Yet more possibilities are waiting to be explored, particularly in the application areas. Many new questions of physical, numerical or analytical nature have emerged. All these make HMM an extremely fruitful and promising area of research and development.

The purpose of this article is to give a coherent summary of the status of HMM. It is our hope that this summary will help to understand the design principle behind the HMM philosophy, the main obstacles that one has to overcome when using HMM for a particular problem, and the immediate problems that we have to solve in order to make HMM a more powerful tool.

Just what *is* HMM? After all most of the multiscale modeling strategies discussed in the applied communities are heterogeneous in nature, i.e. they involve models of different nature at different scales. So is HMM something so broad that it lacks specifics? Or is it so narrow that it has only very limited applications? Through this review we will show that HMM is a specific framework that can be applied to a wide variety of applications. Its effectiveness rests upon the fact that it allows us to make maximum use of the knowledge that we have about the particular problem at all scales, macro and micro, as well as the special features that the problem might have, such as scale separation or self-similarity. For instance if the macro and micro time scales are separated, they are automatically decoupled in HMM. In addition, HMM also suggests a unified approach for carrying out error analysis for multiscale methods.

Despite all that, we will also see from this review that HMM only gives us a good starting point, applications of HMM to specific problems can be a highly non-trivial task. Issues of how do we formulate the constrained microscale problem have to be resolved and technical tools have to be developed along the way. The situation is similar to that of finite element method: On one hand, finite element offers a very attractive framework for designing numerical methods for a wide variety of problems; on the other hand, applying this framework to specific problems can be quite non-trivial.

Very briefly let us summarize the main features of HMM. HMM is a framework for linking models at different scales. It follows a top-down strategy: The basic starting point is an incomplete macroscale model, with the mi-

croscale model used as a supplement. It consists of two main components: The macroscale solver and a procedure for estimating the missing numerical data from the microscale model. The macroscale solver is knowledge-based, namely its design takes into account as much as possible the knowledge we have about the macroscale process. The key to the data estimation step is the design of the constrained microscale solver. The constraints are necessary in order to ensure that the microscale solution lives in an environment that is consistent with the macroscale state of the system. This is often the most difficult step in HMM technically, and its details are highly problem-dependent. Overall the coupling between the macro and microscales is accomplished as follows: The macro state provides the environment (the constraints) for the microscale solver; the microscale solver provides the data (such as numerical fluxes, forces, stiffness matrices, etc) for the macroscale solver. Such a data-based coupling strategy provides much needed flexibility compared with solution-based coupling strategies used in [ABB99, KGH03, OT95].

In the last few years, a general strategy has emerged for the design of multiscale methods by linking together microscale solvers on boxes distributed over the entire computational domain in order to capture the macroscale behavior of the solutions. The quasicontinuum method [KO01], kinetic scheme, HMM, and the gap-tooth scheme [KGH03] all make use of this idea. In general there are two steps in such a computational procedure. The first is to localize the microscale problem. The second is to assemble the information from the different microscale solvers. It is fair to say that HMM has proven to be a very effective tool for the second task. The first task, as we mentioned above, depends on the particular problem, and is certainly not to be neglected.

1.1 Classical and new multiscale methods

Almost all problems in science and engineering are multiscale in nature. Things are made up of atoms and electrons at the atomic scale, and at the same time are characterized by their own geometric dimensions which are usually several orders of magnitude larger. In the same way, atomic processes occur at the time scale of femto-seconds (10^{-15} second), but events in our daily lives are happening at a much slower pace. Thus for every specific problem that we encounter, we speak of the macroscopic scale as the particular scale that we are interested in. All smaller scales are referred to as microscopic scales.

For many problems though, this multiscale nature is not that important. Effective models can be obtained with satisfactory accuracy to account for the effects of microscopic processes. In fact most scientific models are of this type. Consider the example of classical molecular dynamics. There we are interested in the positions and momenta of the nuclei; the effects of the electrons, which are at the microscale compared with the nuclei, are modeled by empirical potentials. In fluid mechanics, we are interested in the density and velocity fields of the fluid; the effect of the molecular processes are modeled by the

equations of state and the constitutive relations. Most of these effective models are empirical, but there is also a substantial amount of work on analytical derivations of these effective models from microscopic theories [Spo91, Yau00].

In spite of their tremendous successes, the effective models also have their limitations. One main limitation is accuracy. This is particularly an issue for complex systems, such as complex fluids. When the modeling error is larger than the solution error, the usefulness of the model becomes a concern. A second limitation is the complete neglect of microscopic mechanisms which are sometimes of interest. Take the example of polymeric fluids. It is often of interest to know the microstructural information such as the conformation of the polymers, not just the macroscopic flow field. The third limitation is associated with the empirical nature of the models – especially for complex systems: These effective models often do not have a solid foundation. For these reasons, one might be tempted to switch completely to a microscopic model that has better accuracy, better physics and better foundation. However this is not an optimal strategy not only because the microscopic models are often too complex to be dealt with, but also because the answers we get will likely contain too much information that is of little interest, further complicating the task of extracting useful data. Indeed if we simulate crack propagation in a solid using molecular dynamics, the data we obtain will be overwhelmed by the trajectories of atoms away from the crack tip, which are of very little interest.

This is where multiscale modeling comes in. By coupling macroscopic and microscopic models, we hope to take advantage of both the simplicity and efficiency of the macroscopic models, as well as the accuracy of the microscopic models. Indeed the basic task of multiscale modeling is to design combined macroscopic-microscopic computational methods that are much more efficient than solving the full microscopic model and at the same time gives the information we need to the desired accuracy.

From the viewpoint of numerical methods, there has already been a long history of using multiscale ideas in methods such as the multi-grid method, fast multipole method and adaptive mesh refinement. Wavelet representation makes the multiscale idea even more explicit. So what is new in the new breed of multiscale methods, such as the quasi-continuum method and HMM? How are they different from the more traditional multiscale methods such as multi-grid [Bra77, Xu96]?

The difference between traditional multiscale methods such as multi-grid, and the new multiscale methods is that traditional multiscale methods are microscale solvers. Their purpose is to resolve the details of the solutions of the microscale model and as a result, their cost is that of a full microscale solver. The recently developed multiscale methods aim at one step further: Their objective is to capture the macroscale behavior of the system with a cost that is much less than the cost of full microscale solvers. Specifically the new multiscale methods are designed to satisfy the *minimum requirement*:

$$\frac{\text{cost of multiscale method}}{\text{cost of microscale solver}} \ll 1 \tag{1}$$

This is achieved only at some expenses:

1. We have to ask for less about the solutions of the microscale problem, e.g. we have to be satisfied with getting only the gross behavior of the solutions, not the details.
2. We must explore possible special features of the microscale problem, such as scale separation, self-similarity, etc.

To put it differently, multiscale problems are commonly recognized for their complexity, yet the main challenge in multiscale modeling is to recognize their simplicity, and make use of it. This has been a common theme in modern multiscale modeling. The disparity of time scales, for example, has long been a major obstacle in atomistic simulations such as molecular dynamics. But in methods such as HMM, it is used as an asset.

To be more concrete, let us first discuss this point at the level of signal representation. Consider the signals shown in Figure 1. They all have multiple scales. For the first signal, a traditional method along the lines of adaptive mesh refinement already gives an optimal representation. There is little room for improvement. For the second and third signals, traditional real space adaptive mesh refinement would represent the signal on a grid that is fine everywhere, with a cost of $O(\varepsilon^{-1})$ where ε is the size of the small scale. In contrast, modern multiscale techniques would recognize the fact that the microstructure itself varies only on a large scale, and use this feature to arrive at a much more efficient representation, by recording the microscale information on a coarsely-distributed fine grid, as shown in the figure, and therefore avoiding repetitive calculation at the microscale level. This idea is used in many modern multiscale methods and analysis, such as the quasi-continuum method [TOP96], two-scale regularity analysis [MM02], HMM [EE03a] and the gap-tooth scheme [KGH03] (see Figures 5, 6).

To look at this point further at the level of modeling, consider the classical elliptic problem

$$-\nabla \cdot (a(\mathbf{x})\nabla u(\mathbf{x})) = f(\mathbf{x}) \tag{2}$$

on a smooth domain Ω with some boundary conditions. We will assume that f as well as the boundary conditions are nice, with no small scales. But for a, let us distinguish three different cases:

- The first is when a is a nice function with no small scales.
- The second case is when a has small scales, but the small scales have some special features such as separation of scales. In this case, we write $a = a^{\varepsilon}$ where ε signifies the small scale.
- The third case is when a has small scales and the small scales do not have any special features.

The first case is clearly the simplest and the third case the most difficult. But despite that the method for dealing with problems in these two extreme

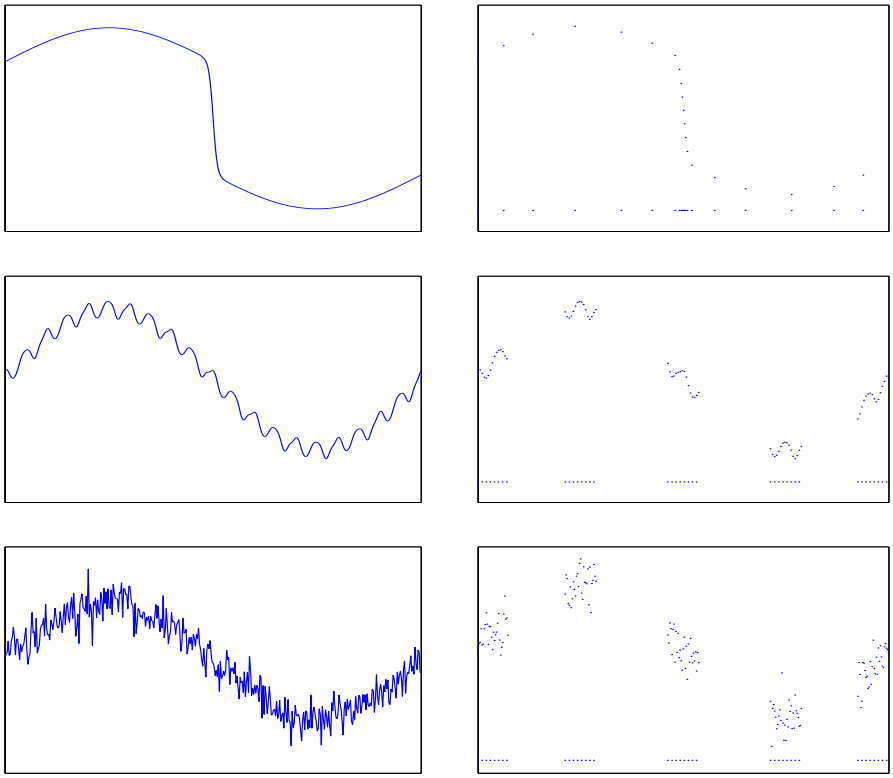

Fig. 1. Multiscale data representation: The signal in the top figures is represented very efficiently by traditional adaptive real space mesh refinement methods. The data in the middle and bottom figures are represented more efficiently on a coarsely-distributed fine mesh by noting that the microstructure itself varies on a large scale

cases are not very different: We just have to use efficient fine scale solvers, such as multi-grid and adaptive mesh refinement methods. Even though in the third case the problems contain multiple scales, it is not very helpful to write $a = a^\varepsilon$ since no particular values of ε matter and we just have to think of it as a very tough problem.

The minimum requirement in this case amounts to "beat the multi-grid method", and we see that this is only possible for the second class of problems. In this case, we have the possibility of capturing the large scale features of the solutions, using methods that are much less costly than full fine scale solvers. This is the focus of methods such as HMM.

To summarize what is said so far, we should distinguish the practice of solving multiscale problems from that of developing multiscale methods. Many multiscale problems are currently solved using ad hoc methods. A good example is fully developed turbulent flows which are typically treated using ad hoc turbulence models. One purpose of multiscale modeling is precisely to change

Table 1. Classical and modern multiscale techniques. Classical multiscale techniques focus on resolving the fine scale problem. The more recent multiscale techniques aim at reducing the computational complexity further by using special features in the fine scale problem, such as scale separation

Classical Techniques	Recent Techniques
Multigrid Method	Car - Parrinello Method
Domain Decomposition	Quasi-continuum Method
Wavelet-based Methods	Optimal Prediction
Adaptive Mesh Refinement	Heterogeneous Multiscale Method
Fast Multipole Method	Gap-Tooth Scheme
Conjugate Gradient Method	Coarse-grained Monte Carlo Models
	Adaptive Model Refinement

that, and to remove as much as possible the ad hoc steps in the modeling process. This can be done in two ways: Either we go back to the original problem and develop efficient and accurate ways of resolving the details, or look for special features that help us to simplify the problem. These features can then be used in developing multiscale modeling strategies.

1.2 Classification of multiscale problems

As we just discussed, the first step in multiscale modeling is to recognize the special features of the problem that one might take advantage of in order to design multiscale methods that satisfy the minimum requirement. For this purpose, it is useful to divide multiscale problems into several categories according to their common features:

Type A: These are problems that contain isolated defects or singularities such as cracks, dislocations, shocks and contact lines. For these problems, the microscopic model is only necessary near defects or singularities. Further away it is adequate to use some macroscopic model. Such a combined macro-micro strategy should satisfy the minimum requirement if the microscale model is limited to a small part of the computational domain.

Type B: These are problems for which a closed macroscopic model should exist for a properly selected set of macroscopic variables, but the macroscale model is not explicit enough to be used directly as an efficient computational tool. One example is the homogenization problem for equations of the type (2). If the coefficient is of the form $a^\varepsilon(\mathbf{x}) = a(\mathbf{x}, \frac{\mathbf{x}}{\varepsilon})$ where ε is the scale of the microstructure, and if the dependence of a on the fast variable $\mathbf{y} = \frac{\mathbf{x}}{\varepsilon}$ has certain structure such as periodicity, then there exists an effective equation, the homogenized equation, for the leading order behavior of the solutions of (2) [BLP78]. The homogenized equation takes the form

$$-\nabla \cdot (A(\mathbf{x})\nabla U(\mathbf{x})) = f(\mathbf{x}) \tag{3}$$

where $A(\mathbf{x})$ is called the homogenized coefficient. Even though the homogenized coefficient can in principle be expressed in terms of the solutions of the

so-called cell problems, they are not explicitly given except for very special problems such as one-dimensional problems. Therefore it is difficult to make use of (3) directly as a computational tool.

The task of multiscale modeling is to carry out macroscale simulations without making use of ad hoc constitutive relations. Instead, the necessary macroscale constitutive information is extracted from the microscale models.

The existence of a closed macroscopic model is often associated with time scale separation, and this can be exploited in order to design multiscale methods that satisfy the minimum requirement.

Type C: These are problems that have features of both type A and type B.

Type D: These are problems that exhibit self-similarity in scales. Examples include critical phenomena in statistical physics, fractals and turbulent transport.

Problems in each category share some common features that can be used when designing multiscale methods. For type A and type B problems, the special feature is scale separation. For type D problem, the special feature is statistical self-similarity.

Clearly as multiscale research goes on, other types of problems will be identified.

1.3 Sequential and concurrent coupling

Most current work on multiscale modeling is in the setting of the so-called "concurrent coupling" methods [ABB99], i.e. the microscale and the macroscale models are linked together "on-the-fly" as the computation goes on. More recently, this approach has also been referred to as "solving equations without equations" or "equation-free" [KGH03]. This is in contrast to the "sequential (serial) coupling" method which determines an effective macroscale model in a pre-processing step from the microscale model and uses the resulted macroscale model in further applications. Sequential coupling methods have been largely limited to "parameter passing", and as such it is very widely used in applications, such as constructing empirical atomistic potentials from quantum mechanics simulations, assigning hopping rates in kinetic Monte Carlo schemes using data from molecular dynamics, computing transport coefficients using microscopic models, etc. But there is no reason why it should be limited to this case. As long as the needed constitutive equation is known to depend on very few variables, sequential coupling provides a viable alternative to concurrent coupling techniques. Concurrent coupling methods are preferred when the constitutive relation depends on many variables so it is difficult to extract it by precomputing.

From a numerical viewpoint, the two strategies are very much related. For both sequential and concurrent coupling methods, the key issue is to design microscopic simulations that would give us the needed macroscopic data. In addition, the results of a concurrent simulation can be used to suggest

the function form of the constitutive relation, which can then be used in a sequential coupling method. Therefore the two strategies can be combined to yield optimal efficiency.

The HMM framework can be used both for concurrent and sequential coupling methods.

In the following, we will first present the HMM framework, illustrated by some relatively simple examples, both for type A and type B problems. We then discuss the heterogeneous multiscale finite element method, with application to the elliptic homogenization problem. After that we focus on the two main applications of HMM that have been pursued so far: coupled molecular dynamics and continuum mechanics modeling of fluids and solids. This is followed by three additional areas of application: Interface problems, stochastic ODEs and statistically self-similar problems. Error analysis and limitations of HMM are discussed next, followed by a summary and some new directions of research.

2 The HMM framework

2.1 The structure of HMM

We now turn to the framework of HMM. The general setting is as follows. We are given a microscopic system whose state variable is denoted by u, together with a microscale model, which can be abstractly written as

$$f(u, b) = 0 \tag{4}$$

where b is the set of auxiliary conditions, such as initial and boundary conditions for the problem. We are not interested in the microscopic details of u, but rather a coarse-grained state of the system which we denote by U. U satisfies some abstract macroscopic equation:

$$F(U, D) = 0 \tag{5}$$

where D stands for the macroscopic data that are necessary in order for the model to be complete.

Given a multiscale problem, the first question one should ask is: What is U? For type B problems, the answer is in principle straightforward: U should be the macroscopic state variables with which a closed macroscale model should in principle exist. These are often averaged quantities. For type A problems, it is less straightforward, since in this case we are also interested in some microstructural information that characterizes the defects. In any case, let us denote by Q the compression operator that maps u to U, and R any operator that reconstructs u from U:

$$Qu = U, \qquad RU = u \tag{6}$$

Q and R should satisfy: $QR = I$ where I is the identity operator. Q is called a compression operator instead of a projection operator since it can be more general than projection. Nevertheless in many cases, it *is* a projection operator. The terminology of reconstruction operator is adopted from Godunov schemes for nonlinear conservation laws [LeV90] and gas-kinetic schemes [SP94]. Compression and reconstruction operators are the same as the projection and prolongation operators used in multi-grid methods, or the restriction and lifting operators in [KGH03].

Examples of Q and R were given in [EE03a].

Fig. 2. Schematics of HMM framework

The goal of HMM is to compute U using the abstract form of F and the microscale model. It consists of two main components.

1. Selection of a macroscopic solver. Even though the macroscopic model is not available completely or is invalid on part of the computational domain, one uses whatever knowledge that is available on the form of F to select a suitable macroscale solver.
2. Estimating the missing macroscale data D using the microscale model. This is typically done in two steps:
   a) Constrained microscale simulation: At each point where some macroscale data is needed, perform a series of constrained microscopic simulations. The microscale solution needs to be constrained so that it is consistent with the local macroscopic state, i.e. $b = b(U)$. In practice, this is often the most important technical step.
   b) Data processing: Use the microscale data generated from the microscopic simulations to extract the needed macroscale data.

The data estimation can either be performed "on the fly" as in a concurrent coupling method, or in a pre-processing step as in a serial coupling method.

The latter is often advantageous if the needed data depends on very few variables.

The guidelines for selecting the macroscale solver are that it should be stable and it should facilitate the task of coupling with the microscale solver [EL04a].

Some remarks are in order. First of all, as we can already see, HMM is a top-down procedure, i.e. it is based on the macroscale process and it goes down to the microscale model only when necessary. Secondly, HMM is an example of data-driven coupling methodology, i.e. the link between different models at different scales is done through the data, which can be stresses, fluxes, forces or elastic coefficients, etc. This is in contrast with many other methods proposed in the literature for which the linking between different scales is done through the solutions directly [ABB98, ABB99, KGH03, WL03]. Thirdly, the influence of the macroscale state on the microscale model is manifested through the constraints on the microscale solver. These constraints play the role of constitutive assumptions in HMM. Therefore HMM does require specifying what macroscale variables the needed data should depend on. But it does not require knowing the functional form of the dependence.

Before we turn to concrete examples, we should emphasize that HMM is not a specific method, it is a framework for designing methods. For any particular problem, there is usually a considerable amount of work, such as designing the constrained microscopic solvers, that is necessary in order to turn HMM into a specific numerical method.

In the remaining part of this section, we will discuss examples of how HMM can be used for some relatively simple problems.

2.2 Type B examples

ODEs with multiple time scales

We will discuss two simple examples of ODEs with multiple time scales. The first is stiff ODEs with spectrum on the negative real axis, a prototypical example being:

$$\begin{cases} \dot{x} = -\dfrac{1}{\varepsilon}(x - f(y)) \\ \dot{y} = g(x, y) \end{cases} \tag{7}$$

The second is ODEs with oscillatory solutions. In this case the spectrum is located close to the imaginary axis. A prototypical example is

$$\begin{cases} \dot{\varphi} = \dfrac{1}{\varepsilon}\omega(I) + f(\varphi, I) \\ \dot{I} = g(\varphi, I) \end{cases} \tag{8}$$

in action-angle variables, studied in averaging methods [Arn89]. Here f and g are assumed to be periodic in φ with period 2π and bounded as $\varepsilon \to 0$. In

these examples x and φ are the fast variables, y and I are the slow variables, which are also our macroscale variable U.

Analytical and numerical issues for these problems have been studied for a long time. We refer to standard reference books such as [Arn89, HW91] where limiting equations as $\varepsilon \to 0$ are given for both (7) and (8). For (7), the fast variable x is rapidly attracted to the slow manifold where $x = f(y)$ and the effective equation for y is

$$\dot{y} = g(f(y), y) =: G(y). \tag{9}$$

For (8), the quasi-periodic motion of φ can be averaged out as $\varepsilon \to 0$ and the effective equation for I reads

$$\dot{I} = G(I) \quad \text{where} \quad G(I) := \frac{1}{2\pi} \int_0^{2\pi} g(\varphi, I) d\varphi. \tag{10}$$

The idea of HMM is to use the existence of the limiting equations such as (9) or (10), and some knowledge about their explicit form, to construct numerical schemes for (7) or (8). These schemes will be useful for more complex situations where the limiting equations are not given explicitly.

Consider (7) first. As the macroscale solver, we may select a conventional explicit ODE solver such as a Runge-Kutta scheme or a linear multi-step method. We may also select special purpose solvers such as the symplectic integrators. For illustration, let us assume that we will use forward Euler as the macroscale solver. We can express it as

$$y^{n+1} = y^n + \Delta t \tilde{G}^n(y^n) \tag{11}$$

The time step Δt resolves the macroscale dynamics of interest, but not the small scales.

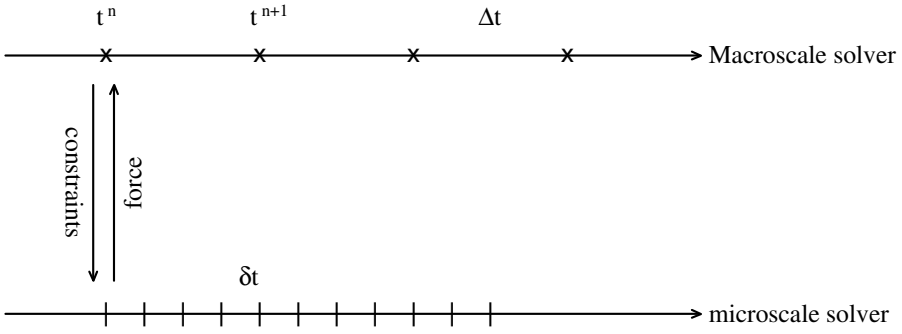

Fig. 3. Schematics of HMM for ODEs

The data that need to be estimated from the microscale model are the forces $\tilde{G}^n(y^n) \approx G(y^n)$. To estimate this data, we solve a modified microscale

model with the constraint that the slow variables are kept fixed. For the example (7), this modified microscale model is simply the equation for x, with y kept fixed, e.g.

$$x^{n,m+1} = x^{n,m} - \frac{\delta t}{\varepsilon}(x^{n,m} - f(y^n)) \tag{12}$$

$m = 0, 1, \cdots, N-1$. N should be large enough such that $x^{n,m}$ has converged to a stationary value with the desired accuracy. We then take

$$\tilde{G}(y^n) = g(x^{n,N}, y^n) \tag{13}$$

Notice that N is still independent of ε, which indicates that the overall cost of HMM is independent of ε. This is the reason for the gain in efficiency when $\varepsilon \ll 1$.

The case of (8) can be treated similarly. Assuming that we use forward Euler as the macroscale solver, we have

$$I^{n+1} = I^n + \Delta t \tilde{G}^n(I^n) \tag{14}$$

where $\tilde{G}^n(I^n) \approx G(I^n)$ must be estimated from the microscale model. This can be done using

$$\varphi^{n,m+1} = \varphi^{n,m} + \frac{\delta t}{\varepsilon}\omega(I^n) + \delta t f(\varphi^{n,m}, I^n)$$

The difference with the previous example is that the estimate of $\tilde{G}^n(I^n)$ must now involve an explicit time-averaging:

$$\tilde{G}^n(I^n) = \frac{1}{N}\sum_{m=1}^{N} K_{m,N} g(\varphi^{n,m}, I^n) \tag{15}$$

where the weights $\{K_{m,N}\}$ should satisfy the constraint

$$\frac{1}{N}\sum_{m=1}^{N} K_{m,N} = 1 \tag{16}$$

The specific choice of $\{K_{m,N}\}$ will affect the overall accuracy of HMM. (15) is called an F-estimator [EE03a]. Extensive analytical and numerical results using this methodology can be found in [ET04].

The choice of (13) can be viewed as a special case of (15) when $K_{m,N} = 1$ for $m = N$ and $K_{m,N} = 0$, otherwise. This choice is optimal for stiff ODEs since the fast variable exhibits a purely relaxational behavior.

The above strategy can be easily extended to more general problems in the form

$$\dot{z} = h(z, \varepsilon) \tag{17}$$

provided that one has explicit knowledge of the slow variables in the system, which will be denoted by $y = Y(z)$. Note that $h(z, \varepsilon)$ is in general unbounded as $\varepsilon \to 0$ due to the existence of fast dynamics. Again, let us use the forward Euler as the macro solver for illustration:

$$y^{n+1} = y^n + \Delta t \tilde{F}^n(y^n) \tag{18}$$

To estimate the force $\tilde{F}^n(y^n)$, we solve the microscale problem (17) with the constraint that $Y(z^{n,m}) = y^n$. As before, we used m as index for the time steps in the micro solver. Using the relation

$$\frac{dy}{dt} = \nabla_z Y(z) \cdot h(z, \varepsilon)$$

we obtain an estimate of the effective force in the limiting equation for y by time averaging:

$$\tilde{F}^n = \frac{1}{N} \sum_{m=0}^{N-1} K_{m,N} \nabla_z Y(z^{n,m}) \cdot h(z^{n,m}, \varepsilon) \tag{19}$$

where the weights $\{K_{m,N}\}$ must satisfy (16).

There is also a seamless version of HMM which does not require explicit knowledge of the slow variables [ET04]. In this version, for both the macro solver and the micro solver, we use the original microscale equations (in the original form). The only difference is in their time-step size. For stiff ODEs, this version of HMM can be viewed as a simple and crude version of the so-called Chebychev methods developed by Lebedev, Abdulle, etc. [HW91, Abd02], or simply an adaptive microscale ODE solver. The cost in this case increases logarithmically in ε as $\varepsilon \to 0$

The seamless version of HMM may also be applied in certain cases (but not always) to the oscillatory problems, though its cost then increases as a negative power of ε and to gain in efficiency requires using sophisticated choice of weights $\{K_{m,M}\}$ in the F-estimator. For examples, see [ET04].

Elliptic equation with multiscale coefficients

Our last example was in the time domain. We next discuss an example in the spatial domain. Consider the classical elliptic problem

$$\begin{cases} -\operatorname{div}\big(a^\varepsilon(\mathbf{x})\nabla u^\varepsilon(\mathbf{x})\big) = f(\mathbf{x}) & \mathbf{x} \in D \subset \mathbb{R}^d, \\ u^\varepsilon(\mathbf{x}) = 0 & \mathbf{x} \in \partial D. \end{cases} \tag{20}$$

Here ε is a small parameter that signifies explicitly the multiscale nature of the coefficient $a^\varepsilon(\mathbf{x})$: It is the ratio between the scale of the coefficient and the scale of the computational domain D. In the next section we will discuss finite element methods for problems of this kind. Here we discuss an approach

based on the finite volume method. This is a simplified version of the methods presented in [AE03]. Similar ideas can also be found in [Dur91].

As the macroscale solver, we choose a finite volume method on a macroscale grid, and we will denote by $\Delta x, \Delta y$ the grid size. The grid points are at the center of the cells, the fluxes are defined at the boundaries of the cells. The macroscale scheme is simply that on each cell, the total fluxes are balanced by the total source or sink terms:

$$-J_{i-\frac{1}{2},j} + J_{i+\frac{1}{2},j} - J_{i,j-\frac{1}{2}} + J_{i,j+\frac{1}{2}} = \int_{K_{i,j}} f(\mathbf{x}) d\mathbf{x} \tag{21}$$

Here $K_{i,j}$ denotes the (i,j)-th cell.

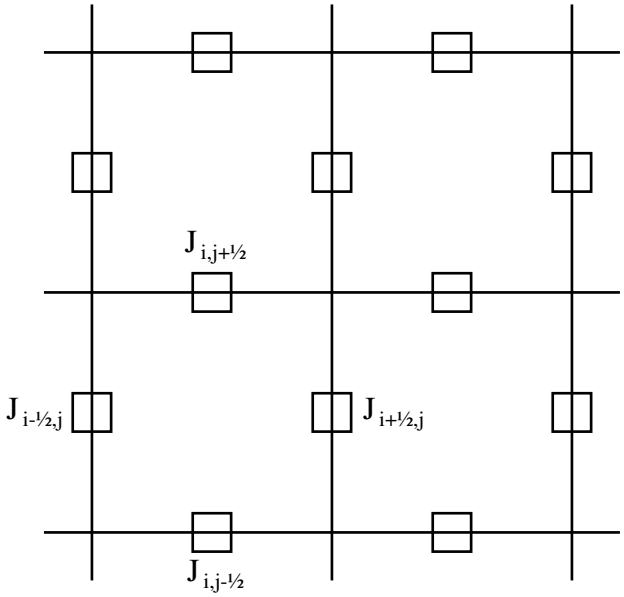

Fig. 4. HMM finite volume method

The data that need to be estimated are the fluxes. This is done as follows. At each point where the fluxes are needed, we solve the original microscale model (20) on a square domain of size δ, subject to the constraint that the average gradient is equal to ∇U at this point, where $U(\mathbf{x})$ is a linear function constructed from the macro state at the two neighboring cells, e.g. for computing $J_{i+\frac{1}{2},j}$, we have

$$\begin{aligned} U(x,y) = \frac{1}{2}(U_{i,j} + U_{i+1,j}) + \frac{U_{i+1,j} - U_{i,j}}{\Delta x}(x - x_{i+\frac{1}{2}}) \\ + \frac{1}{2}\frac{U_{i+1,j+1} + U_{i,j+1} - (U_{i+1,j-1} + U_{i,j-1})}{2\Delta y}(y - y_j) \end{aligned} \tag{22}$$

This constraint can be implemented through boundary condition for u^ε, e.g. we may impose the boundary condition that $u^\varepsilon(\mathbf{x}) - U(\mathbf{x})$ is periodic. We then use

$$J_{i+\frac{1}{2},j} = \frac{1}{\delta^2}\int_{I_\delta} j_1^\varepsilon(\mathbf{x})d\mathbf{x}, J_{i,j+\frac{1}{2}} = \frac{1}{\delta^2}\int_{I_\delta} j_2^\varepsilon(\mathbf{x})d\mathbf{x} \tag{23}$$

where $\mathbf{j}^\varepsilon(\mathbf{x}) = (j_1^\varepsilon(\mathbf{x}), j_2^\varepsilon(\mathbf{x})) = a^\varepsilon(\mathbf{x})\nabla u^\varepsilon(\mathbf{x})$, to compute an approximation to the needed flux.

The periodic boundary condition for the microscale problem is not the only choice. Other boundary conditions might be used. We refer to section 3 for a discussion in the finite element setting. More thorough discussion is found in [YE05]. To reduce the influence of the boundary conditions, a weight function can be inserted in (23), similar to what is done in the time domain earlier.

To implement this idea, note that the J's are linear functions of $\{U_{i,j}\}$. Therefore to compute the fluxes, we first solve the local problems with U replaced by the nodal basis functions: $\Phi_{k,l}$ is the nodal basis function (vector) associated with the (k,l)-th cell if $\Phi_{k,l}$ is zero everywhere except at the (k,l)-th cell center where it is 1. For each such basis function, there are only few local problems that need to be solved, since the basis function vanishes on most cells. Since U can be written as a linear combination of these nodal basis functions, the fluxes correspond to U can also be written as a linear combination of the fluxes correspond to these nodal basis functions. In this way, (21) is turned into a system of linear equations for U. The overall procedure is similar to procedure of heterogeneous multiscale finite element method discussed below.

Now how do we choose δ? Clearly the smaller the δ, the less the cost of the algorithm. If the original problem (20) has scale separation, i.e. the microscale length ε is much smaller than O(1), then we can choose δ such that $\varepsilon \ll \delta \ll 1$. This results in savings of cost for HMM, compared with solving the original microscale problem on the whole domain D.

Similar ideas are used in the modeling of transport in porous medium. The cells we used here are referred to as the representative elementary volumes (REV) [Dur91]. However, there it is customary to use a mixed boundary condition for the microscale problem, i.e. Dirichlet boundary condition with the required gradient in one direction and no-flux boundary condition in the other direction. This is known to produce very bad results [Dur91]. It turns out the error comes from the fact that the microscale problem does not satisfy the average gradient constraint mentioned above [YE05]. This can be corrected very simply as demonstrated in [YE05]. It is interesting to note that such mistakes are automatically avoided if the HMM framework is followed.

Kinetic schemes

Our next example is the derivation of numerical schemes for gas-dynamics that uses only the kinetic model. Such schemes are called kinetic schemes (see

for example [SP74, Pul80, Per91, SP94, Des95], see also the related work on Lattice Boltzmann methods [CD98, SFM01]). This example played an important role in developing the HMM framework. However, as will be seen below, our viewpoint is slightly different from that of the kinetic schemes.

The microscale model here is the kinetic equation, such as the Boltzmann equation:

$$\partial_t f + \mathbf{v} \cdot \nabla f = \frac{1}{\varepsilon} C(f). \tag{24}$$

Here f is the one-particle phase-space distribution function, which is also our microscale state variable; $C(f)$ is the collision kernel; ε is the mean-free path between collisions in the gas. The macroscale state variables U are the usual hydrodynamic variables of mass, momentum and energy densities, which are related to the microscale state variable f by:

$$\rho = \int f d\mathbf{v}, \quad \rho\mathbf{u} = \int f\mathbf{v} d\mathbf{v}, \quad E = \int f \frac{|\mathbf{v}|^2}{2} d\mathbf{v}. \tag{25}$$

(25) defines the compression operator Q.

The connection between Euler's equation and the Boltzmann equation is as follows. From the Boltzmann equation, we have:

$$\partial_t \begin{pmatrix} \rho \\ \rho u \\ E \end{pmatrix} + \nabla \cdot \mathbf{F} = 0 \tag{26}$$

where

$$\mathbf{F} = \int_{\mathbb{R}} f \begin{pmatrix} \mathbf{v} \\ \mathbf{v} \otimes \mathbf{v} \\ \frac{1}{2}|\mathbf{v}|^2 \mathbf{v} \end{pmatrix} d\mathbf{v} \tag{27}$$

When $\varepsilon \ll 1$, the distribution function f is close to local equilibrium states, or the local Maxwellians,

$$M(\mathbf{x}, \mathbf{v}, t) = \frac{\rho(\mathbf{x}, t)}{(2\pi\theta(\mathbf{x}, t))^{3/2}} \exp\Big(-\frac{(\mathbf{v} - \mathbf{u}(\mathbf{x}, t))^2}{2\theta(\mathbf{x}, t)}\Big) \tag{28}$$

with θ being the absolute temperature.

To design an HMM strategy, we first need to select a macroscale solver. We will focus on the one-dimensional case. Since the macroscale model (26) is a set of conservation laws, we will choose as the macroscale solver a finite volume scheme. We first divide the computational domain in the physical space into cells of size Δx. We denote by x_j the center position of the j-th cell, and $x_{j+1/2}$ the cell boundary between the j-th and $j+1$-th cells. For first order method, we represent the solution as piece-wise constants, i.e.

$$(\rho, \rho u, E) = (\rho_j, \rho_j u_j, E_j), \quad x \in (x_{j-1/2}, x_{j+1/2}]$$

The finite volume scheme takes the form:

$$\begin{cases} \rho_j^{n+1} - \rho_j^n + \dfrac{\Delta t}{\Delta x}\big(F^{(1)}_{j+1/2} - F^{(1)}_{j-1/2}\big) = 0, \\ (\rho u)_j^{n+1} - (\rho u)_j^n + \dfrac{\Delta t}{\Delta x}\big(F^{(2)}_{j+1/2} - F^{(2)}_{j-1/2}\big) = 0, \\ E_j^{n+1} - E_j^n + \dfrac{\Delta t}{\Delta x}\big(F^{(3)}_{j+1/2} - F^{(3)}_{j-1/2}\big) = 0 \end{cases} \tag{29}$$

where $\mathbf{F}_{j+1/2} = (F^{(1)}_{j+1/2}, F^{(2)}_{j+1/2}, F^{(3)}_{j+1/2})^T$ is the numerical flux at the cell boundary $x_{j+1/2}$.

The next step is to compute $\mathbf{F}_{j+1/2}$ from solving the kinetic equation. To take into account the wave character of the solutions, we write:

$$\mathbf{F}_{j+1/2} = \mathbf{F}^+_{j+1/2} + \mathbf{F}^-_{j+1/2}, \quad \text{with} \quad \mathbf{F}^\pm_{j+1/2} = \int_{\mathbb{R}^\pm} f(x^\mp_{j+1/2}, v, t) \begin{pmatrix} v \\ v^2 \\ \frac{1}{2}v^3 \end{pmatrix} dv. \tag{30}$$

Normally one would numerically solve the kinetic model to obtain f. For the present problem, it is much simpler to write down an approximate solution analytically. To leading order, we have:

$$f(x, v, t) \sim M(x - vt, v, t^n) \tag{31}$$

Using this in (30), we have

$$\mathbf{F}^\pm = \begin{pmatrix} \rho u A^\pm(S) \pm \dfrac{\rho}{2\sqrt{\pi\beta}} B(S) \\ (p + \rho u^2) A^\pm(S) \pm \dfrac{\rho u}{2\sqrt{\pi\beta}} B(S) \\ (pu + \rho u e) A^\pm(S) \pm \dfrac{\rho}{2\sqrt{\pi\beta}} (\dfrac{p}{2\rho} + e) B(S) \end{pmatrix} \tag{32}$$

where

$$A^\pm = \frac{1 + \mathrm{erf}(S)}{2}, \quad B(S) = e^{-S^2}, \quad S = \frac{u}{\sqrt{2RT}}, \quad p = \rho RT.$$

This is the simplest kinetic scheme. The schematic is shown in Figure 5.

How do we construct higher order kinetic schemes? The standard practice is to consider both higher order reconstructions (for the initial value of f in the shaded-region in Figure 5) and solve the kinetic model to higher order accuracy. This is the path followed, for example, in [Per92, SP94] for constructing second order kinetic schemes. From the viewpoint of HMM, however, one would simply take a higher order macroscale solver, such as the ones in [NT90]. Then it is no longer necessary to have higher order reconstruction for the initial values of the kinetic model.

Large scale MD simulation of gas dynamics

In this example we discuss how HMM can be used to carry out macroscale gas-dynamics calculations using only MD. The macroscopic equations are the

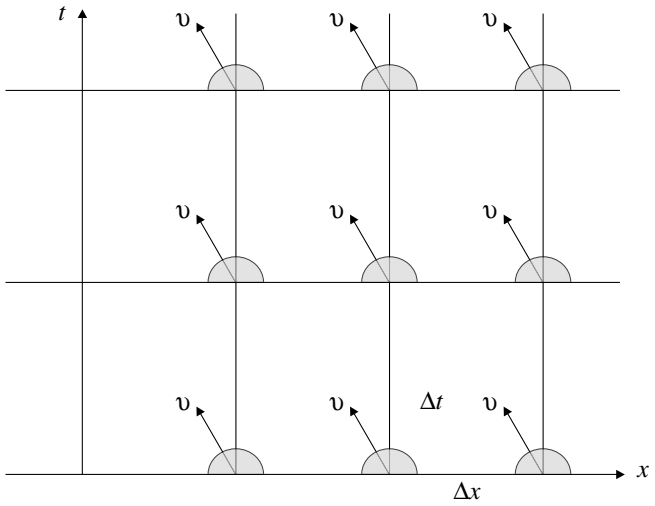

Fig. 5. Schematics for the derivation of kinetic scheme: A finite volume method is imposed in the $x-t$ domain, and the kinetic equation is solved (e.g. analytically) over the shaded region to give the fluxes needed in the finite volume method. The v axis indicates the extra velocity variable in the kinetic model, which represents the microstructure for the present problem

usual conservation laws of density, momentum and energy. In one dimension, it can be expressed in a generic form:

$$\partial_t \mathbf{u} + \partial_x \mathbf{f} = 0 \tag{33}$$

Here $\mathbf{f}$ is the flux. Traditional gas dynamics models assume that $\mathbf{f}$ is a known function of $\mathbf{u}$. Here we do not make that assumption. Instead we will extract $\mathbf{f}$ from an underlying atomistic model.

As the macroscale solver, we select a finite volume method. One example is the central scheme of [NT90] on a staggered grid:

$$\mathbf{u}_{j+1/2}^{n+1} = \frac{\mathbf{u}_j^n + \mathbf{u}_{j+1}^n}{2} - \frac{\Delta t}{\Delta x}\big(\mathbf{f}_{j+1}^n - \mathbf{f}_j^n\big). \tag{34}$$

The data that need to be estimated from MD are again the fluxes. This is done by performing a constrained MD simulation locally at the cell boundaries, which are the cell centers for the previous time step. The constraints are that the average density, momentum and energy of the MD system should agree with the local macro state at the current time step n. This is realized by initializing the MD with such constraints and apply the periodic boundary condition afterwards. Using the Irving-Kirkwood formula (see section 4) which relates the fluxes to the MD data, we can then extract the macroscale fluxes by time averaging the MD data. We refer to [LE05] for more details.

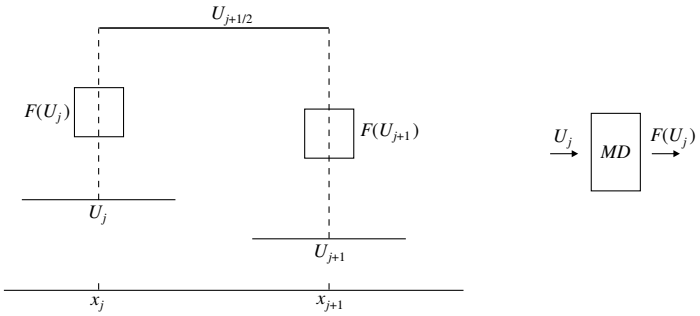

Fig. 6. Central scheme: starting with piecewise constant solution, one computes fluxes at x_j and x_{j+1}, and integrates the conservation laws to the next time step, where the grid points are shifted to the midpoints $x_{j+1/2}$. The numerical fluxes are evaluated with the help of MD

One result from such a method is shown in Figure 7. Here the set-up for the macroscale model is a Riemann problem for one-dimensional wave propagation in solids. The microscale model is two dimensional MD with Lennard-Jone potential. The result of HMM is compared with that of a direct MD simulation.

2.3 A type A example: Coupled kinetic-hydrodynamic simulation of shock propagation

Our next example is continuum gas dynamics locally corrected near shocks by the kinetic model. This is a type A problem. Problems of this type have been studied for a long time in the kinetic theory community using domain decomposition methods (see for example [BLP92, LP98]). The framework of HMM suggests a way of handling this problem that is slightly different from what is done in the literature.

The macroscopic process is gas dynamics, the microscopic process is described by a kinetic model. Therefore as the macroscale solver we will choose the kinetic schemes for gas dynamics. Away from shocks, the numerical fluxes are computed using (32). At the shocks the numerical fluxes are computed by solving locally the kinetic model using micro time steps. The kinetic model is constrained by the local macroscopic state through the boundary conditions. As shown in Figure 8, the kinetic equation is solved in the shaded region between x_l and x_r (assume that the shock is at the cell boundary $x_{k+1/2}$). Boundary condition is needed at x_l for $v > 0$. For this we choose

$$f(x_l, v, t) = M(x_l, v, t), \quad v > 0 \tag{35}$$

where the right hand side is the local Maxwellian corresponding to the macroscopic state at x_l, obtained by extrapolating the macro states in the cells to

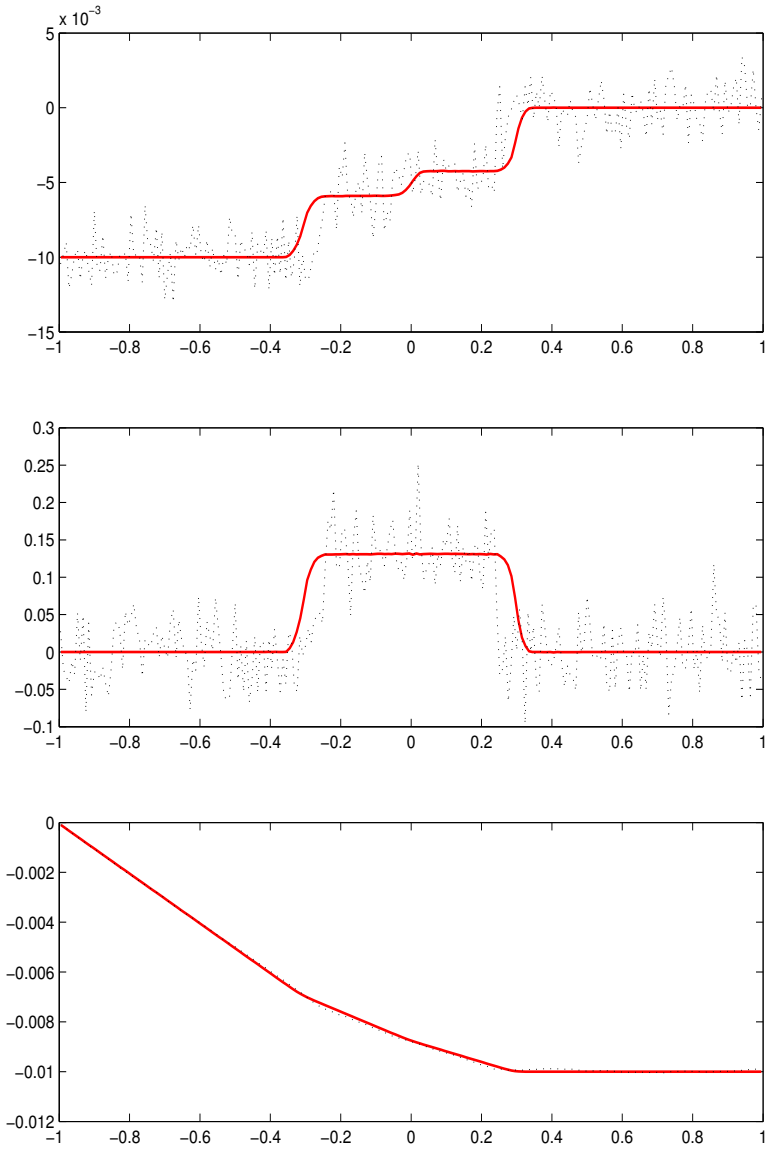

Fig. 7. Numerical test on shock formation and propagation. 200 macro-grid points are used and each local MD simulation consists of 40×10 atoms and 10^4 steps of time integration. The solution is displayed after 40 steps of integration over macro time steps. Solid line: computed solution; dashed line: full atom simulation (one realization). Top: strain; middle: velocity; bottom: displacement

the left of x_l. Boundary condition at x_r can be handled similarly. At $x_{k+1/2}$, we define

$$\mathbf{F}_{k+1/2} = \frac{1}{\tau}\int_{t^n}^{t^n+\tau} dt\Big\{ \int_{\mathbb{R}^+} f(x^-_{k+1/2}, v, t) \begin{pmatrix} v \\ v^2 \\ \frac{1}{2}v^3 \end{pmatrix} dv + \int_{\mathbb{R}^-} f(x^+_{k+1/2}, v, t) \begin{pmatrix} v \\ v^2 \\ \frac{1}{2}v^3 \end{pmatrix} dv \Big\}. \tag{36}$$

for suitably chosen τ.

How do we choose τ? To address this question, we should note that there are potentially two different cases concerning corrections to the gas-dynamics models of shocks. The first is when non-equilibrium effects are important. In this case the relaxation time of the gas inside the shock may become comparable to the hydrodynamic time, and we should simply choose $\tau = \Delta t$. Note in this case there is no time scale separation, and the kinetic model is solved continuously throughout the shock region, with occasional reinitialization as the shock region moves. This is shown schematically in the left panel in Figure 8. The second is when viscous or other higher order gradient effects are important inside the shocks, but there is still time scale separation between the relaxation time of the gas and the hydrodynamic time. In this case we should choose τ to be larger than the relaxation time of the gas, but still smaller than Δt. The specific choice should be made numerically by observing when the numerical fluxes in (36) reach stationary values as a function of τ. At each macro time step, the kinetic model needs to be reinitialized, as discussed earlier for gas-kinetic schemes. A schematic is shown in the right panel in Figure 8.

The final component of the method is a criterion for locating the shock position. At the present time, there is little systematic work in this direction.

Comparison with domain decomposition methods

It is worthwhile to make a comparison between the HMM approach and other approaches for type A problems. With few exceptions, most existing approaches to type A problems are based on the idea of domain decomposition [OT95, HP97, Had99, ABB98, ABB99, FWF00, NC04a, KL04, QWL03, PKL04, BLP92, BLT96, LP98]. If the microscopic model is molecular dynamics and the macroscopic model is continuum mechanics, one solves the continuum model over part of the domain and molecular dynamics over the rest of the domain, typically near defects or singularities. For modeling fluids, it is customary to require that the two domains overlap. The results from the two different models are matched in the overlapping region to ensure compatibility of the two models. The matching is done either over the macroscopic fields or the fluxes. For solids, the two domains usually do not overlap, but

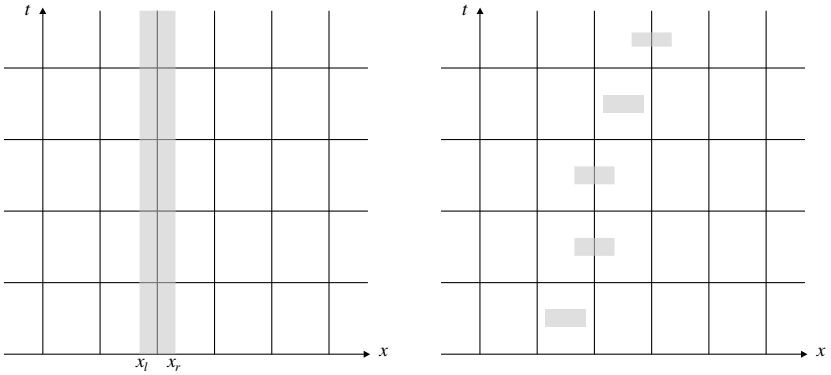

Fig. 8. Schematics for the coupled kinetic-gas dynamics simulation: A finite volume method is imposed everywhere in the $x - t$ domain. The numerical fluxes are computed using the kinetic scheme away from the shocks, and directly from the solutions of the kinetic equations at the shocks. The shaded regions indicate where the kinetic equation needs to be solved. The left panel illustrates the case when there is no scale separation between the relaxation time scale inside the shock and the hydrodynamic time scale. The right panel shows the case when there is time scale separation

rather is connected by some specially designed atomistic-continuum interface condition.

In contrast, in the HMM approach the macroscale solver is imposed over the whole domain. Near defects or singularities (here the shocks), the data (here the flux) required by the macroscale solver is estimated from a microscale model. Therefore the HMM methodology resembles that of an **(adaptive) model refinement**: Near defects or singularities, a more refined model is used to supply the data. Ideas similar to this were used in [GBC99, OV00].

For the example discussed above, the model is adaptively refined at the shocks and is replaced by the kinetic model for flux evaluation. The overall algorithm is still that of a finite volume method. The kinetic model is used inside the finite volume scheme to provide part of the data. In addition, HMM provides ways of further limiting the size of the computational domain for the microscopic model, by exploiting time scale separation so that the kinetic equation does not have to be solved for all time, or spatial scale separation so that the kinetic equation is solved only in a very thin strip inside the macro cells. This philosophy is opposite to that of over-lapping – it is more in the spirit of "under-lapping". See Figure 8.

3 The heterogeneous multiscale finite element method

In this section we discuss the application of HMM to problems with a variational structure. Many microscale problems are of this type. One example is

the elliptic problem with multiscale coefficients $a^\varepsilon(\mathbf{x})$ discussed in section 2.2 (20). Here ε is the small parameter that characterizes the rapid variations in the coefficient a^ε, e.g. ε might be the correlation length for the small scale variation. Special cases of these problems have been studied analytically in homogenization theory [BLP78, PV81].

Another type of interesting microscale models are the discrete models such as network models. Examples of network models include the pore network models of porous media, resistor network models, and percolation models [Sah95, Tor02].

A third type of microscale variational models are the molecular mechanics models that are used in connection with the quasi-continuum method [TOP96, MT04]. They are relevant for studying the structure of solids at low temperature.

In the following we will focus on the case when the microscale models are PDE models of the type (20).

3.1 The macroscale solver

To construct a HMM finite element method, we choose as the macroscale solver the conventional finite element method. As an example, we will use the standard C^0 piecewise linear element, on a triangulation T_H where H denotes the element size. We will denote by X_H the finite element space.

3.2 Estimating the stiffness matrix

The data that need to be estimated from the microscale model is the effective stiffness matrix on T_H:

$$A = (A_{ij}) \tag{37}$$

where

$$A_{ij} = \int_D (\nabla \Phi_i(\mathbf{x}))^T \mathcal{A}_H(\mathbf{x}) \nabla \Phi_j(\mathbf{x})\, d\mathbf{x} \tag{38}$$

and $\mathcal{A}_H(\mathbf{x})$ is the effective coefficient (say conductivity) at the scale H and $\{\Phi_i(\mathbf{x})\}$ are the basis functions for X_H. Had we known $\mathcal{A}_H(\mathbf{x})$, we could have evaluated (A_{ij}) by numerical quadrature. Let $f_{ij}(\mathbf{x}) = (\nabla \Phi_i(\mathbf{x}))^T \mathcal{A}_H(\mathbf{x}) \cdot \nabla \Phi_j(\mathbf{x})$, then

$$A_{ij} = \int_D f_{ij}(\mathbf{x}) dx \simeq \sum_{K \in T_H} |K| \sum_{x_\ell \in K} w_\ell f_{ij}(\mathbf{x}_\ell) \tag{39}$$

where $\{\mathbf{x}_\ell\}$ and $\{w_\ell\}$ are the quadrature points and weights respectively, $|K|$ is the volume of the element K. Therefore our problem reduces to the approximation of $\{f_{ij}(\mathbf{x}_\ell)\}$. This will be done by solving the original microscale model locally around each quadrature point $\{\mathbf{x}_\ell\}$.

Let us first discuss the case when $i = j$. Our formulation of the local microscale problem is motivated by the following general principle. Given an arbitrary microscale variational problem $\min_u e(u)$,

$$\min_u e(u) = \min_U E(U) \tag{40}$$

where

$$E(U) = \min_{u:Qu=U} e(u) \tag{41}$$

Here Q is some compression operator. Using this, computing A_{ii} is equivalent to computing $E(\Phi_i)$.

Let $I_\delta(\mathbf{x}_\ell)$ be a cube of size δ. On each cell $I_\delta(\mathbf{x}_\ell)$, we define Q as follows: $Qu = U$ if

$$\frac{1}{\delta^d}\int_{I_\delta(\mathbf{x}_\ell)} \nabla u(\mathbf{x})\, d\mathbf{x} = \nabla U(\mathbf{x}_\ell) \tag{42}$$

With these, we can define the microscale problem to be solved on $I_\delta(\mathbf{x}_\ell)$. Let φ_i^ε be the solution of the following problem

$$\min_{Qu=\Phi_i} \int_{I_\delta(\mathbf{x}_\ell)} (\nabla u(\mathbf{x}))^T a^\varepsilon(\mathbf{x}) \nabla u(\mathbf{x}) d\mathbf{x}, \tag{43}$$

we approximate $f_{ii}(\mathbf{x}_\ell)$ by

$$f_{ii}(\mathbf{x}_\ell) \simeq \frac{1}{\delta^d}\int_{I_\delta(\mathbf{x}_\ell)} (\nabla \varphi_i^\varepsilon(\mathbf{x}))^T a^\varepsilon(\mathbf{x}) \nabla \varphi_i^\varepsilon(\mathbf{x})\, d\mathbf{x} \tag{44}$$

Similarly we approximate $f_{ij}(\mathbf{x}_\ell)$ by

$$f_{ij}(\mathbf{x}_\ell) \simeq \frac{1}{\delta^d}\int_{I_\delta(\mathbf{x}_\ell)} (\nabla \varphi_i^\varepsilon(\mathbf{x}))^T a^\varepsilon(\mathbf{x}) \nabla \varphi_j^\varepsilon(\mathbf{x})\, d\mathbf{x} \tag{45}$$

Knowing $\{f_{ij}(\mathbf{x}_\ell)\}$, we obtain the stiffness matrix A by (39).

(43) is equivalent to solving

$$-\mathrm{div}(a^\varepsilon(\mathbf{x}) \nabla \varphi_i^\varepsilon(\mathbf{x})) = 0 \quad \text{on } I_\delta(\mathbf{x}_\ell) \tag{46}$$

with boundary condition

$$a^\varepsilon(\mathbf{x}) \frac{\partial \varphi_i^\varepsilon}{\partial n} = \lambda^T \hat{\mathbf{n}} \quad \text{on } \partial I_\delta(\mathbf{x}_\ell) \tag{47}$$

where λ is the Lagrange multiplier for the constraints that $\frac{1}{\delta^d}\int_{I_\delta(\mathbf{x}_\ell)} \nabla \varphi_i^\varepsilon\, d\mathbf{x} = (\nabla \Phi_i)(\mathbf{x}_\ell)$, $\hat{\mathbf{n}}$ is the outward normal on $\partial I_\delta(\mathbf{x}_\ell)$.

Other formulations of boundary conditions that preserve the constraint (42) are discussed in [YE05]. The effect of boundary conditions for the microscale problem, as well as the influence of δ, the size of the micro-cell, is systematically studied numerically in [YE05]. In the analysis presented later

in section 9.2, it is more convenient to consider the boundary condition that $\varphi_i^\varepsilon(\mathbf{x}) - \Phi_i(\mathbf{x})$ is periodic with period $I_\delta(\mathbf{x}_\ell)$.

To reduce the effect of the boundary conditions, we may introduce a weight function w_δ in the evaluation of $f_{ij}(\mathbf{x}_\ell)$:

$$f_{ij}(\mathbf{x}_\ell) \simeq \frac{1}{\delta^d} \int_{I_\delta(\mathbf{x}_\ell)} w_\delta(\mathbf{x}) (\nabla \varphi_i^\varepsilon(\mathbf{x}))^T a^\varepsilon(\mathbf{x}) \nabla \varphi_j^\varepsilon(\mathbf{x}) \, d\mathbf{x} \tag{48}$$

where w_δ should satisfy the condition that

$$\frac{1}{\delta^d} \int_{I_\delta(\mathbf{x}_\ell)} w_\delta(\mathbf{x}) \, d\mathbf{x} = 1 \tag{49}$$

w_δ should be chosen so that it assigns smaller weights to regions near the boundary. The considerations for the choice of the weight function is similar to the same problem in the time domain, which is discussed in subsection 9.2.

The overall procedure goes as follows:

- Solve for $\varphi_1^\varepsilon, \cdots, \varphi_d^\varepsilon$ at each $\mathbf{x}_\ell$.
- Assemble the effective stiffness matrix using (48).
- Solve the macroscale finite element equation using the effective stiffness-matrix. If we express the macroscale solution in X_H in the form of $U_H(\mathbf{x}) = \sum U_j \Phi_j(\mathbf{x})$, then the macroscale finite element equation takes the standard form:

$$AU = F \tag{50}$$

  where $U = (U_1, \cdots, U_N)^T, F = (F_1, \cdots, F_N)^T, F_j = (f(\mathbf{x}), \Phi_j(\mathbf{x}))$, $f(\mathbf{x})$ is the macroscale forcing function.

The savings compared with solving the full fine scale problem comes from the fact that we can choose $I_\delta(\mathbf{x}_\ell)$ to be smaller than K. The size of $I_\delta(\mathbf{x}_\ell)$ is determined by many factors, including the accuracy and cost requirement, the degree of scale separation, and the microstructure in $a^\varepsilon(\mathbf{x})$. One purpose for the error estimates that we present in section 9.2 is to give guidelines on how to select $I_\delta(\mathbf{x}_\ell)$. If $a^\varepsilon(\mathbf{x}) = a(\mathbf{x}, \mathbf{x}/\varepsilon)$ and $a(\mathbf{x}, \mathbf{y})$ is periodic in $\mathbf{y}$, we can simply choose $I_\delta(\mathbf{x}_\ell)$ to be $\mathbf{x}_\ell + \varepsilon I$, i.e., $\delta = \varepsilon$. If $a(\mathbf{x}, \mathbf{y})$ is random, then δ should be a few times larger than the local correlation length of a^ε. In the former case, the total cost is independent of ε. In the latter case, the total cost depends only weakly on ε (see [MY03]).

Some related ideas exist in the literature. Durlofsky [Dur91] proposed an up-scaling method, which directly solves some local problems for obtaining the effective coefficients [MT77, Spa76, Tar00]. Oden and Vemaganti [OV00] proposed a method that aims at recovering the oscillations in ∇u^ε locally by solving a local problem with some given approximation to the macroscopic state U as the boundary condition. This idea is sometimes used in HMM to recover the microstructural information.

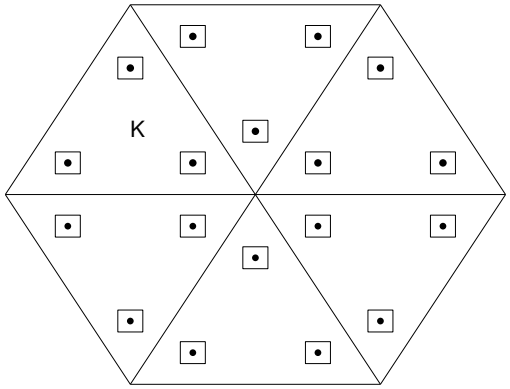

Fig. 9. Illustration of HMM for solving (20). The dots are the quadrature points. The little squares are the microcell $I_\delta(\mathbf{x}_\ell)$

3.3 Other multiscale finite element methods

Another proposal for constructing multiscale finite element method has been made in [Bab76, BCO94, BBO03, BBO04, HW97, LZR91] based on modifying the basis functions in the finite element space by solving, for each element, the original microscale problem with vanishing right hand side and suitable boundary conditions. The modified basis functions are used to constructive the effective stiffness matrix on the coarse grid. This idea was first introduced by Babuska et al. [BCO94] in the context generalized finite element methods for solving elliptic equations with general rough coefficients. For problems with multiscale coefficients, Hou et al. [HW97] introduced overlapping in order to alleviate the difficulties with local boundary conditions. Some rudimentary versions of this idea was also suggested in [LZR91] for solving Helmholtz equations by using oscillatory functions as basis functions.

Once the basis functions and the effective stiffness matrix is computed, the modified basis function method works efficiently as a coarse grid method. The main problem, however, is in the overhead for computing the basis functions. This overhead is already comparable with solving the original microscopic problem, if a linear scaling method such as multi-grid is used. As all other upscaling methods, the goal of both HMM-FEM and the modified basis function method is to obtain the effective stiffness matrix at the macroscale. The difference lies in whether the procedure is tied with modifying the original finite element space, say through basis functions. HMM-FEM approximates the stiffness matrix *directly* by performing local simulations of the original microscale model. The size of the local simulation can be chosen according to the special features of the problem. In particular, one may choose the domains of the local problems to overlap with each other so that their union covers the original computational domain. This would make it very close to the modified basis function methods, and most likely also defeat the purpose

of HMM-FEM. In contrast, the modified basis function method does this by going through an intermediate step, namely modifying the basis functions and as a result, the original finite element space. This greatly limits its flexibility in exploring the multiscale features of the underlying problem. Indeed, except for simple cases such as the periodic homogenization problem, solving a problem *with* structure using such ideas is as hard as solving a problem *without* structure. On the other hand, these techniques might be of some use if the problem (20) is solved repeatedly with different right hand side, in which case they can be used as pre-processing techniques, in the same way as LU decomposition, computation of Schur complements [ER02], and sub-structuring methods [BPS86].

For a more detailed discussion of these methods and their relative performance, we refer to [MY03]. It was found, among other things, that the accuracies of HMM-FEM and the modified basis function method are generally comparable, for the examples considered there, despite the difference in cost.

For the special case when the microstructure of a^ε is locally periodic, several other methods have been proposed. Some are based on solving the homogenized equations, plus next order terms [CC95]. One particularly interesting idea, proposed by Schwab et al. [SM02a, SM02b], uses multiscale test functions. In this case, the finite element space has a tensor product structure, which can be exploited to compensate for the increase of dimensionality caused by using the multiscale test functions.

4 Complex fluids and microfluidics

The behavior of liquids is usually very well described by the classical Navier-Stokes equations with the no-slip boundary condition. There are two notable exceptions. The first is non-Newtonian fluids such as polymeric fluids. In this case the constitutive equations are more complex than that of Newtonian fluids, for which the viscous stress is simply a linear function of the rate of strain. The second is micro-fluidics. In this case the geometry of the flow domain is so small that the no-slip boundary condition is no longer sufficiently accurate.

Three different levels of models are commonly used in the modeling of liquids: molecular dynamics, Brownian dynamics, and hydrodynamics. We will discuss the case when the microscale model is molecular dynamics and the macroscale model is hydrodynamics. But some of the issues that we will discuss are also relevant if the microscale model is Brownian dynamics. For simplicity we will assume that the flow is incompressible. Extending the methodology to deal with compressibility is quite straightforward. This section is taken mostly from [RE05a].

4.1 The macroscale and microscale models

At the continuum level, the dynamics of incompressible flow have to obey conservation laws of mass and momentum:

$$\begin{cases} \rho \partial_t \mathbf{u} = \nabla \cdot \tau \\ \nabla \cdot \mathbf{u} = 0 \end{cases} \tag{51}$$

where the momentum flux $-\tau = \rho\, \mathbf{u} \otimes \mathbf{u} - \tau_d$. Here ρ is the density of the fluid which is assumed to be a constant, $\mathbf{u} = (u, v)$ is the velocity field, and τ_d is the stress tensor. At this stage the system is not closed since the stress tensor is yet to be specified. Traditionally the idea has been to close this system by an empirically postulated constitutive relation, such as

$$\tau_d = -pI + \mu(\nabla \mathbf{u} + \nabla \mathbf{u}^T) \tag{52}$$

for simple fluids. In this case, all information about the molecular structure is lumped into one number, the viscosity μ. Here we are interested in the situation when empirical constitutive relations are no longer accurate enough, as for the case of polymeric fluids, and more information at the microscopic level is needed.

Another important component in the model is the boundary condition. Almost all macroscopic models assume the no-slip boundary condition

$$\mathbf{u} = \mathbf{u}_0 \tag{53}$$

where $\mathbf{u}_0$ is the velocity of the boundary. This is adequate in many situations, but becomes questionable for some problems in micro-fluidics.

For the microscopic model, we will use molecular dynamics (MD). Using standard notations for liquids, we have

$$\begin{cases} m_i \dot{\mathbf{x}}_i(t) = \mathbf{p}_i(t) \\ \dot{\mathbf{p}}_i(t) = \mathbf{F}_i \end{cases} \tag{54}$$

$i = 1, 2, \cdots, N$. Here m_i is the mass of the i-th particle, $\mathbf{x}_i$ and $\mathbf{p}_i$ are its position and momentum respectively, $\mathbf{F}_i$ is the force acting on the i-th particle. To examine the behavior of the fluid flow near a solid boundary, we should also model the vibration of the atoms in the solid next to the fluid-solid interface. Therefore one should consider the fluid-solid system as a whole. Normally one works in the isothermal setting, and the Nosé-Hoover thermostat can be used to control the temperature of the system [FS01].

The connection between the atomistic and the continuum models is made as follows. Given the microscopic state of the system $\{\mathbf{x}_i(t), \mathbf{p}_i(t)\}_{i=1,2,\cdots,N}$, we define the empirical momentum distribution

$$\mathbf{m}(\mathbf{x}, t) = \sum_i \mathbf{p}_i(t) \delta(\mathbf{x}_i(t) - \mathbf{x}) \tag{55}$$

where δ is the Delta function. Momentum conservation can then be expressed in terms of the microscopic variables as:

$$\partial_t \mathbf{m} = \nabla \cdot \tau(\mathbf{x}, t) \tag{56}$$

where the momentum current density $\tau(\mathbf{x}, t)$ is given by the following Irving-Kirkwood formula [IK50]:

$$\begin{aligned}\tau(\mathbf{x}, t) = &-\sum_i \tfrac{1}{m_i}(\mathbf{p}_i(t) \otimes \mathbf{p}_i(t))\delta(\mathbf{x}_i(t) - \mathbf{x}) \\ &-\tfrac{1}{2}\sum_{j \neq i} \left((\mathbf{x}_i(t) - \mathbf{x}_j(t)) \otimes \mathbf{F}_{ij}(t)\right) \int_0^1 \delta(\lambda \mathbf{x}_i(t) + (1-\lambda)\mathbf{x}_j(t) - \mathbf{x})\, d\lambda\end{aligned} \tag{57}$$

where $\mathbf{F}_{ij}(t)$ is the force acting on the i-th particle by the j-th particle.

An important issue in molecular dynamics is how to model the atomistic forces accurately. The algorithms that we will discuss are quite insensitive to the details of the atomistic potential. For simplicity we will work with the simplest situation when the interaction between particles is pair-wise and the pair potential is the Lennard-Jones (LJ) potential in a slightly modified form:

$$V^{LJ}(r) = 4\varepsilon \left(\left(\frac{\sigma}{r}\right)^{12} - \eta \left(\frac{\sigma}{r}\right)^{6} \right) \tag{58}$$

Here r is the distance between the particles, ε and σ are characteristic energy and length scales respectively. The parameter η controls the nature of the interaction between particles. When $\eta = 1$, (58) defines the usual LJ potential which is attractive at long distance. Repulsion between particles of different species can be modeled using negative values of η. For simplicity we have restricted ourselves to macroscopically two-dimensional systems and will continue to do so. But it is important to note that the MD simulations are done in three dimensions. Two dimensional MD systems may exhibit non-physical effects.

It proves convenient to use the reduced atomic units. The unit of length is σ. The unit of time is $\sigma\sqrt{m/\varepsilon}$. For temperature it is ε/k_B where k_B is the Boltzmann constant, and for density it is m/σ^3. The unit of viscosity is $(\varepsilon m)^{1/2}/\sigma^2$. The unit of surface tension is ε/σ^2.

4.2 Type B problems: Atomistic-based constitutive modeling

Macroscale solver

As the macroscopic solver, we choose the projection method on a staggered grid [Cho68, Cho89]. The projection method is a fractional step method. At each time step, we first discretize the time derivative in the momentum equation by the forward Euler scheme to obtain an intermediate velocity field:

$$\rho \frac{\tilde{\mathbf{u}}^{n+1} - \mathbf{u}^n}{\Delta t} = \nabla \cdot \tau^n \tag{59}$$

where τ^n is the momentum flux. For the moment, pressure as well as the incompressibility condition are neglected. Next the velocity field $\tilde{\mathbf{u}}^{n+1}$ is projected onto the divergence-free subspace:

$$\rho \frac{\mathbf{u}^{n+1} - \tilde{\mathbf{u}}^{n+1}}{\Delta t} + \nabla p^{n+1} = 0 \tag{60}$$

where p^{n+1} is determined by

$$\Delta p^{n+1} = \frac{\rho}{\Delta t} \nabla \cdot \tilde{\mathbf{u}}^{n+1} \tag{61}$$

usually with Neumann boundary condition.

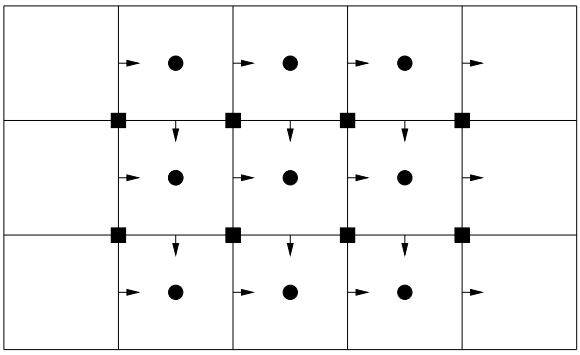

Fig. 10. Schematic of the spatial discretization of the continuum equations in (51). u is defined at $(x_i, y_{j+\frac{1}{2}})$, v is defined at $(x_{i+\frac{1}{2}}, y_j)$, and p is at the cell center $(x_{i+\frac{1}{2}}, y_{j+\frac{1}{2}})$. τ_{11} and τ_{22} are calculated at the cell center indicated by circles, and τ_{12} is calculated at the grid points indicated by squares

The spatial discretization is shown in Figure 10. For integer values of i and j, we define u at $(x_i, y_{j+\frac{1}{2}})$, v at $(x_{i+\frac{1}{2}}, y_j)$, and p at the cell center $(x_{i+\frac{1}{2}}, y_{j+\frac{1}{2}})$. The diagonals of the flux τ are defined at $(x_{i+\frac{1}{2}}, y_{j+\frac{1}{2}})$, and the off-diagonals are defined at (x_i, y_j). The operators ∇ and Δ are discretized by standard central difference and the five-point formula respectively. The use of this grid simplifies the coupling with molecular dynamics.

Estimating the stress

The data that need to be estimated from molecular dynamics are the stresses. Here we will make a constitutive assumption, namely that the stress depends only on the rate of strain. We do not need to know anything about the specific functional form of this dependence.

The key component in estimating the stress is to construct a constant rate-of-strain ensemble for the MD. This is done through a modified periodic boundary condition.

Constrained microscopic solver: Constant rate-of-strain MD

There exists an earlier work due to Lees and Edwards [LE72] in which the periodic boundary condition is modified to maintain a constant shear in one direction. This is done by shifting the periodic copies of the simulation box above and below in opposite directions according to the given shear profile. This idea was extended to situations with general linear velocity profiles in [RE05a].

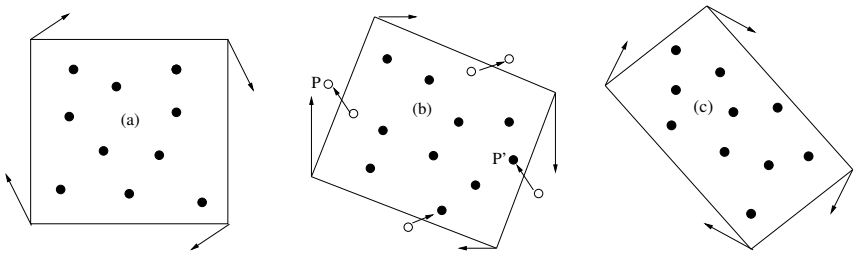

Fig. 11. Periodic boundary conditions on a dynamically deforming box

Without loss of generality, we will consider the situation when the macroscopic velocity profile is of the form

$$\begin{pmatrix} u \\ v \\ w \end{pmatrix} = \begin{pmatrix} a & b & 0 \\ c & -a & 0 \\ 0 & 0 & 0 \end{pmatrix} \begin{pmatrix} x \\ y \\ z \end{pmatrix} = A\mathbf{x}. \tag{62}$$

To initialize the MD calculation, one may simply start with a perfect lattice configuration in a rectangular box. Each particle is given a mean velocity according to (62), plus a random component with mean 0 and variance $k_B T$, where T is the desired temperature and k_B is the Boltzmann constant.

Deforming the simulation box. Periodic boundary condition is imposed on a dynamically deforming simulation box, whose vertices move according to

$$\dot{\mathbf{x}} = A\mathbf{x}, \quad A = \begin{pmatrix} a & b & 0 \\ c & -a & 0 \\ 0 & 0 & 0 \end{pmatrix}. \tag{63}$$

Intuitively it is helpful to think of the simulation box as been embedded in the whole space.

The shape of the deformed box at a later time is shown in Figure 11(b). Suppose at this point a particle crosses the boundary at $P(\mathbf{x})$, with velocity $\mathbf{u}$, it will return to the box at $P'(\mathbf{x}')$ with a modified velocity

$$\mathbf{u}' = \mathbf{u} + A(\mathbf{x}' - \mathbf{x}). \tag{64}$$

where P' is the periodic image of P with respect to the deformed box.

It is easy to see that if the velocity field is a pure shear

$$A = \begin{pmatrix} 0 & b & 0 \\ 0 & 0 & 0 \\ 0 & 0 & 0 \end{pmatrix} \tag{65}$$

then this boundary condition becomes simply the Lees-Edwards boundary condition.

Reinitialization. As the simulation proceeds, the simulation box will in general become quite elongated in one direction and narrowed in the other direction (see Figure 11(c)). If the box is significantly deformed, we need to reinitialize the configuration. The details of the reinitialization procedure is discussed in [RE05a, RE05b].

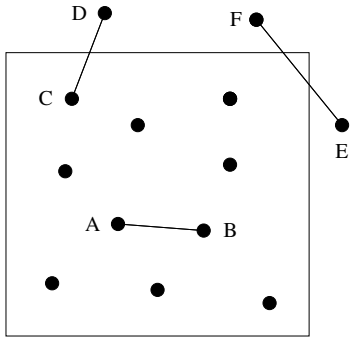

Fig. 12. Computing averaged stress: Besides the contributions from the particles inside the box to the averaged stress, the particles outside the box also contribute, such as CD and EF

The MD simulation keeps track of the positions and velocities of all particles as functions of time, from which the momentum flux tensor can be calculated using the Irving-Kirkwood formula (57).

In practice, (57) is averaged over the simulation box. This gives

$$-\tau(t) = \frac{1}{|\Omega|} \sum_{\mathbf{x}_i \in \Omega(t)} \frac{1}{m_i} (\mathbf{p}_i \otimes \mathbf{p}_i) + \frac{1}{2|\Omega|} \sum_{j \neq i} d_{ij}(\mathbf{x}_i - \mathbf{x}_j) \otimes \mathbf{F}_{ij} \tag{66}$$

where in the first term the summation runs over particles inside the box, and in the second term the summation is over all pairs of particles including their images. Here d_{ij} is defined as

$$d_{ij} = \begin{cases} 1, \text{ if } \mathbf{x}_i, \mathbf{x}_j \in \Omega, \\ 0, \text{ if } \mathbf{x}_i, \mathbf{x}_j \notin \Omega, \\ c, \text{ if only one of } \mathbf{x}_i, \mathbf{x}_j \text{ in } \Omega \end{cases} \tag{67}$$

where $0 \leq c \leq 1$ is the fraction of $|\mathbf{x}_i - \mathbf{x}_j|$ being cut by the box. Therefore besides contributions from the particles inside the box, particles outside the box also contribute to the stress, as illustrated in Figure 12.

(66) gives the instantaneous stress at the microscopic time t (see Figure 13). To extract the macroscopic stress, (66) is averaged over time to give an estimate for the macroscale stress:

$$\tau = \frac{1}{T - T_0} \int_{T_0}^{T} \tau(t) dt \tag{68}$$

where T_0 is some relaxation time.

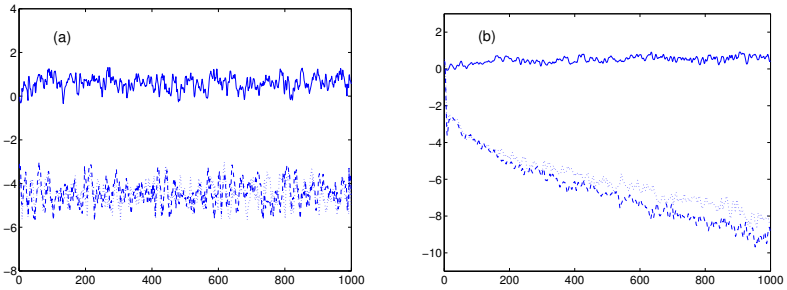

Fig. 13. Instantaneous stress as a function of the microscopic time. Solid line: $-\tau_{12}$; dashed line: $-\tau_{11}$; dotted line : $-\tau_{22}$. The temperature is fixed in **(a)** but not in **(b)**, where the stress diverges due to viscous heating. In both case, $u = 0.18y, v = 0$

In Figure 13, we show two numerical examples of the calculated stress. In atomic units the density is $\rho = 0.79$ and the temperature is fixed at 1.0 in the first example but not in the second which is not coupled to any thermostats. The stress diverges in this case due to viscous heating.

As a simple validation of this procedure, we show in Figure 14 the computed shear stress as a function of shear rate for LJ fluids. These data fit quite well to a linear function indicating a linear relation between stress and the rate of strain. The viscosity can be computed by estimating the slope. This gives a value of 2 which agrees well with result in the literature [TR89].

To summarize, at each macro time step k, the overall algorithm looks as follows:

1. Step 1. Calculate the needed stresses by constrained local MD simulations;
2. Step 2. Using the projection method and the computed stresses to get $\mathbf{u}^{k+1}$.

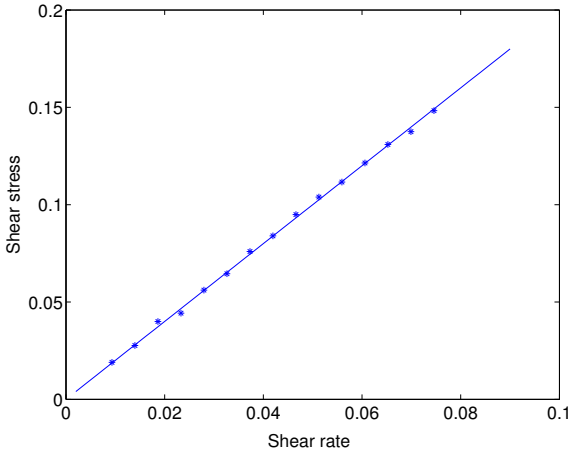

Fig. 14. Shear stress as a function of shear rate for simple LJ fluids. The discrete points are obtained from 3d MD simulation, and they fit very well to a linear function with slope 2 which is the viscosity. All the quantities are expressed in the atomic unit

Fluid dynamics of chain molecules

This algorithm was validated on a simple example of pressure-driven cavity flow, and applied to a number of other examples, including the driven cavity flow, and a system of dumbbell fluids with FENE potential. Here we briefly report the results for the dynamics of chain molecules that represent flexible polymers. More details are found in [RE05b].

In [RE05b] a bead-spring model of chain molecules is used to represent the flexible polymers, with a total of N beads for each chain. The interaction potential between the beads has two parts. The first is the LJ potential which acts on all beads in the system. The second is the spring force given by the FENE potential:

$$V^{FENE}(r) = \begin{cases} -\frac{1}{2}kr_0^2 \ln(1-(\frac{r}{r_0})^2), & r < r_0 \\ \infty, & r \geq r_0 \end{cases} \tag{69}$$

The values $k = 1$ and $r_0 = 2.5$ were used. The density of the beads is 0.79. $N = 12$. The slip boundary condition suggested in [PT04] was used. [RE05b] also reports results from computations that treat this as a type C problem and extract boundary conditions using the algorithm described next for type A problems. The results are basically the same.

At small driving force, there is only partial slip between the fluid the solid. The velocity profile converges to steady state, as shown in Figure 15. This steady state profile is compared with the standard Poiseuille profile at the

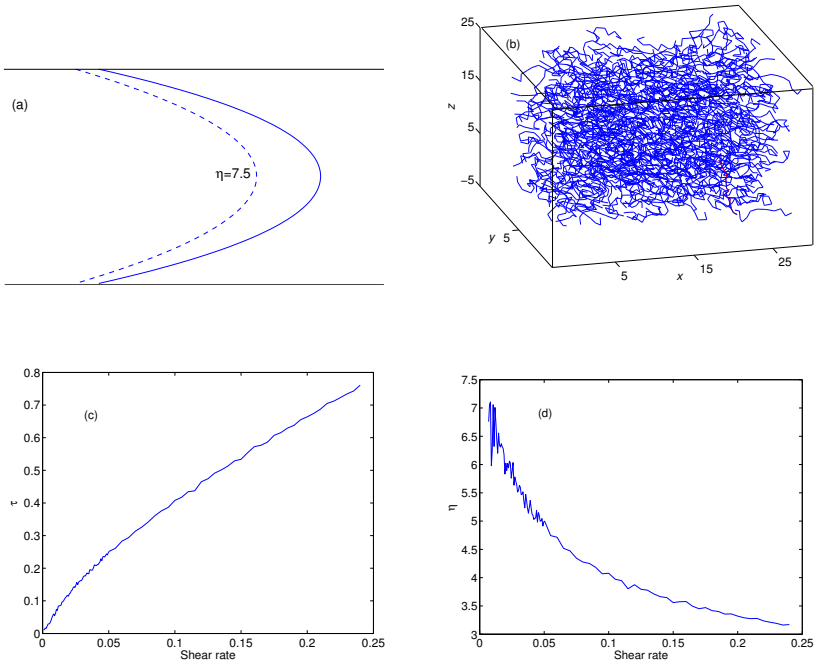

Fig. 15. (a) Steady state velocity profile for the polymer fluid made up of chain molecules (solid line), compared with that of the Newtonian fluid (dashed line). We observe partial slip, as well as shear-thinning. **(b)** A partial sample of the conformation of the chain molecules in a typical MD simulation. **(c)** Shear stress as a function of shear rate. **(d)** Viscosity as a function of shear rate. In **(c)** and **(d)**, to make the results more transparent, we supplemented the results from the HMM calculation by results from pre-computing: The more noisy results at small shear rates are from HMM calculation, the more smooth results at higher shear rates are from pre-computing

zero-shear-rate viscosity. Besides the partial slip, we also see that the profile for the chain molecules has larger curvature, a characteristic of shear thinning fluids. This is confirmed by the plot of the effective constitutive relation used in the HMM simulation at the steady state.

4.3 Type A problems: Modeling boundary conditions

In the discussions above we were concerned with the constitutive relations for complex fluids. Here we will discuss boundary conditions for micro-fluidics. One most important aspect of micro-fluidics is the significance of line and surface tension. Therefore as our primary examples, we choose the Marangoni flow and the contact line problem. For these problems, the need for coupling with MD comes from the complex solid-fluid and fluid-fluid interaction near the wall.

Marangoni flows

We will discuss a specific example of the Marangoni flow, namely channel flow driven by complex solid-fluid interactions which are modeled by molecular dynamics.

The HMM procedure goes as follows. The macroscopic solver is the same as before, i.e. a finite-volume projection method on a staggered grid. This simplifies the next step, which is to obtain the boundary condition from MD.

The needed data in the finite volume projection method are the *tangential* stresses at the boundary.

The schematic of the MD is shown in Figure 16. Periodic boundary condition is imposed in the x- and z-direction. In the y-direction, the fluid is confined by a solid wall at AB and a repulsive force at GH. One choice of this repulsive potential is the repulsive part of the LJ potential:

$$P(r) = \varepsilon \left(\frac{\sigma}{r}\right)^{12} \tag{70}$$

where r is the distance to GH. Similar techniques for confining particles were used in [HP97, Had99].

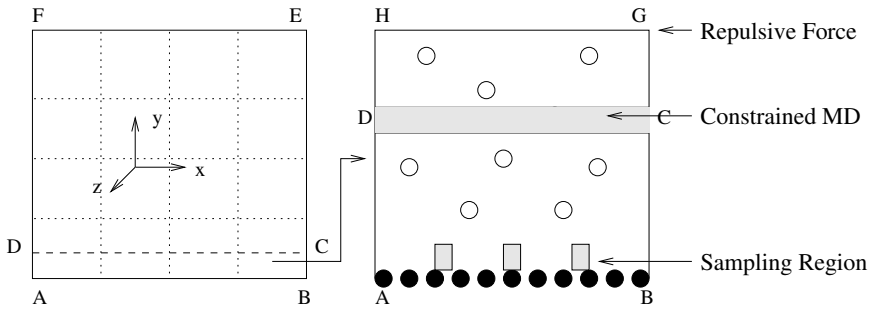

Fig. 16. Schematic of the multiscale method for the example of Marangoni flow. In the left panel, the finite volume grid is indicated by the dotted lines. The boundary condition at AB is extracted from molecular dynamics simulations confined in $ABCD$. The set-up of the MD simulation is shown in the right panel. Particles are confined by a repulsive force at GH and the solid wall at AB. The dynamics of the particles in the strip CD are constrained by the continuum velocity field. The boundary conditions are extracted from the small bins at the lower boundary. Black dots represent atoms in the solid

The MD is constrained by the macroscale velocity field. This is done as follows. Each particle in the strip CD is assigned the velocity: $\mathbf{u}(\mathbf{x}) = \mathbf{u}^c(\mathbf{x}) + \tilde{\mathbf{u}}$, where $\mathbf{u}^c(\mathbf{x})$ is the velocity from the continuum calculation and $\tilde{\mathbf{u}}$ is the thermal velocity that obeys the Maxwellian distribution at some temperature T. Therefore the strip plays a two-fold role here: As a momentum reservoir

it maintains the non-equilibrium dynamics at the steady state; as a thermal reservoir it releases heat generated by viscous flow from the system.

The solid wall also needs to be explicitly modeled, here as a crystal lattice. Geometric as well as chemical heterogeneities can be modeled by choosing appropriate atomistic potentials (see [RE05a, QW04]).

After a relatively short equilibration time, the stresses are estimated using the Irving-Kirkwood formula, as was done before.

Figure 17 shows some results of the effective boundary conditions extracted from the molecular dynamics simulation. For more numerical results, we refer to [RE05a].

The overall algorithm for a typical macro time step k is as follows:

Step 1. Calculate the stress at the boundary AB by local MD simulation. The MD is constrained by $\mathbf{u}^k$;
Step 2. Solve the continuum equations to get $\mathbf{u}^{k+1}$.

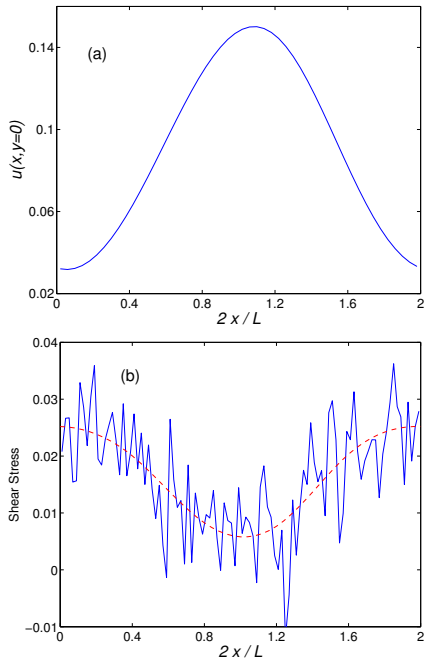

Fig. 17. (a) the velocity at the lower boundary; **(b)** the stress extracted from MD (solid curve) and fitted by fourth-order B-splines (dashed curve)

Contact line dynamics

We next consider the motion of two immiscible fluids on a solid surface. Continuum hydrodynamics breaks down in the vicinity of the contact line, where the fluid-fluid interface meets the solid surface. Specifically the usual no-slip boundary condition used in macroscopic fluid dynamics leads to an unphysical divergent shear stress and dissipation rate [Dus79]. Molecular dynamics simulations of Couette or Poiseuille flow show relative slip between the fluid and the wall around the contact line [TR89, QWS03].

As for the previous example, a HMM procedure is called for in order to obtain boundary conditions from MD. However the present problem is quite a bit more complicated.

Macroscale solver

As the macroscale model, we take

$$\begin{cases} \rho\, \partial_t \mathbf{u} = \nabla \cdot \tau \\ \nabla \cdot \mathbf{u} = 0 \\ \dot{\mathbf{x}}_\Gamma = \mathbf{u} \end{cases} \tag{71}$$

where the momentum flux in continuum theory is given by

$$-\tau = \rho\, \mathbf{u} \otimes \mathbf{u} + pI - \mu(\nabla \mathbf{u} + \nabla \mathbf{u}^T) + \gamma(I - \hat{\mathbf{n}} \otimes \hat{\mathbf{n}})\delta_\Gamma - f_0 x I. \tag{72}$$

The last equation in (71) says that the fluid-fluid interface $\mathbf{x}_\Gamma(t)$ is advected by the velocity field of the fluid. The first term in the momentum flux is due to convection, the second term is the pressure, the third term is the viscous stress, the fourth term corresponds to the surface tension force which is concentrated at the fluid-fluid interface $\mathbf{x}_\Gamma$ (δ_Γ is the surface delta function), and the last term is the external force. I is the identity matrix, γ is the the surface tension coefficient and $\hat{\mathbf{n}}$ is the unit normal of the interface.

In the numerical calculations, it is standard to replace the surface tension term $\tau_\Gamma = \gamma(I - \hat{\mathbf{n}} \otimes \hat{\mathbf{n}})\delta_\Gamma$ as a body force defined by

$$\tilde{\tau}_\Gamma(\mathbf{x}) = \int_{R^2} D(\mathbf{x} - \mathbf{y})\tau_\Gamma(\mathbf{y}) d\mathbf{y} \tag{73}$$

One choice for the kernel D is given by

$$D(\mathbf{x}) = \begin{cases} (2d)^{-2}(1 + \cos(\frac{\pi}{d}x))(1 + \cos(\frac{\pi}{d}y)), & \text{if } |x| < d, |y| < d; \\ 0, & \text{otherwise} \end{cases} \tag{74}$$

This was first introduced by Peskin [Pes77]. In the examples reported below, d, the width of the smoothing region, is taken to be twice the cell size. After

being interpolated from the interface to the grid points by (73), the total flux is conserved.

As before we use the projection method for the macroscale equation. The interface is updated by forward Euler method:

$$\frac{(\mathbf{x}_\Gamma)^{n+1} - (\mathbf{x}_\Gamma)^n}{\Delta t} = \mathbf{u}^n. \tag{75}$$

The interface is represented by a collection of discrete points $\{(\mathbf{x}_\Gamma)_i, i = 0, 1, \cdots, N\}$, where the two end points $(\mathbf{x}_\Gamma)_0$ and $(\mathbf{x}_\Gamma)_N$ are the contact points, i.e. the intersections of the interface with the solid walls. Surface tension force is calculated at the middle of each segment. Neumann condition on velocity is used at the in-flow and out-flow boundaries. At the solid wall away from the contact point, no-slip boundary condition is used. Other details of the macroscale solver can be found in [RE05a].

Microscopic solver and estimating boundary conditions

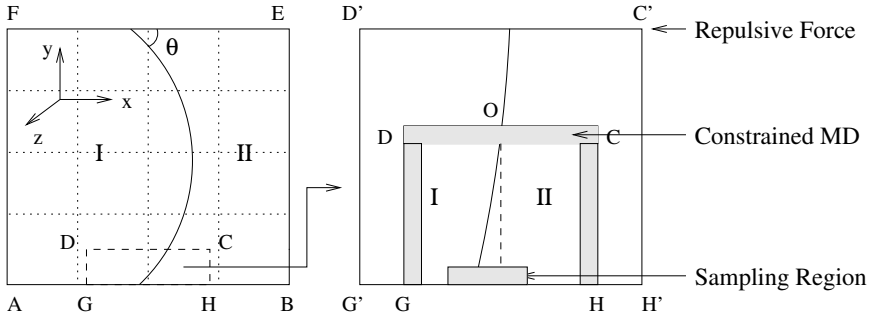

Fig. 18. Schematic of the multiscale method for the contact line problem. Macro grid used in the computation is represented by dotted lines in the left panel. MD is carried out in a local region around the contact line. Periodic boundary conditions are imposed on the boundaries of the enlarged box $G'D'$ and $H'C'$. The dynamics in the shaded strips GD, DC and CH are constrained by continuum velocity field. The shear stress and the position of the contact point are computed in the strip along GH

The data that need to be estimated from MD are:

1. shear stress near the contact line (here the contact point);
2. velocity of the contact line.

The schematics of the molecular simulation around the contact line is shown in Figure 18. Periodic boundary conditions are imposed in the z-direction. In the x-direction, the flow field is not necessarily periodic, so we

enlarge the simulation box to $G'H'C'D'$ and impose periodic boundary conditions on $G'D'$ and $H'C'$ instead (see the right panel in Figure 18). The enlarged part serves as a particle reservoir. In this system we have two species of fluids, fluid I on the left and fluid II on the right. When a fluid particle of species II crosses $H'C'$, it will enter the box through $G'D'$ and become species I, and vice versa.

In the y-direction, the particles are confined by the solid wall at $G'H'$ and a repulsive force at $C'D'$. The repulsive force is modeled by the repulsive part of the LJ potential, as given in (70). The repulsive force is used to keep the particles from escaping the MD domain. More detailed information on the microscale solver is given in [RE05a].

For consistency between the molecular dynamics and the continuum dynamics, a modified Andersen thermostat is used in the strips GD, DC, and CH: At Poisson distributed times with certain frequency ν, a random particle is selected from the strips and its velocity is replaced by $\mathbf{u}(\mathbf{x}) = \mathbf{u}^c(\mathbf{x}) + \tilde{\mathbf{u}}$, where $\mathbf{u}^c$ is the velocity from continuum dynamics and $\tilde{\mathbf{u}}$ is a random variable with Maxwell-Boltzmann distribution at the specified temperature T.

The shear stress is calculated using the formula (57) in the bins which are a few (about 3) atomic lengths above the wall.

To estimate the position of the contact line, we first calculate the particle density function along the fluid-solid interface (remember O is fixed):

$$\rho(x) = \sum_i \rho_i \, \delta(x_i - x) \tag{76}$$

where the sum is over all particles in the strip above the solid wall, x_i is the x coordinate of the i-th particle, ρ_i is 1 for particles of species I and -1 for particles of species II. The position of the contact line is determined by $\rho(x) = 0$. [RE05a] suggests taking a strip which is again a few atomic lengths above the wall and partition it into uniform bins in x direction. Then the density is obtained by taking the sum of ρ_i in each bin. The position of the contact line is given by

$$(x_\Gamma)_0 = x_0 + \int_{x_0}^{x_1} \tilde{\rho}(x) dx \tag{77}$$

where x_0 and x_1 are the positions of the leftmost and the rightmost bins respectively. $\tilde{\rho}(x)$, which is between 0 and 1, is the rescaled density:

$$\tilde{\rho}(x) = \frac{\rho(x) - \min_x \rho(x)}{\max_x \{\rho(x) - \min_x \rho(x)\}}. \tag{78}$$

Numerical results

The overall algorithm for a typical macro time step k looks like the following:

Step 1. Carry out a constrained MD simulation near the contact line, from which the shear stress and the position of the contact line are estimated;
Step 2. Solve equations in (71) for $\mathbf{u}^{k+1}$ and $(\mathbf{x}_\Gamma)^{k+1}$.

We will discuss two examples from [RE05a]. The first example is a validation study. The second is an example of asymmetric fluid-solid interactions.

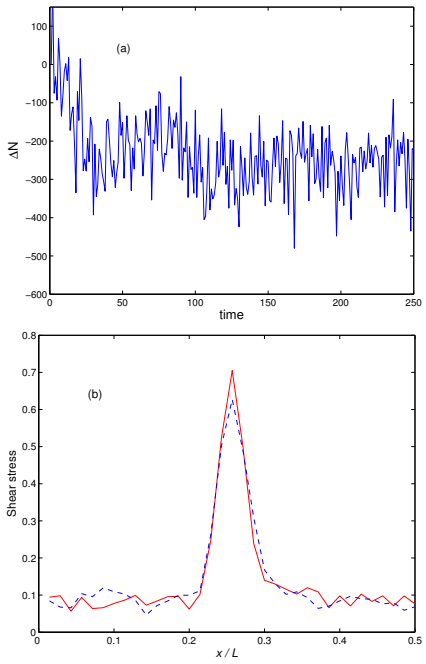

Fig. 19. Results of the constrained MD simulation. **(a)** The time series of $\Delta N = N_I(t) - N_{II}(t)$, where $N_I(t)$ and $N_{II}(t)$ are the particle numbers of the two species in the box $GDCH$ (see Figure 18) respectively; **(b)** The shear stress measured at the solid wall. The solid curve is calculated from the full MD simulation and the dashed curve is from the constrained MD simulation

Example 1. Two immiscible fluids are confined in a channel and driven by an external force $f_0 = 0.02$ in the x direction. The system measures $69.7 \times 22.5 \times 5.16$ and contains 2944 particles of each fluid and 1728 solid particles. The system is periodic in the x and z directions.

To check the validity of the constrained molecular dynamics used in the hybrid method, a local MD simulation is performed around the contact line. The left panel of Figure 19 shows the time series for the difference of the particle numbers of both species inside $GDCH$ (see Figure 18). We clearly see a transient time during which the particles of species I flow out of the box

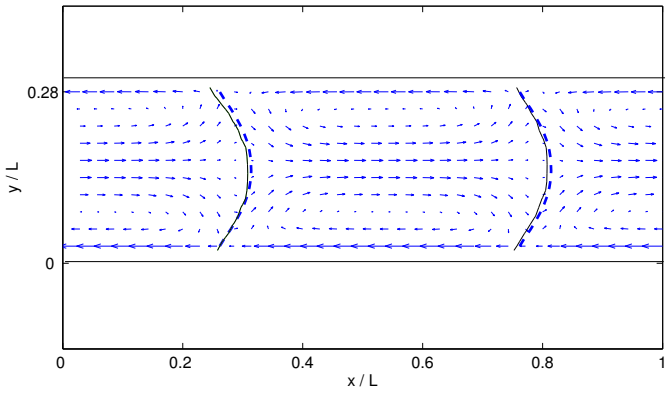

Fig. 20. The steady-state solution of Example 1 by the hybrid method and comparison with the results of full MD. The interface is shown in dashed curve. The solid curve shows the interface obtained by full MD simulation

and particles of species II flow into the box. The right panel of Figure 19 is a comparison between the shear stress calculated on the surface of the solid wall in the full MD simulation and in the local constrained MD simulation, and we see good agreements.

The validation study was also carried out for the steady-state solution. The parameters in the continuum model are $\rho = 0.81, \mu = 2.0$ and $\gamma = 3.7$. 70×20 grid points are used in the spatial discretization, and the time step is $\Delta t = 0.05$. A static configuration was used as the initial data and the external force is slowly increased to 0.02. The steady-state velocity field and the interface (dashed line) are shown in Figure 20. These results agree well with the full MD results.

Example 2. In our next example, we consider the case for which the fluid-solid interaction is different for the two fluid phases. Specifically the attraction between fluid I and the solid is decreased by taking $\eta = 0.7$ in the potential (58). All other parameters in the potential are kept unchanged from the previous example. The static contact angle θ in this case is 65°.

Again the static configuration is used as the initial state and an external force $f_0(t) = 5.35 \times 10^{-11} t$ in x-direction is applied until it reaches $f_0 = 2.2 \times 10^{-5}$. The force is then decreased at the same rate until it reaches $f_0 = -7.0 \times 10^{-5}$. The fluid-fluid interfaces at different times are shown in Figure 21a . The left-most dashed line is the interface at the static position, and it travels in the stream-wise direction as the external force increases. The right-most dashed line corresponds to $f_0 = 2.2 \times 10^{-5}$. The solid lines from the right to the left show the shapes of the interfaces as the external force decreases. Figure 21b shows the dynamic contact angle as a function of the applied force. Again, the dashed curve corresponds to the dynamics as the

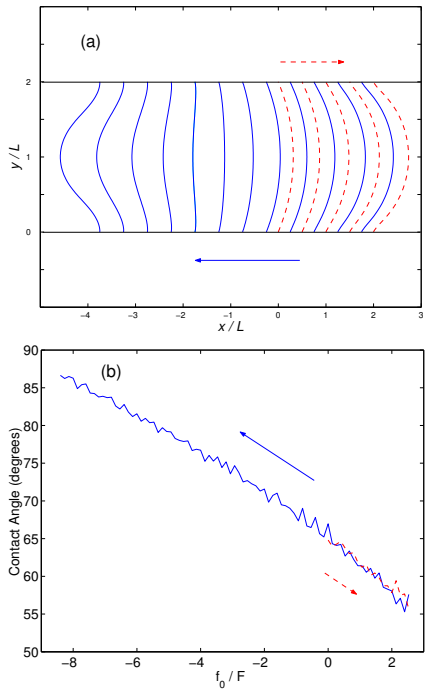

Fig. 21. Dynamics of the contact line problem with asymmetric fluid-solid interactions. **(a)** Fluid-fluid interfaces at different times. For dashed curves from left to right, the external force increases from 0 to 2.2×10^{-5}; For solid curves from right to left, the external force decreases from 2.2×10^{-5} to -7.0×10^{-5}; **(b)** Dynamic contact angle as a function of external force. The external force is rescaled by $F = 8.1 \times 10^{-6}$

force increases, and the solid curve corresponds to the dynamics as the force decreases.

5 Dynamics of solids at finite temperature

Unlike fluids, the multiscale nature of solids is much more pronounced. On the modeling side, there is no analog of the Navier-Stokes equation as the fundamental macroscopic model. On the physics side, solids often contain a hierarchy of structures and defects at different scales [Phi01]. These include point defects such as vacancies and impurities, dislocations and structures formed by dislocations, grain boundaries, and even cracks. As a result, multiscale modeling has received more attention in solids than in fluids.

We will again focus our discussion on the situation when the macroscopic model is continuum mechanics and the microscopic model is molecular dynamics. For the analysis of static properties of solids at zero temperature, in

which case the mathematical models reduce to minimization problems, the quasi-continuum method has had a great deal of success [TOP96]. Here we will discuss multiscale methods that handles the dynamics of solids at finite temperature. This part of the presentation follows mainly [LE05].

5.1 Macroscopic and microscopic models

Again the continuum model is expressed in terms of the conservation laws. For solids it is more convenient to work with Lagrangian coordinates. Denote by $\mathbf{x}^0$ the reference coordinate for the solid and $\mathbf{x} = \mathbf{x}^0 + \mathbf{u}(\mathbf{x}^0, t)$, the position after deformation, with $\mathbf{u}$ being the displacement. Then the conservation laws take the form:

$$\begin{cases} \partial_t \mathbf{A} - \nabla_{\mathbf{x}^0} \mathbf{v} &= 0, \\ \partial_t \mathbf{v} - \nabla_{\mathbf{x}^0} \cdot \boldsymbol{\sigma} &= 0, \\ \rho_0 \partial_t e + \nabla_{\mathbf{x}^0} \cdot \mathbf{j} &= 0. \end{cases} \tag{79}$$

Here $\mathbf{A}, \mathbf{v}, e$ are the deformation gradient, velocity and total energy per particle respectively, ρ_0 is the initial density, $\boldsymbol{\sigma}$ is the first Piola-Kirchhoff stress tensor and $\mathbf{j}$ is the energy flux. The first equation in (79) is a statement of compatibility between the deformation gradient and the velocity. The second and third equations are conservation of momentum and energy respectively. In continuum mechanics [LL80b], these equations are supplemented by the empirical constitutive relations for stress and energy fluxes. Our interest here is to develop multiscale strategies that bypass these empirical constitutive laws when their accuracy is in doubt.

The microscopic model is again MD. The first step is to express MD in the form of (79). For this purpose, we define the following empirical distributions [LE05],

$$\begin{cases} \widetilde{\rho}(\mathbf{x}^0, t) = \sum_i m_i \delta(\mathbf{x}^0 - \mathbf{x}_i^0), \\ \widetilde{\mathbf{v}}(\mathbf{x}^0, t) = \sum_i \mathbf{v}_i(t) \delta(\mathbf{x}^0 - \mathbf{x}_i^0), \\ \widetilde{\mathbf{q}}(\mathbf{x}^0, t) = \sum_i m_i \mathbf{v}_i(t) \delta(\mathbf{x}^0 - \mathbf{x}_i^0), \\ \widetilde{e}(\mathbf{x}^0, t) = \frac{1}{2} \sum_i \Big[m_i \mathbf{v}_i(t)^2 + \sum_{j \neq i} \phi\big(\mathbf{x}_i(t) - \mathbf{x}_j(t)\big) \Big] \delta(\mathbf{x}^0 - \mathbf{x}_i^0). \end{cases} \tag{80}$$

Here as before we denote by $\mathbf{x}_i^0$ the position of the i-th atom in the undeformed configuration, which is also taken to the initial position of the i-th atom, $\mathbf{x}_i(t)$ and $\mathbf{v}_i(t)$ are respectively the position and velocity of the i-th atom at time t. Note that $\mathbf{x}_i^0$ is independent of t. Let

$$\begin{cases} \widetilde{\boldsymbol{\sigma}}_{\alpha\beta}(\mathbf{x}^0,t) = -\dfrac{1}{2}\displaystyle\sum_{i\neq j} f_\alpha\big(\mathbf{x}_i(t)-\mathbf{x}_j(t)\big)(x^0_{i\beta}-x^0_{j\beta}) \\ \qquad\qquad \times \displaystyle\int_0^1 \delta\big(\mathbf{x}^0-(\mathbf{x}^0_j+\lambda(\mathbf{x}^0_i-\mathbf{x}^0_j))\big)d\lambda, \\ \widetilde{\mathbf{j}}(\mathbf{x}^0,t) = \dfrac{1}{4}\displaystyle\sum_{i\neq j}\big(\mathbf{v}_i(t)+\mathbf{v}_j(t)\big)\cdot\mathbf{f}\big(\mathbf{x}_j(t)-\mathbf{x}_i(t)\big)(\mathbf{x}^0_i-\mathbf{x}^0_j) \\ \qquad\qquad \times \displaystyle\int_0^1 \delta\big(\mathbf{x}^0-(\mathbf{x}^0_j+\lambda(\mathbf{x}^0_i-\mathbf{x}^0_j))\big)d\lambda. \end{cases} \tag{81}$$

where $\mathbf{f}=-\nabla V$ is the force and we have only considered two-body interaction in the atomistic potential – extension to general cases can be found in [LE05]. We have

$$\begin{cases} \partial_t\widetilde{\mathbf{q}} - \nabla_{\mathbf{x}^0}\cdot\widetilde{\boldsymbol{\sigma}} = 0, \\ \rho_0\partial_t\widetilde{e} + \nabla_{\mathbf{x}^0}\cdot\widetilde{\mathbf{j}} = 0. \end{cases} \tag{82}$$

The expressions in (81) are nothing but the generalizations of the classical Irving-Kirkwood formula.

5.2 Type B problem: Atomistic-based constitutive modeling

Macroscale solver

Since our basic macroscopic model is a set of conservation laws, we will choose a finite volume method as the macroscale solver. Although there are a variety of finite volume methods available for solving conservation laws [LeV90, GR96], many of them involve computing the Jacobian of the flux functions, which dramatically increases the computational complexity in a coupled multiscale method when the constitutive relation has to be extracted from atomistic models. An exception is the central scheme of Lax-Friedrichs type, such as the one developed in [NT90] which is formulated over a staggered-grid. Below we will choose such central schemes as our macroscale solver.

For convenience, we rewrite the conservation laws in the generic form,

$$\mathbf{w}_t + \mathbf{f}_x = 0. \tag{83}$$

where $\mathbf{w}$ denotes the conserved quantities, and $\mathbf{f}$ is some (unknown) flux function. Figure 22 shows the overall structure of the method. The first order central scheme represents the solutions by piece-wise constants, which are the average values over each cell:

$$\mathbf{w}^n_k = \frac{1}{\Delta x}\int_{x_{k-1/2}}^{x_{k+1/2}} \mathbf{w}(x,t^n)dx.$$

Here Δx is the size of the cell. Integrating (83) over $[x_j,\ x_{j+1}]\times[t^n,\ t^{n+1})$ leads to the following,

$$\mathbf{w}_{k+1/2}^{n+1} = \frac{\mathbf{w}_k^n + \mathbf{w}_{k+1}^n}{2} - \frac{\Delta t}{\Delta x}\left(\mathbf{f}_{k+1}^n - \mathbf{f}_k^n\right) \tag{84}$$

where

$$\mathbf{f}_k^n = \frac{1}{\Delta t}\int_{t^n}^{t^{n+1}} \mathbf{f}(x_k, t)dt$$

This is then approximated by numerical quadrature such as the mid-point formula. A simple choice is $\mathbf{f}_k^n \sim \mathbf{f}(x_k, t^n)$.

With this choice of the macro-solver, the HMM procedure is shown schematically in Figure 22 (see also Figure 6). At each time step, the scheme (84) requires as input the fluxes at the grid points x_k. These flux values are obtained by performing local MD simulations that are constrained by the local macro state variables $\mathbf{A}$, $\mathbf{v}$, e. After the MD system equilibrates, we estimate the fluxes by time/ensemble averaging.

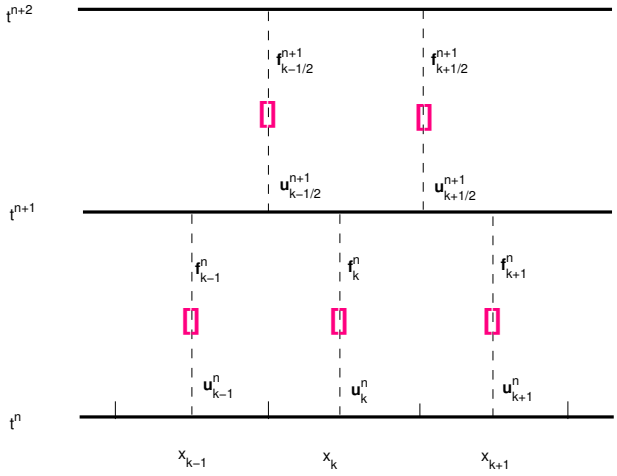

Fig. 22. A schematic illustration of the numerical procedure: starting from piecewise constant solutions $\{\mathbf{w}_k^n\}$, one integrates (83) in time and in the cell $[x_k, x_{k+1}]$. To estimate $\mathbf{f}$ at x_k, we perform a MD simulation using $\mathbf{w}_k^n$ as constraints

Higher order schemes and generalization to high dimensions are discussed in see [LE05].

Constrained microscale solver

Next we discuss how to set up the MD in order to measure the fluxes. As for the case of fluids, we will make a constitutive assumption that the fluxes depend only on the local values of the conserved densities. More general constitutive assumptions can be accommodated, but the constrained MD that we discuss below will have to be modified.

First we initialize the MD. The basic requirement is that the initial condition has to be consistent with the local conserved quantities of the macroscopic state, and has the correct crystal structure. Given the local macroscopic state $\mathbf{A}, \mathbf{v}, e$, we first determine the shape of the MD cell from the deformation gradient tensor. Consider the situation that the crystal is a simple Bravais lattice and let $\mathbf{E}$ be a basis for the undeformed unit cell. The deformed lattice is generated by the basis vectors $\tilde{\mathbf{E}} = \mathbf{AE}$. We then place the atoms on the deformed lattice, possibly with small perturbations. The potential energy $\mathcal{U}$ of this trial configuration and the kinetic energy associated with the mean velocity is subtracted from the total energy e to give us the thermal energy. If this value is positive, the trial configuration is accepted. Otherwise, it is rejected. From the thermal energy one computes the temperature. The velocities of the atoms are initialized according to the Maxwell-Boltzmann distribution with the mean and variance given by the macroscale velocity and the temperature respectively.

We should remark that if the local relaxation time is very short compared with the macro time scale, then there is not much difference in the performance of different initialization procedures, as long as the initial configuration has the correct crystal structure. However, as the relaxation time increases, there can be considerable advantage in using the previously computed microscopic state as the initial configuration for the new MD simulation. Of course the previously computed microscopic state has to be modified in order to be consistent with the current macro state. This can be done as follows.

1. The configuration is deformed linearly to be consistent with the current deformation gradient.

2. The average velocity is shifted to the current average velocity.

3. The temperature is changed using the same procedure as discussed above to arrive at the required total energy.

The choice of the size of the MD system is affected by two competing factors. On one hand the size of the system has to be large enough in order to minimize the effect of the boundary conditions. On the other hand, as the system size goes up, not only the cost goes up, the relaxation time also goes up. We refer to [EL04b] for some careful numerical studies of these effects.

Boundary conditions have to be imposed on the microscopic system in order to guarantee consistency with the local macroscale variables. In the present case since the system is homogeneous (constant mean velocity, temperature and deformation gradient), the most convenient boundary condition is the periodic boundary condition. The MD is performed in a deformed box as described earlier and periodically extended to the whole space.

The periodic boundary condition excludes the possibility of accounting for inhomogeneous effects such as effects of thermal gradients, strain gradients, etc. Extending the methodology to cover these effects is still on-going work.

From the MD data, we can compute the microscopic fluxes using the formulas in (81). The final step is to average the microscopic fluxes to obtain the fluxes needed by the macroscopic scheme. This is very similar to the situation

for fluids and therefore we will omit the details. The interested reader can consult [LE05].

We remark that this procedure allows us to automatically decouple the micro time scales from the macro time scales.

An error analysis of the overall method can be found in [EL04b].

Modeling thermal expansion using MD

As an example, we study the effect of thermal expansion. Our atomistic model is a 3D Lennard-Jones solid in a FCC (face-centered cubic) lattice. We set up the example so that the macroscale behavior is two dimensional. Initially the material is at rest with homogeneous temperature distribution $T \equiv 0.1$. We then increase the temperature in the middle instantaneously to $T = 0.4$. This results in a thermal expansion that propagates outward. The result of HMM is shown in Figure 23 where we display the numerical results for the temperature distribution as well as the velocity field. One clearly observes that the material is expanding outward as heat is spread out.

5.3 Type A problem: Dealing with isolated defects

We now turn to another class of problems that can be treated using multiscale methods, the problem of isolated defects. Solids often contain a variety of defects, such as vacancies, dislocations, twin boundaries and grain boundaries. To a large extent, the structure and dynamics of these defects determine the properties of the solid [Phi01].

A common idea for the multiscale modeling of defects is to use atomistic models near defects and continuum models away from defects, e.g. in a domain decomposition framework. MAAD is a good example of such an approach [ABB98, ABB99]. The HMM philosophy, on the other hand, suggests a strategy that is closer to adaptive model refinement.

The idea of adaptive model refinement is to start with a macroscale model on a macro-grid (which might be locally refined) in the entire computational domain and couple with a more refined model locally near the defects. For the present problem, the macroscale model is the same as before, namely the conservation laws. The macroscale solver can also be chosen as before, i.e. central type of finite volume schemes. But when it comes to computing the fluxes, the cells (more precisely, the cell boundaries where flux evaluation is carried out) are divided into two types: cells that contain defects and cells that do not contain defects. In cells that do not contain defects we evaluate the fluxes using either empirical constitutive relations or the method discussed in the previous section. In cells that do contain defects we compute the fluxes using MD.

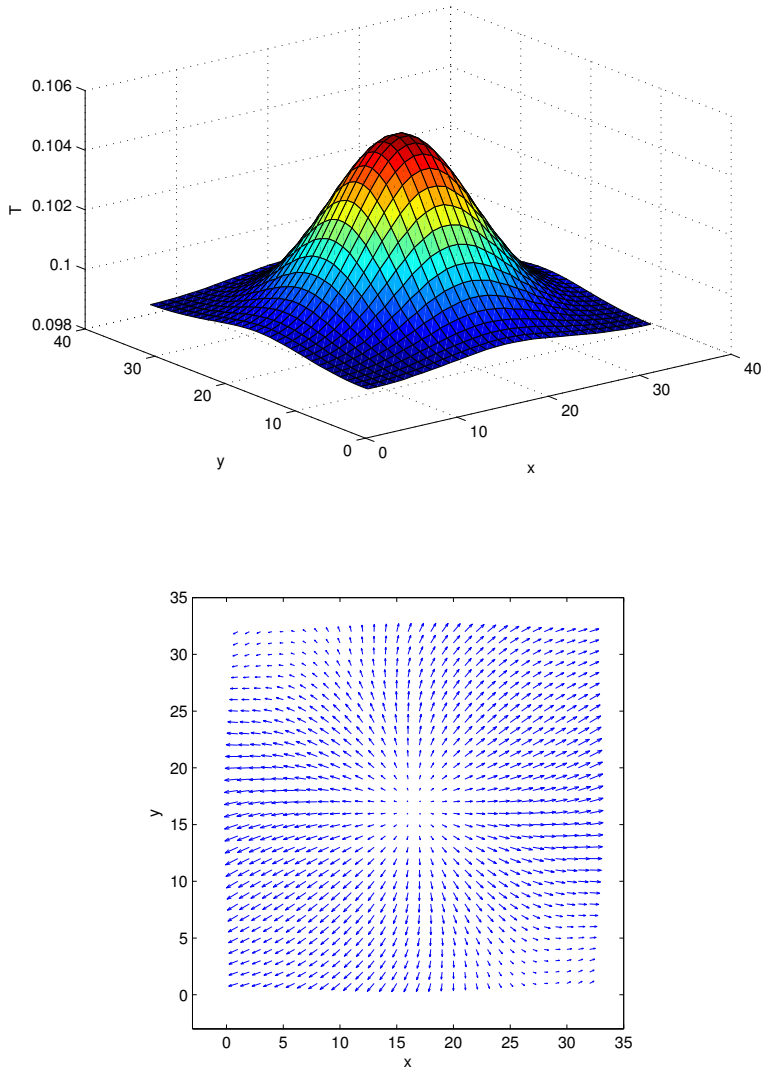

Fig. 23. Thermal expansion: temperature distribution (top) and the velocity field (bottom). The macro mesh consists of 36×36 grid points. Each MD cell contains $36 \times 36 \times 3 \times 4$ atoms, and the MD system is evolved for 10^4 time steps

The relevant time scales

To formulate the procedure of coupling MD with the continuum models near defects, we distinguish two different situations depending on whether there is scale separation between the time scale for the dynamics of the defects and the time scale for the local relaxation of the defect structure. We denote the former by T_d and the latter by T_r.

If T_d is much larger than T_r, we can extend the macroscale model to include the velocity and character of the defect. The macroscale scheme then contains two components: a solver for the conservation laws (a central type finite volume scheme or discontinuous Galerkin method) and defect tracking. The data to be measured from MD include the fluxes, the defect velocity and the local environment variables, of the defect. This procedure naturally decouples the two time scales T_r and T_d.

If T_d is comparable to T_r, then the time history of the defect is important for its future dynamics. There is no decoupling of time scales since there is no time scale separation. In this case reinitializing the defect structure at macro time steps is no longer accurate enough. We will have to track the entire history of the local atomic structures near the defect. This situation often arises when dealing with small-size materials.

Figure 24 illustrates the procedure for both cases.

When $T_r \ll T_d$, we can extract information on the dynamics of the defect from *local* MD simulations, and use it to advance the defects over macro time steps. At the same time the macro solver needs to be modified near the interface to take into account the defect structure. This defect tracking procedure is similar in spirit to the front tracking algorithms in computational fluid dynamics [GMM86], except that the velocity of front is not obtained from macroscopic jump conditions but from molecular dynamics.

The defect tracking procedure has been constructed in [LE05] for co-dimension one defects, such as twin and grain boundaries. Extending this procedure to dealing with high co-dimensional defects such as point defects and dislocations still remains open.

MD boundary conditions

Another difference with the type B problems discussed earlier is that the local MD simulations are no longer homogeneous, e.g. temperature may not be constant in the local MD system. This complicates issues such as boundary conditions.

Since the local MD system is no longer homogeneous, we need to modify the boundary condition that needs to be imposed on the MD system. The issue of boundary condition is still very much the topic of on-going research. We refer to [CKB00, EH01, KWL05] for some representative work on boundary conditions. We expect that whatever future developments may have on this

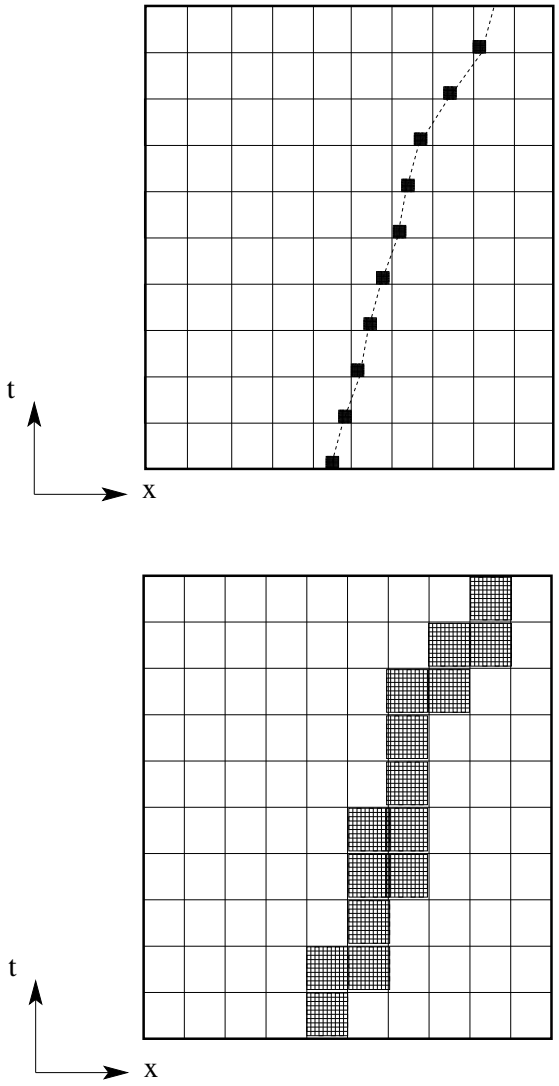

Fig. 24. Schematic of the adaptive modeling refinement. The top figure shows the case where $T_r \ll T_d$. The MD simulations are carried out inside the black boxes. The dashed lines represents the interface. The bottom figure shows the other case where T_r and T_d are comparable. Here one has to keep track the local defect structure for all time by MD simulation

issue, we should be able to incorporate them readily into the overall scheme discussed here.

Here we describe a simple boundary condition using the idea of border regions. The first step is to extend the atomistic system by appending atoms to the border of the MD simulation cell. The border region is divided into bins as indicated in Figure 25. Next we define macroscale variables, namely displacement, velocity and temperature, on the bins by interpolating from their values on the macro grid. We denote these continuum values at the boundary by $(\mathbf{u}_b, \mathbf{v}_b, T_b)$.

To obtain the boundary condition for MD, we separate out the mean from the fluctuating part, i.e. we rewrite the position and velocity of the atoms in the border region as,

$$\mathbf{x}_j = \mathbf{x}_j^{(0)} + \mathbf{x}_j^{(1)}, \quad \mathbf{v}_j = \mathbf{v}_j^{(0)} + \mathbf{v}_j^{(1)}.$$

The *macro* components, $\mathbf{x}_j^{(0)}$ and $\mathbf{v}_j^{(0)}$, are computed from $\mathbf{u}_b$ and $\mathbf{v}_b$, by interpolation if necessary. For the *micro* part, $\mathbf{x}_j^{(1)}$ and $\mathbf{v}_j^{(1)}$, we apply Nosè-Hoover thermostat on each bin using temperature values from T_b, again using interpolation if necessary.

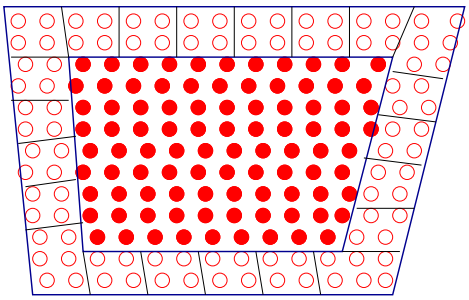

Fig. 25. Boundary conditions imposed on the atomistic system: The border region is divided into bins and Nose-Hoover is applied to each bin

Various validation studies were conducted on this boundary condition, including a study of the Fourier's law for thermal conduction. We refer to [LE05] for details.

Twin boundary dynamics in Ni-Al alloy

To see how these ideas can be applied to a realistic problem, we summarize the results of [LE05] for the example of twin boundary dynamics in a $Ni_{62.5}Al_{37.5}$ alloy. The atomistic model uses the EAM potential developed by Voter and Chen [VC87], which is specifically designed for Ni-Al alloys. At this percentage twin boundaries have been observed both experimentally [CW76] and in

atomistic simulations (with this EAM potential) [BCR93]. In particular the EAM potential has predicted a tetragonal structure with three variants. The corresponding strain matrices can be written as,

$$U_1 = \begin{pmatrix} \eta_1 & 0 & 0 \\ 0 & \eta_2 & 0 \\ 0 & 0 & \eta_2 \end{pmatrix}, \quad U_2 = \begin{pmatrix} \eta_2 & 0 & 0 \\ 0 & \eta_1 & 0 \\ 0 & 0 & \eta_2 \end{pmatrix}, \quad U_3 = \begin{pmatrix} \eta_2 & 0 & 0 \\ 0 & \eta_2 & 0 \\ 0 & 0 & \eta_1 \end{pmatrix}. \tag{85}$$

The cubic structure with lattice constant $a_0 = 2.871$ Åis chosen as the reference configuration. The parameters η_1 and η_2 can be thought of as being the stretch along the principal axis illustrated in Figure 26. The values of these parameters are obtained from MD simulation: $\eta_1 = 1.2263$ and $\eta_2 = 0.9061$.

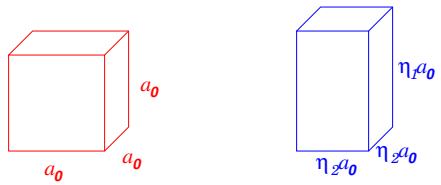

Fig. 26. Cubic and tetragonal phases for Ni-Al alloys

For convenience the material is arranged so that the twin plane coincides with the y-z plane. The deformation corresponding to the undeformed variant I and variant II are:

$$\mathbf{A}_1 = \begin{pmatrix} \frac{\sqrt{2}\eta_1\eta_2}{\sqrt{\eta_1^2+\eta_2^2}} & 0 & 0 \\ \frac{\eta_1^2-\eta_2^2}{\sqrt{2(\eta_1^2+\eta_2^2)}} & \frac{\sqrt{\eta_1^2+\eta_2^2}}{\sqrt{2}} & 0 \\ 0 & 0 & \eta_2 \end{pmatrix}, \quad \mathbf{A}_2 = \begin{pmatrix} \frac{\sqrt{2}\eta_1\eta_2}{\sqrt{\eta_1^2+\eta_2^2}} & 0 & 0 \\ \frac{\eta_2^2-\eta_1^2}{\sqrt{2(\eta_1^2+\eta_2^2)}} & \frac{\sqrt{\eta_1^2+\eta_2^2}}{\sqrt{2}} & 0 \\ 0 & 0 & \eta_2 \end{pmatrix}. \tag{86}$$

The dynamics of the twin boundary is driven by a shear that is applied at the left boundary. Away from the twin boundary, local MD simulations are performed to estimate the stress as was done for type B problems. Each such simulation involves $20 \times 20 \times 5$ atomic units and 2000 steps of time integration. Near the twin boundary the defect tracking technique is applied to estimate the moving speed of the twin boundary and the local strain and stress. Each such MD calculation is carried over a system with $120 \times 20 \times 8$ atomic units for 1200 time steps. In all the MD simulations the time step is taken to be $\delta t = 0.003$ ps. Since the twin boundary simply moves in the x direction, and the continuum quantities do not have appreciable change in the y direction, the continuum equations can be simplified to

$$\begin{cases} \partial_t A_{11} - \partial_x v_1 = 0, \\ \partial_t A_{21} - \partial_x v_2 = 0, \\ \partial_t v_1 + \partial_x \sigma_{11} = 0, \\ \partial_t v_2 + \partial_x \sigma_{21} = 0. \end{cases} \tag{87}$$

For simplicity the energy equation is neglected in this problem, and is replaced by constraining the system at constant temperature. Other components of **A** are assumed not to change in time.

Figure 29 shows the numerical results at the macroscale level after some macro time steps. As the twin boundary propagates, two elastic waves are generated and move away from the twin boundary.

To better understand the mechanism of twin boundary propagation, we plot in Figure 27 some results from the local MD simulation at the twin boundary. We first select an arbitrary plane of atoms and examine their positions at the initial and final times of the MD. Different variants of the twin are easily identified as rectangular lattices with different orientation. We see that at the end of the MD, the twin boundary has clearly moved forward (in a layer by layer fashion).

Next we examine what happens on the twin plane as it propagates forward. For that purpose we plot the atomic positions of the atoms on the twin plane. Figure 28 clearly suggests that the twin plane moves by a nucleation and propagation mechanism, very much similar to the mechanism of epitaxial growth of crystals. New variants are first nucleated and form islands on the twin plane. The edges of the islands then propagate out and induce the transformation on the whole plane.

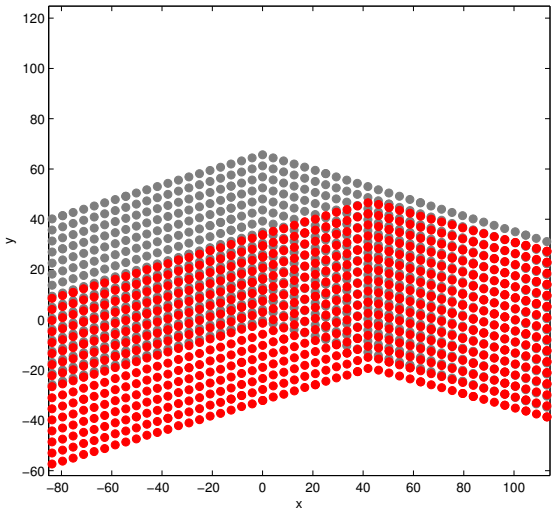

Fig. 27. Propagation of twin boundary under stress: shear stress is applied at the left boundary of the sample. The initial positions of the atoms are plotted in light color. The positions after 1.2 ps are plotted in dark color

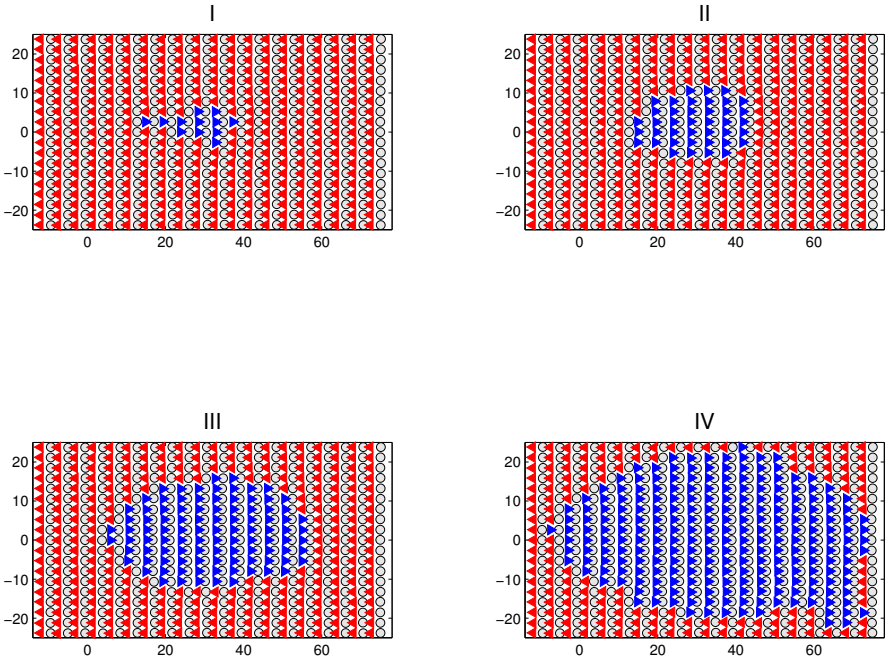

Fig. 28. Nucleation and propagation of new variant: '◁': atoms in the twin plane that are still in the original variant. '▷': atoms that have transformed to the new variant. Circle atoms belong to the layer next to the twin plane which are still in the original variant. They are used as reference atoms. Transformed atoms are closer to circle atoms at the right, whereas untransformed atoms are close to circle atoms at the left

6 Interface problems

In this section we discuss how the HMM philosophy can be applied to the study of interface motion in a multi-scale setting. This discussion follows that of [CE04]. Our main interest is to capture the macroscale dynamics of the interface in cases where the velocity is not explicitly specified. Instead, it has to be extracted from some underlying microscale model. Examples of such microscale models include: 1. Microscale interface dynamics with interfacial velocity of the form

$$V_n(x) = c^\epsilon(x, \gamma) \tag{88}$$

where γ denotes the microscale interface, $\epsilon \ll 1$ is the ratio between the microscale and macroscale. $c^\varepsilon(x, \gamma)$ is a multiscale interfacial velocity function, a simplest example being

$$c^\varepsilon(x) = c\left(x, \frac{x}{\epsilon}, \gamma\right). \tag{89}$$

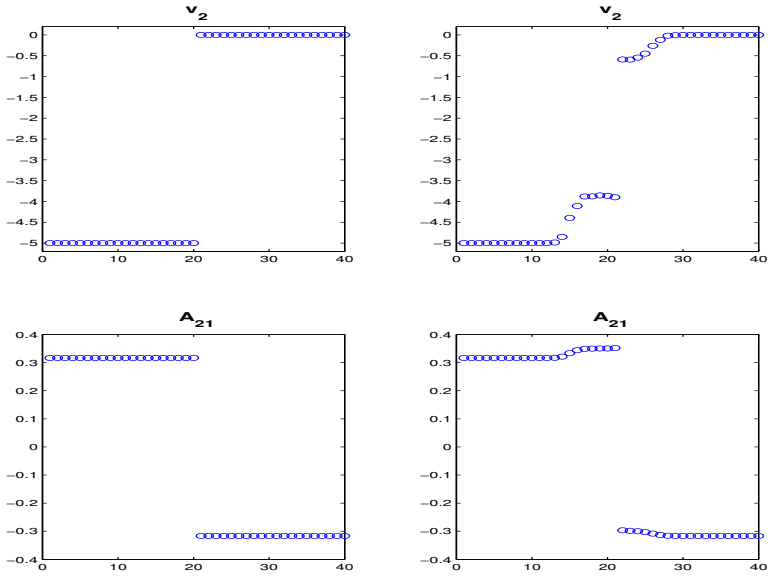

Fig. 29. Left: the initial data for $A_{2,1}$ and v_2 (100 m/s); **Right:** the numerical results in 15 macro time steps

Such models arise in the study of interface propagation in strongly heterogeneous media such as composite materials, polycrystals, material with impurities, and porous media, to name a few.

(89) is a homogenization problem. In the case when the microstructure is periodic, homogenized equations have been derived in [LPV].

2. Front propagation in phase-field models. Consider, for example, the Allen-Cahn equation

$$u_t = \epsilon \Delta u + \frac{1}{\epsilon} u(1 - u^2). \tag{90}$$

It is well-known that for small ϵ, (90) describes the propagation of a front whose inward normal velocity is the mean curvature of the front. In this case, an equation for mean curvature flow can be solved in place of (90) to capture the large scale dynamics of the front. However, if the phase field model takes a more complex form or if non-trivial chemical reactions occur at the front, deriving analytically the effective dynamic laws for the front becomes a difficult task. Therefore it is of interest to develop numerical methods that capture the large scale dynamics of the interface, but is based only on the microscale model of the type (90). Such ideas have been explored in the work of R. Klein et. al [SK03].

3. Discrete microscale models such as kinetic Monte Carlo or molecular dynamics. Examples include the dynamics of step edges on the surface of an epitaxially grown crystal, grain boundaries in solids, and many more.

6.1 Macroscale solver: The level set method

As the macroscale solver we may use any of the conventional methods for interface dynamics such as the level set method [OS88], front tracking [GMM86], or the segment projection method [TE00]. Here we will follow [CE04] and focus on the level set method.

In the framework of the level set method, an interface is described as the zero level set of a globally defined function, ϕ, called a level set function. All operations, in particular evolution, are then performed on this function in place of the interface of interest. The level set function ϕ satisfies the PDE:

$$\phi_t + V \cdot \nabla\phi = 0$$

where V is a globally defined velocity field. On the interface, this is equivalent to

$$\phi_t \pm V_n|\nabla\phi| = 0 \tag{91}$$

which involves the normal velocity only. In many problems, though, the velocity is only naturally specified at the interface. Many techniques are available to extend the velocity to the whole ambient space [AS95, AS99, HPC96, Set96, Tsi95, TCO03].

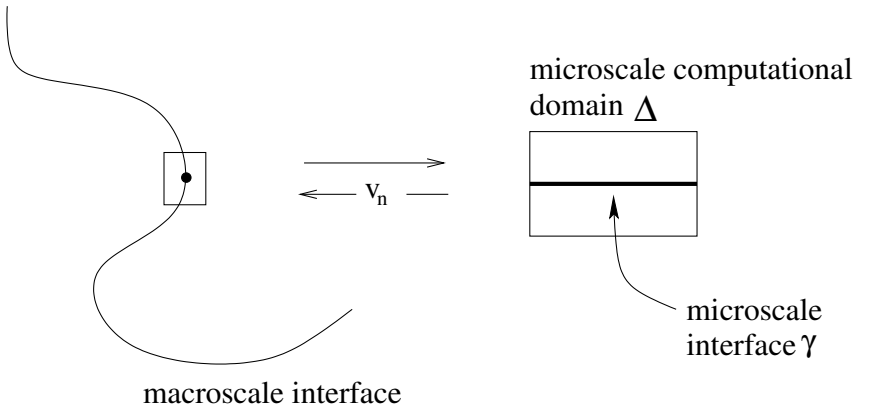

Fig. 30. A pictorial description of the HMM setup showing the link between the macroscopic and microscopic levels

6.2 Estimating the macroscale interface velocity

The data that need to be estimated from the microscale models are the normal velocities of the macroscale interface at each macroscale grid point. The first step is to locally reconstruct the interface. If the normal velocity of the

macroscale interface is known to only depend on the orientation of the local tangent plane of the interface, then we may approximate the interface locally by a hyperplane. On the other hand, if the normal velocity is also known to depend on the local curvature, a quadratic approximation is needed.

As illustration, we first consider the homogenization problem. The level set representation of the microscale model in this case takes the form

$$\phi_t + c\left(x, \frac{x}{\epsilon}\right)|\nabla\phi| = 0, \tag{92}$$

which describes motion in the normal direction at speed c. In this case, we can use the hyperplane reconstruction. [CE04] suggests working on a transformed coordinate through a change of variables so that this hyperplane coincides with the $\{x_n = 0\}$-plane. The original microscale model (92) is then solved in a domain Δ in the transformed space, rectangular with sides orthogonal to the coordinate axes, that should be larger than the size of the periodic cell or the correlation length of c (see Figure 30). Periodic boundary conditions are imposed in the $x_1, x_2, \ldots, x_{n-1}$-directions and a periodic jump condition can be imposed in the x_n-direction.

To extract the quantity of interest, at each microscale time step, the microscale Hamiltonian is averaged in the central region $\tilde{\Delta}$ of the domain to reduce spurious effects that may arise from the boundary and the chosen boundary conditions. Denote this value by $h^\epsilon(t)$

$$h^\varepsilon(t) = \frac{1}{|\tilde{\Delta}|}\int_{\tilde{\Delta}} c^\varepsilon(x)|\nabla\phi(x,t)|dx \tag{93}$$

the velocity of the front at the particular location is obtained from

$$V_n = \frac{1}{|\nabla\phi|}\int_0^{t^*} h^\epsilon(t)K\left(\frac{t}{t^*}\right)\, dt. \tag{94}$$

Here K is an averaging kernel, as discussed earlier. Having obtained V_n at all the macroscale grid points at the interface, the interface can be evolved using standard procedures in the level set method.

[CE04] also considered the case where the microscale model is described by a phase-field equation:

$$u_t = \nabla\cdot\left(b\left(x, \frac{x}{\epsilon}\right)u\right) + \epsilon\nabla\cdot\left(a\left(x, \frac{x}{\epsilon}\right)\nabla u\right) - \frac{1}{\epsilon}\frac{\partial V}{\partial u}(u), \tag{95}$$

where $a(x,y) > 0$ and $b(x,y)$ are smooth functions that are either periodic in y or stationary random in y with rapidly decaying correlation at large distances and V is a double well potential with minima at $u = \alpha, \beta$. For the details concerning this example, as well as the numerical results, we refer to [CE04].

7 Stochastic ODEs with multiple time scales

Consider the following generic example for $(x, y) \in \mathbb{R}^n \times \mathbb{R}^m$:

$$\begin{cases} \dot{X}_t^\epsilon = f(X_t^\epsilon, Y_t^\epsilon, \epsilon), & X_0^\epsilon = x, \\ \dot{Y}_t^\epsilon = \dfrac{1}{\epsilon} g(X_t^\epsilon, Y_t^\epsilon, \epsilon), & Y_0^\epsilon = y. \end{cases} \tag{96}$$

Here $f(\cdot) \in \mathbb{R}^n$ and $g(\cdot) \in \mathbb{R}^m$ are (possibly random) functions that are $O(1)$ in ϵ, and ϵ is a small parameter representing the ratio of the time-scales in the system. We have assumed that the phase space can be decomposed into slow degrees of freedom x and fast ones y. Depending on the problem, we may be interested in the $O(1)$ (advective) or $O(\epsilon^{-1})$ (diffusive) time-scales.

There has been numerous analytical work on systems of the type (96) [FW98, Kur73, MTV01, Pap77]. On the advective time-scale, if the dynamics for Y_t^ϵ with $X_t^\epsilon = x$ fixed has an invariant probability measure $\mu_x^\epsilon(dy)$ and the following limit exists:

$$\bar{f}(x) = \lim_{\epsilon \to 0} \int_{\mathbb{R}^m} f(x, y, \epsilon) \mu_x^\epsilon(dy), \tag{97}$$

then in the limit as $\epsilon \to 0$, X_t^ϵ converges to the solution of

$$\dot{\bar{X}}_t = \bar{f}(\bar{X}_t), \qquad \bar{X}_0 = x. \tag{98}$$

Leading order optimal prediction of Chorin et al. applied to this problem gives the same result [CKK98, CHK02]. On the diffusive time-scale, fluctuations become important. With the rescaled time $s = \epsilon t$, (96) becomes:

$$\begin{cases} \dot{X}_s^\epsilon = \dfrac{1}{\epsilon} f(X_s^\epsilon, Y_s^\epsilon, \epsilon), & X_0^\epsilon = x, \\ \dot{Y}_s^\epsilon = \dfrac{1}{\epsilon^2} g(X_s^\epsilon, Y_s^\epsilon, \epsilon), & Y_0^\epsilon = y. \end{cases} \tag{99}$$

Under appropriate assumptions on f and g, the effective dynamics for X_s^ϵ in the limit of $\epsilon \to 0$ is a stochastic differential equation,

$$\dot{\bar{X}}_s = \bar{b}(\bar{X}_s) + \bar{\sigma}(\bar{X}_s) \dot{W}_s, \qquad \bar{X}_0 = x, \tag{100}$$

where W_s is a Wiener process and the coefficients $\bar{b}$ and $\bar{\sigma}$ are expressed in terms of limits of expectations similar to (97). Details can be found in [EL04b].

We will only discuss the dynamics over the advective time scale, and refer to [EL04b] for discussions on the diffusive time scale.

In order to facilitate the discussion that we will present later on error analysis, we consider a more special form of stochastic ODEs:

$$\begin{cases} \dot{X}_t^\epsilon = a(X_t^\epsilon, Y_t^\epsilon, \varepsilon), & X_0^\epsilon = x, \\ \dot{Y}_t^\epsilon = \dfrac{1}{\epsilon} b(X_t^\epsilon, Y_t^\epsilon, \varepsilon) + \dfrac{1}{\sqrt{\epsilon}} \sigma(X_t^\epsilon, Y_t^\epsilon, \varepsilon) \dot{W}_t, & Y_0^\epsilon = y, \end{cases} \tag{101}$$

where $a \in \mathbb{R}^n$, $b \in \mathbb{R}^m$, $\sigma \in \mathbb{R}^m \times \mathbb{R}^d$ are deterministic functions and W_t is a d-dimensional standard Wiener process.

Based on the assumption that for small ε, the dynamics of X_t^ε is approximated by that of

$$\dot{\bar{X}}_t = \bar{a}(\bar{X}_t), \qquad \bar{X}_0 = x, \tag{102}$$

an HMM type of strategy was independently proposed in [Van03]. The basic idea is to solve (102) with a macro-solver in which $\bar{a}$ is estimated by solving the micro-scale problem (101).

As the macroscale solver we may use any stable explicit ODE solver such as the forward Euler, Runge-Kutta, or a linear multi-step method. In the simplest case when forward Euler is selected as the macro-solver, we have

$$X_{n+1} = X_n + \tilde{a}_n \Delta t, \tag{103}$$

where Δt is the macro time step size.

The data that need to be estimated is $\tilde{a}_n$ which is an approximation of $\bar{a}(X_n)$. We estimate this data in two steps:

1. We solve (101) using a micro-solver for stochastic ODEs and denote the solution by $\{Y_{n,m}\}$ where m labels the micro-time-steps. Multiple independent replicas can be used, in which case we denote the solutions by $\{Y_{n,m,j}\}$ where j is the replica number.
2. We then define an approximation of $\bar{a}(X_n)$ by the following time and ensemble average:

$$\tilde{a}_n = \frac{1}{MN} \sum_{j=1}^{M} \sum_{m=n_T}^{n_T+N-1} a(X_n, Y_{n,m,j}, \varepsilon),$$

where M is the number of replicas, N is the number of steps in the time averaging, and n_T is the number of time steps we skip to eliminate transients.

For the micro-solver, for each realization we may use the following first order scheme

$$\begin{aligned} Y^i_{n,m+1} = Y^i_{n,m} &+ \frac{1}{\sqrt{\varepsilon}} \sum_j \sigma^{ij}(X_n, Y_{n,m}, \varepsilon) \xi^j_{m+1} \sqrt{\delta t} \\ &+ \frac{1}{\varepsilon} b^i(X_n, Y_{n,m}, \varepsilon)\delta t + \frac{1}{\varepsilon} \sum_{jk} A^{ijk}(X_n, Y_{n,m}, \varepsilon) s^{kj}_{m+1} \delta t, \end{aligned} \tag{104}$$

where δt is the micro-time-step size (note that it only appears in term of the ratio $\delta t/\varepsilon =: \Delta\tau$), and

$$A^{ijk} = \sum_l (\partial^l \sigma^{ij}) \sigma^{lk} \tag{105}$$

Here the derivatives are taken with respect to y. The random variables $\{\xi^j_m\}$ are i.i.d Gaussian with mean zero and variance one, and

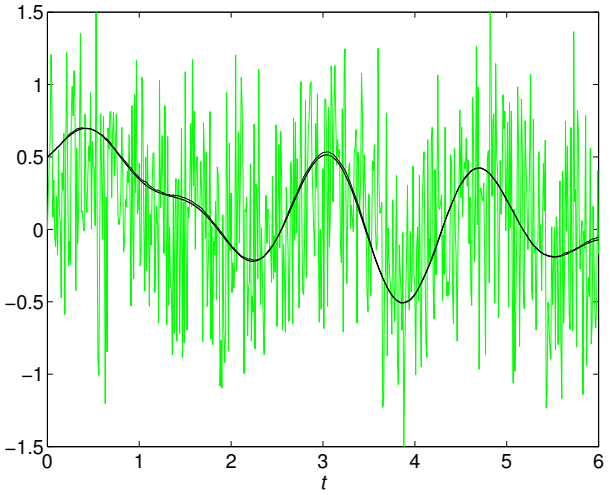

Fig. 31. The comparison between $\bar{X}_n$ and X_n produced by the multiscale scheme with $p = 4$ (black curves). Also shown is the fast process Y_{n,n_T+N} used in the micro-solver (grey curve).

$$s_m^{kj} = \begin{cases} \frac{1}{2}\xi_m^k \xi_m^j + z_m^{kj}, & k < j, \\ \frac{1}{2}\xi_m^k \xi_m^j - z_m^{jk}, & k > j, \\ \frac{1}{2}\left((\xi_m^j)^2 - 1\right), & k = j, \end{cases}$$

where $\{z_m^{kj}\}$ are i.i.d with $\mathbb{P}\{z_m^{kj} = \frac{1}{2}\} = \mathbb{P}\{z_m^{kj} = -\frac{1}{2}\} = \frac{1}{2}$. High order schemes are discussed in [EL04b]. For the initial condition, we take $Y_{0,0} = 0$ and

$$Y_{n,0} = Y_{n-1,n_T+N-1}, \tag{106}$$

i.e. the initial values for the micro variables at macro-time-step n are chosen to be their final values from macro-time-step $n-1$. This choice of initial condition is not necessary for the convergence of the scheme, e.g.

$$Y_{n,0} = 0 \tag{107}$$

would work as well, but it improves the convergence properties, as we will discuss in section 9.2.

As an illustration, consider the following example with $(X, Y) \in \mathbb{R}^2$:

$$\begin{cases} \dot{X}_t = -Y_t - Y_t^3 + \cos(\pi t) + \sin(\sqrt{2}\pi t), & X_0 = x, \\ \dot{Y}_t = -\dfrac{1}{\epsilon}(Y_t + Y_t^3 - X_t) + \dfrac{1}{\sqrt{\epsilon}}\dot{W}_t, & Y_0 = y. \end{cases} \tag{108}$$

From (102) the effective equation for $\bar{X}_t$ is

$$\dot{\bar{X}}_t = -\bar{X}_t + \cos(\pi t) + \sin(\sqrt{2}\pi t), \qquad \bar{X}_0 = x. \tag{109}$$

The following numerical parameters are used:

$$(T_0, \Delta t, \delta t/\varepsilon, n_T, M, N) = (6,\ 0.01,\ 0.01 \times 2^{-p},\ 100,\ 1,\ 10 \times 2^{3p}) \tag{110}$$

The results for $p = 2$ is shown in Fig. 31, and compared with solution of the effective equation $\bar{X}_t$.

8 Exploring statistical self-similarity: An example without scale separation

8.1 General strategy for data estimation

In the problems discussed above, scale separation was very important for the efficiency of HMM: It allows us to choose small microscale simulation box and still retain sufficient accuracy for the estimated data. It is important to realize that this is not the only situation for which HMM works efficiently. There is a more general philosophy behind it which works as follows. Suppose that the size of the macroscale mesh is H. We need to estimate some effective data such as transport coefficients at that scale, which is a function of H. Let us denote by $f = f(L)$ the value of that data at the scale L. If there is scale separation in the system, then $f(L)$ is essentially independent of L

$$f(L) \approx \text{Const} \tag{111}$$

as long as L is much larger than some characteristic scale of the microscopic model, which might just be the correlation length. This allows us to take advantage of the scale separation by choosing the size of the microscale simulation box, δ, to be much larger than the microscopic scale, but still much smaller than H. However, so long as the scale dependence of $f = f(L)$ is of a simple form with a few parameters, we can make use of this simple relationship by performing a few (not just one as was done for problems with scale separation) small scale simulations and use the results to predict the needed quantities at a much larger scale. One example of such a situation is when the system exhibits local self-similarity. In this case the dependence in (111) is of the form $f(L) = C_0 L^\beta$ with only two parameters. Therefore we can use results of microscopic simulations at two different scales to predict the result at a much larger scale, namely H.

This is a poor-man's version of renormalization group method. Other numerical methods that use renormalization ideas are found in [Cho98, Cho03].

8.2 Transport on a percolation network at criticality

This idea was demonstrated in [EY04] on the example of effective transport on a two-dimensional bond percolation network at the percolation threshold.

In the standard two dimensional bond percolation model with parameter $p, 0 \leq p \leq 1$, we start with a square lattice, each bond of the lattice is either kept with probability p or deleted with probability $1-p$. Of particular interest is the size of the percolation clusters formed by the remaining bonds in the network (see Figure 32 for a sample of bond percolation). The critical value

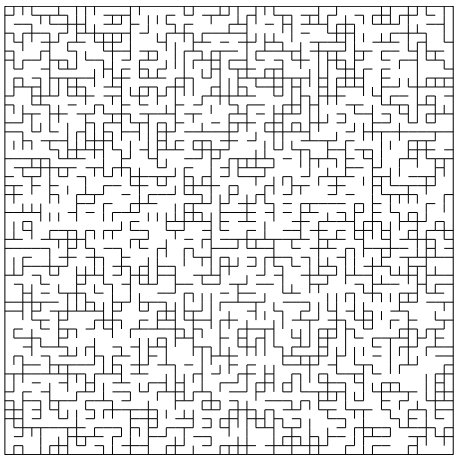

Fig. 32. Bond percolation network on a square lattice at $p = 0.5$

for this model is at $p = p^* = 0.5$. For an infinite lattice, if $p < p^*$, the probability of having infinite size clusters is zero. For $p > p^*$, the probability of having infinite size clusters is 1. Given the parameter value p, the network has a characteristic length scale – the correlation length, denoted by ξ_p. As $p \to p^*, \xi_p$ diverges as

$$\xi_p \sim |p - p^*|^\alpha, \tag{112}$$

where $\alpha = -4/3$ (see [Sah95]). At $p = p^*$, $\xi_p = \infty$. In this case, the system has a continuum distribution of scales, i.e. it has clusters of all sizes. In the following we will consider the case when $p = p^*$.

We are interested in the macroscopic transport on such a network. To study transport, say of some pollutants whose concentration density will be denoted by c, we embed this percolation model into a domain $\Omega \in R^2$. We denote by ε the bond length of the percolation model, and L the length scale for the domain Ω. We will consider the case when ε/L is very small.

The basic microscopic model is that of mass conservation. Denote by $S_{i,j}, i, j = 1, \cdots, N$ the (i, j)-th site of the percolation network, and $c_{i,j}$ the concentration at that site. Define the fluxes

$$\begin{aligned}
\text{the flux from right} \quad & f^r_{i,j} = B^x_{i,j}(c_{i+1,j} - c_{i,j}),\\
\text{the flux from left} \quad & f^l_{i,j} = B^x_{i-1,j}(c_{i-1,j} - c_{i,j}),\\
\text{the flux from top} \quad & f^t_{i,j} = B^y_{i,j}(c_{i,j+1} - c_{i,j}),\\
\text{the flux from bottom} \quad & f^b_{i,j} = B^y_{i,j-1}(c_{i,j-1} - c_{i,j}).
\end{aligned}$$

Here the various B's are bond conductivities for the specified bonds. The bond conductivity is zero if the corresponding bond is deleted, and 1 if the bond is retained. At each site $S_{i,j}$, from mass conservation, we have

$$f^t_{i,j} + f^b_{i,j} + f^r_{i,j} + f^l_{i,j} = 0, \tag{113}$$

i.e. the total flux to this site is zero. This will be our microscale model.

For the macroscale solver, we will choose a finite volume scheme over a macroscale grid Ω_H where H is the size of the finite volume cell (see Fig 4). The data that we need to estimate from the microscale model, here the percolation model, are the fluxes at the mid-points of cell boundaries. Since the present problem is linear, we only need to estimate the effective conductivity for a network of size H. We note that at $p = p^*$, the effective conductivity is strongly size-dependent. In fact there are strong evidences that the following relation holds [Hug96]:

$$\kappa_L = C_0 L^\beta \tag{114}$$

where κ_L is the mean effective conductivity at size L. This is confirmed in Figure 33 where we show a log-log plot of the effective conductivity as a function of scale.

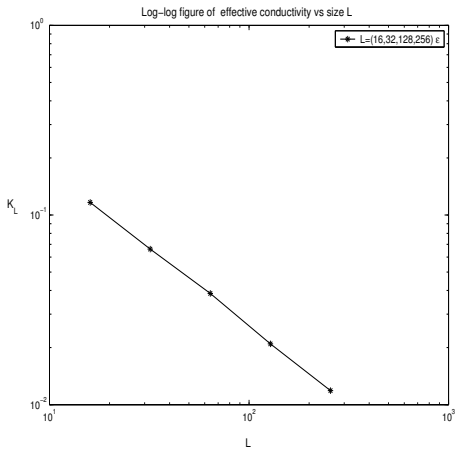

Fig. 33. Effective conductivity at different scale $L = (16, 32, 64, 128, 256)\varepsilon$ for a realization of the percolation network with $p = p^* = 0.5$

Our basic strategy is to make use of such relations in estimating the effective fluxes in the case when $\varepsilon \ll H$. For this purpose, we perform a series of mi-

croscopic simulations on systems of size L_1 and L_2 where $\varepsilon \ll L_1 < L_2 \ll H$. From the results we estimate κ_{L_1} and κ_{L_2}. We then use these results to estimate the parameter values C_0, β in (114). Once we have these parameters, we can use (114) to predict κ_H.

One interesting question is the effect of statistical fluctuations. To see this we plot in Figure 34 the actual and predicted (using self-similarity) values of the conductivity on a sub-lattice of size $L = 128$ for a number of realizations of the percolation network. The predicted values are computed using simulated values from sub-lattices with $L = 16$ and $L = 32$. The predicted values have obviously larger fluctuations than the actual values, implying that the fluctuations are amplified in the process of predicting the mean values. Nevertheless the mean values are predicted with reasonable accuracy, considering the relatively small size of the network.

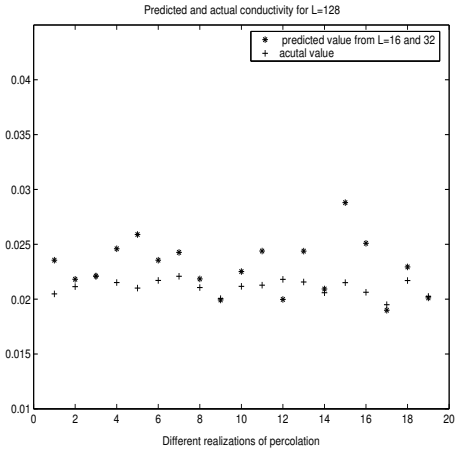

Fig. 34. Effect of fluctuations: Actual and predicted effective conductivity at scale $L = 128\varepsilon$ for different realizations of the percolation network with $p = 0.5$. The predicted values are computed from $L = 16\varepsilon$ and 32ε lattices

More numerical results, including some results of the multiscale method, can be found in [EY04].

9 Error analysis

Error analysis for multiscale methods presents a new challenge to numerical analysis, particularly for problems involving multi-physics. Since multiscale methods are relatively new, and their errors typically involve several different contributions, rigorous results on error control are very much desired for understanding basic issues such as stability and accuracy of multiscale methods.

Indeed, to be able to develop a general strategy for error analysis was one of the motivations for developing the HMM framework.

To begin with, what should we take as the exact or reference solution, to be compared with the numerical solution of a multiscale method? In general, we should not take the detailed solution of the microscopic problem as the reference solution, since approximating that would usually require solving the full microscopic problem, and therefore defeat the whole purpose. For type B problems, we can take the reference solution as the solution to the underlying macroscopic model that we assume exist. Even though the macroscopic model is not used for numerical purposes, it can certainly be used for conceptual and analytical purposes. If we denote by u the solution to the microscopic model, U_0 the solution to the effective macroscale model, and Q the compression operator that maps the microscopic state to the macroscopic state, then by definition, $U_0 - Qu$ should be small. Therefore we can also take Qu as the reference solution. This is preferred since it comes more directly out of the microscopic solution.

These issues have not been discussed much for other types of problems.

Since error analysis is much better understood for type B problems, we will focus our attention to this type of problems. The overall strategy is as follows. We first prove a general statement that if some underlying macroscopic scheme is stable, then the error in the HMM solution is bounded by a standard error term for the macroscopic solver, plus a new term, sometimes denoted by $e(\text{HMM})$ due to the error in estimating the data. We then estimate this new term. The first step is usually quite general. However, specific estimates in the second step are only obtained for specific models.

9.1 Error analysis of the HMM-FEM

Our first example is the HMM finite element method discussed earlier. We will always assume that $a^\varepsilon(\mathbf{x})$ is smooth, symmetric and uniformly elliptic:

$$\lambda I \le a^\varepsilon \le \Lambda I \tag{115}$$

for some $\lambda, \Lambda > 0$ which are independent of ε. We will assume that the quadrature formula used in (39) is exact for polynomials of degree $2k-2$ for $k > 1$ and k for $k = 1$.

As the first step, we will compare the HMM solution to the solutions of a macroscale model of the form:

$$\begin{cases} -\operatorname{div}\big(\mathcal{A}(\mathbf{x})\nabla U_0(\mathbf{x})\big) = f(\mathbf{x}) & \mathbf{x} \in D, \\ U_0(\mathbf{x}) = 0 & \mathbf{x} \in \partial D. \end{cases} \tag{116}$$

We will use standard notions for Sobolev spaces: $\|\cdot\|_1$ and $\|\cdot\|_0$ denote H^1 and L^2 norms respectively, and $\|\cdot\|_{1,\infty}$ denotes the $W^{1,\infty}$ norm. The following results are proved in [EMZ04].

Theorem 1. *Denote by U_0 and $U_{\rm HMM}$ the solution of* (116) *and the* HMM *solution, respectively. Let*

$$e(\mathrm{HMM}) = \max_{\substack{\mathbf{x}_\ell \in K \\ K \in \mathcal{T}_H}} \|\mathcal{A}(\mathbf{x}_\ell) - \mathcal{A}_H(\mathbf{x}_\ell)\|,$$

where $\|\cdot\|$ is the Euclidean norm. If U_0 is sufficiently smooth, then there exists a constant C independent of ε, δ and H, such that

$$\|U_0 - U_{\rm HMM}\|_1 \le C\big(H^k + e(\mathrm{HMM})\big), \tag{117}$$

$$\|U_0 - U_{\rm HMM}\|_0 \le C\big(H^{k+1} + e(\mathrm{HMM})\big). \tag{118}$$

If there exits a constant C_0 such that $e(\mathrm{HMM})|\ln H| < C_0$, then there exists a constant H_0 such that for all $H \le H_0$,

$$\|U_0 - U_{\rm HMM}\|_{1,\infty} \le C\big(H^k + e(\mathrm{HMM})\big)|\ln H|. \tag{119}$$

So far no assumption on the form of $a^\varepsilon(\mathbf{x})$ or $\mathcal{A}(\mathbf{x})$ is necessary. U_0 can be the solution of an arbitrary macroscopic equation with the same right-hand side as in (20). Of course for $U_{\rm HMM}$ to converge to U_0, i.e., $e(\mathrm{HMM}) \to 0$, U_0 must be chosen as the solution of the homogenized equation, which we now assume exists. To obtain quantitative estimates on $e(\mathrm{HMM})$, we must restrict ourselves to more specific situations.

The simplest example of such a specific problem is when

$$a^\varepsilon(\mathbf{x}) = a\Big(\mathbf{x}, \frac{\mathbf{x}}{\varepsilon}\Big), \tag{120}$$

where $a(\mathbf{x}, \mathbf{y})$ can either be periodic in $\mathbf{y}$, in which case we assume the period to be $I = [-1/2, 1/2]^d$, or random but stationary under shifts in $\mathbf{y}$, for each fixed $\mathbf{x} \in D$. In both cases, it has been shown that [BLP78, PV81]

$$\|u^\varepsilon(\mathbf{x}) - U_0(\mathbf{x})\|_0 \to 0, \tag{121}$$

where $U_0(\mathbf{x})$ is the solution of the homogenized equation. We will take (116) to the homogenized equation with coefficients computed from solving the relevant cell problems [BLP78, PV81].

For the following results we assume that the periodic boundary condition is used for the microscale problems in HMM.

Theorem 2. *For the periodic homogenization problem, we have*

$$e(\mathrm{HMM}) \le \begin{cases} C\varepsilon & \text{if } I_\delta(\mathbf{x}_\ell) = \mathbf{x}_\ell + \varepsilon I, \\ C\Big(\dfrac{\varepsilon}{\delta} + \delta\Big) & \text{otherwise.} \end{cases}$$

The difference between the two results lies in the choice of $I_\delta(\mathbf{x}_\ell)$. For the second result we do not need to assume that the period of $a(\mathbf{x}, \cdot)$ is a cube: In

fact it can be of arbitrary shape as long as its translation tiles up the whole space.

Another important case for which specific estimates on $e(\mathrm{HMM})$ have been obtained is the random homogenization problem. However the results for this case are less satisfactory. The following result was proved in [EMZ04] following the work of [Yur86]. Here we assume for simplicity that the coefficient $a(\mathbf{x}, \mathbf{y}, \omega)$ is independent of $\mathbf{x}$.

Theorem 3. *For the random homogenization problem, assuming that a mixing condition holds. We have*

$$\mathbb{E}\, e(\mathrm{HMM}) \leq \begin{cases} C(\kappa)\Big(\dfrac{\varepsilon}{\delta}\Big)^{\kappa}, & d = 3 \\ \textit{remains open}, & d = 2 \\ C\Big(\dfrac{\varepsilon}{\delta}\Big)^{1/2}, & d = 1 \end{cases}$$

where

$$\kappa = \frac{6 - 12\gamma}{25 - 8\gamma}$$

for any $0 < \gamma < 1/2$. *By choosing* γ *small,* κ *can be arbitrarily close to* $6/25$. $\mathbb{E}$ *denotes expectation with respect to the probability space for the random coefficients.*

The proper probablistic set-up is discussed in [PV81]. The mixing condition is stated in [EMZ04]. Roughly speaking it says that the correlation of the random coefficients $a_{i,j}(\mathbf{y}, \omega)$ decays exponentially fast at large distances.

U_{HMM} by itself does not give any information on the gradients of u^ε which is important for many applications since it is related to physically important quantities such as stress in the elastic problem and velocity in the porous medium problem. This information can be recovered using a simple post-processing technique. For the general case, having U_{HMM}, one can obtain locally the microstructural information using an idea in [OV00]. Assume that we are interested in recovering u^ε and ∇u^ε only in the subdomain $\Omega \subset D$. Consider the following auxiliary problem:

$$\begin{cases} -\operatorname{div}\big(a^{\,\varepsilon}(\mathbf{x})\nabla \tilde{u}^{\,\varepsilon}(\mathbf{x})\big) = f(\mathbf{x}) & \mathbf{x} \in \Omega_\eta, \\ \tilde{u}^{\,\varepsilon}(\mathbf{x}) = U_{\mathrm{HMM}}(\mathbf{x}) & \mathbf{x} \in \partial\Omega_\eta, \end{cases} \tag{122}$$

where Ω_η satisfies $\Omega \subset \Omega_\eta \subset D$ and $\operatorname{dist}(\partial\Omega, \partial\Omega_\eta) = \eta$. We then have: There exists a constant C such that

$$\Big(\fint_\Omega |\nabla(u^\varepsilon - \tilde{u}^{\,\varepsilon})|^2 \mathbf{x}\Big)^{1/2} \leq \frac{C}{\eta} \|u^\varepsilon - U_{\mathrm{HMM}}\|_{L^\infty(\Omega_\eta)} \tag{123}$$

There is a much simpler procedure for the periodic homogenization problem [EE02]. Consider the case when $k = 1$ and choose $I_\delta = \mathbf{x}_K + \varepsilon I$, where $\mathbf{x}_K$ is the barycenter of K. We also assume that the quadrature point in the element K is at $\mathbf{x}_K$. Define $\tilde{u}^{\,\varepsilon}$ by:

1. $\tilde{u}^{\varepsilon}|_{I_\delta} = v_K^{\varepsilon}$, where v_K^{ε} is the solution of (46) with the boundary condition that $v_K^{\varepsilon} - U_{\mathrm{HMM}}$ is periodic with period εI and $\int_{I_\delta}(\tilde{u}^{\varepsilon} - U_{\mathrm{HMM}})(\mathbf{x})\mathbf{x} = 0$.
2. $\big(\tilde{u}^{\varepsilon} - U_{\mathrm{HMM}}\big)|_K$ is periodic with period εI.

We then have [EMZ04]

Theorem 4. *Let $\tilde{u}^{\varepsilon}$ be defined as above. Then*

$$\Big(\sum_{K\in\mathcal{T}_H} \|\nabla(u^{\varepsilon} - \tilde{u}^{\varepsilon})\|_{0,K}^2\Big)^{1/2} \le C\big(\sqrt{\varepsilon} + H\big). \tag{124}$$

Similar results are also proved for nonlinear elliptic problems. For details, see [EMZ04].

[YE05] presents systematic numerical studies on the effect of the boundary conditions for the microscale problems as well as the microscale cell size.

9.2 Dynamic problems

The main strategy proposed in [EE03a] is to compare the HMM solution with that of some underlying macroscale solver, or effective macroscale method. The basic result, proved in [EE03a], is that if this effective macroscale method is stable and k-th order accurate, then

$$||U_{\mathrm{HMM}} - U_0|| \le ||U_{\mathrm{HMM}} - \bar{U}_H|| + ||\bar{U}_H - U_0|| \le C(e(\mathrm{HMM}) + (\Delta t)^k) \tag{125}$$

where U_0 is the solution of the macroscale model, $e(\mathrm{HMM})$ is the error in estimating the effective force. In proving (125), it is assumed that both HMM and the effective macroscale method are expressed in the form:

$$U^{n+1} = U^n + \Delta t F^{\varepsilon}(U) \tag{126}$$

$$\bar{U}^{n+1} = \bar{U}^n + \Delta t \bar{F}(\bar{U}) \tag{127}$$

and $e(\mathrm{HMM})$ is defined as

$$e(\mathrm{HMM}) = \max_U \|\bar{F}(U) - F^{\varepsilon}(U)\| \tag{128}$$

We also have:

$$||Qu^{\varepsilon} - U_{\mathrm{HMM}}|| \le ||Qu^{\varepsilon} - U_0|| + ||\bar{U}_H - U_0|| + ||U_{\mathrm{HMM}} - \bar{U}_H|| \tag{129}$$

Here the first term on the right hand side is due to the error in the effective model; the second term is due to the error in the macroscale solver; the third term is the HMM error, due to the fact the macroscale data are not given by an explicit model but are estimated from the microscale model. Denote by ε the parameter that characterizes the small scale in the problem. (129) suggests an estimate of the type:

$$||Qu^{\varepsilon} - U_0|| \le C(\varepsilon^{\alpha} + (\Delta t)^k + e(\mathrm{HMM})) \tag{130}$$

We now apply this general result to some concrete examples.

ODEs with multiple time scales

The problems and algorithms were discussed in section 2.2. If we apply the general principles discussed above, we get:

Theorem 5. HMM is stable if the macroscale solver is stable. Moreover for any given constant T there exists a constant C such that

$$|E^n| \leq C((\Delta t)^k + e(\text{HMM}))$$

if $n\Delta t \leq T$, where E^n is the error between the HMM solution and the slow component of the exact solution (a precise definition is given below), k is the order of the macroscale solver, $e(\text{HMM})$ is the error in the estimation of the macroscale data.

Next we estimate $e(\text{HMM})$. This depends on a number of important components of HMM, in particular the filter K. We first discuss the case of dissipative systems. For clarity, we will consider the example of (7). We will further assume that f and g are smooth and bounded. We will also assume that $\{Z^{n,0}\}$ is bounded.

In the limit as $\varepsilon \to 0$, one expects that x will be close to $f(y)$, and hence the effective dynamics for the slow variable y is given by

$$\dot{\bar{y}} = g(f(\bar{y}), \bar{y}) = G(\bar{y}) \tag{131}$$

In fact it can be easily shown that if we denote by $(x_\varepsilon, y_\varepsilon)$ the solution of (7) and if $y_\varepsilon(0) = \bar{y}(0)$. Then

$$|y_\varepsilon(t) - y_0(t)| \leq C_1 \exp\left(-\frac{t}{\varepsilon}\right) + C_2\varepsilon.$$

First let us consider the case when the macroscale solver is forward Euler. In this case we can express HMM as:

$$y^{n+1} = y^n + \Delta t \tilde{g}(y^n)$$

Let $E^n = y^n - y_0(t^n)$, where $t^n = n\Delta t$, for $n\Delta t \leq T$. We have

$$\begin{aligned}
\frac{E^{n+1} - E^n}{\Delta t} &= \tilde{g}(y^n) - G(y_0(t^n)) + O(\Delta t) \\
&= G(y^n) - G(y_0(t^n)) + \tilde{g}(y^n) - G(y^n) + O(\Delta t) \\
&= G'(y_0(t^n) + \theta E^n)E^n + \tilde{g}(y^n) - G(y^n) + O(\Delta t)
\end{aligned}$$

If we let $L = \max |G'(y)|$, then we get

$$|E^n| \leq e^{Lt}(C\Delta t + \max_{n\Delta t \leq T} |\tilde{g}(y^n) - G(y^n)|)$$

where $C = \max_{t \leq T} |y_0''(t)|$. Here the first term on the right hand side is the standard truncation error at the macroscale. The second term $|\tilde{g}(y^n) - G(y^n)|$

is what we usually call e(HMM). With (13), it is a simple matter to prove [E03]:

$$e(\text{HMM}) \leq C\left(\Delta t + \left|1 - \frac{\delta t}{\varepsilon}\right|^N\right) \tag{132}$$

In the general case when k-th order stable macroscale solvers are used, we have [E03]:

Theorem 6. Assume that the macroscale solver is k-th order accurate and stable, i.e. for linear multi-step methods the root condition is satisfied. Let $A(\lambda\delta t)$ be the amplification factor of the microscale solver for the ODE $\dot{y} = -\lambda y$. Then there exists a constant C, independent of $\Delta t, \varepsilon, \delta t$ and N, such that, for $n\Delta t \leq T$,

$$|E^n| \leq C\left(\Delta t^k + \left|A\left(\frac{\delta t}{\varepsilon}\right)\right|^N\right)$$

Next we consider the oscillatory case. As before we will discuss a simple and yet canonical example, namely (8). The dynamics for the slow variable I obeys the equation

$$\dot{\bar{I}} = \frac{1}{2\pi}\int_0^{2\pi} g(\varphi, \bar{I})d\varphi = G(\bar{I}) \tag{133}$$

See for example [Arn89]. We will assume that $\omega(I)$ never vanishes:

$$\omega(I) \geq \omega_0 > 0 \tag{134}$$

We will restrict ourselves to the situation when the weights $\{K_{m,N}\}$ are given by

$$K_{m,N} = K_0\left(1 - \frac{m}{N}\right) \tag{135}$$

for $m = 0, 1, \ldots, N$, where K_0 is a filtering kernel.

A crucial component in the analysis in this case is the effect of the kernel K_0. This is examined in detail in [ET04]. Consider an example for which the microscopic data takes the form:

$$f^\varepsilon(t) = f_0(t) + f_1\left(\frac{t}{\varepsilon}\right)$$

where $f_1(\tau)$ is periodic in τ with period 1. The marcoscale component of $\{f^\varepsilon(t)\}$ is

$$F(t) = f_0(t) + \int_0^1 f_1(\tau)d\tau$$

The macroscale data of interest is $F_0 = F(0)$. Assume that the F-estimator has the form

$$\tilde{F}_0 = \frac{1}{T}\int_0^T K_0\left(1 - \frac{\tau}{T}\right) f^\varepsilon(\tau)d\tau$$

Then one has

Lemma: Assume that K_0 satisfies the following conditions

1. (A1). Moment condition

$$\int_0^1 K_0(\tau)d\tau = 1$$
$$\int_0^1 (1-\tau)^\alpha K_0(\tau)d\tau = 0$$

   for $\alpha = 1, 2, \ldots \ell - 1$
2. (A2). Regularity condition

$$K_0^{(\alpha)}(0) = K_0^{(\alpha)}(1) = 0$$

   for $\alpha = 0, 1, \ldots, q-1$ and

$$\int_0^1 |K_0^{(\alpha)}(\tau)|\alpha\tau \ < +\infty$$

   for $\alpha = 0, 1, \ldots, q$.

Then

$$|F_0 - \tilde{F}_0| \leq C\left(T^\ell + \left(\frac{\varepsilon}{T}\right)^q\right)$$

Using this result, one has,

Theorem 7. Under the same assumption as before, we have

$$|E^n| \leq C\left((\Delta t)^k + \left(\frac{\delta t}{\varepsilon}\right)^r + \left(\frac{\varepsilon}{N\delta t}\right)^q\right)$$

where $r = \min(l, p)$ and p is the order of the microscale solver.

As expected, the size of δt should be chosen to resolve the small time scale ε, and N should be large enough so that $N\delta t$ is larger than ε in order to sample adequately the dynamics at the small scale.

The effect of the fast variable reinitialization

The error estimates given in the last subsection were for the general case when the initialization of the fast variables in the microscale solver is quite arbitrary. Suitable reinitialization of the fast variables at each macro-time-step may result in significant gain in efficiency. Precise estimates are given below for the case of stochastic ODEs, but it is usefull to first illustrate the influence of fast variables initialization on a simple example, (7).

Suppose that the initial condition for (12) is taken to be $x^{n,0} = 0$. Then N must be taken large enough so that (12) has converged, i.e. $x^{n,N} \approx f(y^m)$, and the error estimate for e(HMM) is given in (132).

Suppose on the contrary that we take $x^{n,0} = x^{n-1,N}$. Then it can be shown that the error estimate improves to

$$e(\text{HMM}) \leq C\left(\Delta t + \frac{\varepsilon \Delta t}{N\delta t} + \Delta t\left|1 - \frac{\delta t}{\varepsilon}\right|^N\right). \tag{136}$$

which indicates, in particular that the scheme converges as $\Delta t, \delta t \to 0$ provided that $\varepsilon\Delta t/N\delta t \to 0$. Notice that this can happen even if $N = 1$. Notice also that accuracy requires that

$$\varepsilon\Delta t/N\delta t \ll 1$$

whereas gaining in efficiency in the sense of (1) requires

$$\Delta t/N\delta t \gg 1$$

For small ε both constraints can be satisfied at the same time.

The simplest way to justify (136) is to re-write (12) as

$$x^{n,m+1} = x^{n,m} - \frac{1}{\gamma}\frac{\Delta t}{N}(x^{n,m} - f(y^m)) \tag{137}$$

where

$$\gamma = \frac{\varepsilon \Delta t}{N\delta t} \tag{138}$$

It is easy to see that in the limit as $\delta t, \Delta t \to 0$ with γ kept fixed, HMM is consistent with the modified equation

$$\begin{cases} \dot{x} = -\dfrac{1}{\gamma}(x - f(y)) \\ \dot{y} = g(x, y) \end{cases} \tag{139}$$

If $\gamma \gg \varepsilon$, this equation is less stiff than (7) and correspondingly HMM gains in efficiency over a direct scheme for (7). On the other hand, for $\varepsilon \ll 1$ it is possible to also satisfy $1 \gg \gamma \gg \varepsilon$. In this case, the y component of the solutions of (7) and (139) remains close because of the existence of a limiting dynamics. But the choice of γ is now dictated by the error tolerance that one wants to achieve and not by the value of ε in the original equation.

Stochastic ODEs with multiple time scales

Here we discuss some of the results proved in [EL04b] for stochastic ODEs. The algorithms were described in section 7. Again we will focus on the case of advective time scale. The algorithm over the diffusion time scale was also analyzed in [EL04b].

We will make the following assumptions:

(1). The coefficients a, b and σ, viewed as functions of (x, y, ε), are in $\mathbb{C}_b^\infty$, a and σ are bounded. Here $\mathbb{C}_b^\infty$ is the space of smooth functions with bounded derivatives of any order.

(2). There exists an $\alpha > 0$ such that $\forall\ (x, y, \varepsilon)$,

$$|\sigma^T(x,y,\varepsilon)y|^2 \geq \alpha|y|^2.$$

(3). There exists a $\beta > 0$ such that $\forall\ (x, y_1, y_2, \varepsilon)$,

$$\begin{aligned}\langle (y_1 - y_2), (b(x,y_1,\varepsilon) - b(x,y_2,\varepsilon))\rangle + \|\sigma(x,y_1,\varepsilon) - \sigma(x,y_2,\varepsilon)\|^2 \\ \leq -\beta|y_1 - y_2|^2,\end{aligned}$$

where $\|\cdot\|$ denotes the Frobenius norm.

Under these assumptions, we have:

Theorem 8. *Assume that the macro solver is stable and kth order accurate for* (102)*. Then for any $T_0 > 0$, there exists a constant $C > 0$, independent of $(\epsilon, \Delta t, \delta t, n_T, M, N)$, such that*

$$\sup_{n \leq T_0/\Delta t} \mathbb{E}|X^\epsilon_{t_n} - X_n| \leq C\left(\sqrt{\epsilon} + (\Delta t)^k + e_D\right) \tag{140}$$

where $t_n = n\Delta t$, and

$$e_D = (\delta t/\varepsilon)^\ell + \frac{e^{-\frac{1}{2}\beta n_T(\delta t/\varepsilon)}}{\sqrt{N(\delta t/\varepsilon)+1}}(R + \sqrt{R}) + \frac{\sqrt{\Delta t}}{\sqrt{M(N(\delta t/\varepsilon)+1)}} \tag{141}$$

Here ℓ is the weak order of the micro solver,

$$R = \frac{\Delta t}{1 - e^{-\frac{1}{2}\beta(n_T+N-1)(\delta t/\varepsilon)}}. \tag{142}$$

if the fast variable is initialized as in (106) *and $R = 1$ if the fast variable is initialized as in* (107)*.*

The basic idea for proving this result is as follows. The error $|X^\epsilon_{t_n} - X_n|$ in (140) is decomposed into three parts:

1. $|X^\epsilon_t - \bar{X}_t|$, where $\bar{X}_t$ is the solution of the effective equation (102).
2. $|\bar{X}_{t_n} - \bar{X}_n|$, where $\bar{X}_n$ is the approximation of $\bar{X}_{t_n}$ given by the selected macro solver assuming that $\bar{a}(x)$ is known.
3. $|\bar{X}_n - X_n|$.

The first part is the error in using the averaging principle. As shown in [EL04b], we have

$$\sup_{0 \leq t \leq T_0} \mathbb{E}|X^\epsilon_t - \bar{X}_t| \leq C\sqrt{\epsilon}.$$

This is the first term in (140).

The second part is a standard ODE estimate:

$$\sup_{n \leq T_0/\Delta t} |\bar{X}_{t_n} - \bar{X}_n| \leq C(\Delta t)^k. \tag{143}$$

This is the second term in (140).

The third part, e_D, accounts for the error caused by using $\tilde{a}_n$ instead of $\bar{a}(X_n)$ in the macro solver. Here the term $(\delta t/\varepsilon)^\ell$ is due to the micro-time discretization which induces a difference between the invariant measures of the continuous and discrete dynamical systems. The term

$$\frac{e^{-\frac{1}{2}\beta n_T(\delta t/\varepsilon)}}{\sqrt{N(\delta t/\varepsilon)+1}}(R+\sqrt{R})$$

accounts for the errors caused by relaxation of the fast variables. The factor R reflects the particular initialization procedure used for the fast variables at each macro time step. Different initialization will lead to a similar estimate with different values of R. For example if we use $Y_{n,0}=0$, then $R=1$. Finally, the term

$$\frac{\sqrt{\Delta t}}{\sqrt{M(N(\delta t/\varepsilon)+1)}}$$

accounts for the sampling errors after the fast variable reaches local equilibrium. This is a central limit theorem type of estimate.

(140) suggests a somewhat surprising fact, namely that the HMM scheme converges as $\Delta t \to 0$, $\delta t \to 0$ on any sequence such that $R \to 0$, even if we take only one realization and one micro time step per macro time step , $M=1, n_T=1$, $N=1$. In this case $R=\Delta t/(\delta t/\varepsilon)$ to leading order. This is the consequence of the particular reinitialization procedure that we have adopted (see (106)), and it is a manifestation of the point made in the last subsection.

We now discuss how these results play out in actual computations. We will focus on strong convergence estimates, and adopt the more accurate initialization procedure for the fast variable. When

$$N_m(\delta t/\varepsilon)=(n_T+N-1)(\delta t/\varepsilon)>1,$$

we have $R=\Delta t$ plus higher order terms, and

$$\begin{aligned}&\sup_{n\le T_0/\Delta t}\mathbb{E}|X_n-\bar{X}_n|\\ &\quad\le C\left((\delta t/\varepsilon)^\ell+\frac{e^{-\frac{1}{2}\beta n_T(\delta t/\varepsilon)}\sqrt{\Delta t}}{\sqrt{N(\delta t/\varepsilon)+1}}+\frac{\sqrt{\Delta t}}{\sqrt{M(N(\delta t/\varepsilon)+1)}}\right).\end{aligned}\tag{144}$$

Here Δt is taken as a fixed parameter. Suppose that we want to bound the error by $O(2^{-p})$ for $p=0,1,\ldots$ and assume that $M=1$. Then as in [EL04b], we have that the optimal parameters are

$$\delta t/\varepsilon=O(2^{-p/\ell}),\qquad n_T=O(1),\qquad N=O(2^{p(2+1/\ell)}),$$

which gives

$$\text{cost }=(n_T+N-1)/\Delta t=O(2^{p(2+1/\ell)}).$$

independent of ε. The magnitudes of the errors for various p and $\ell=1,2$ are listed in the following table and shown in Figure 35. As predicted, we the error scales as $E\ell_p=O(2^{-\ell p})$.

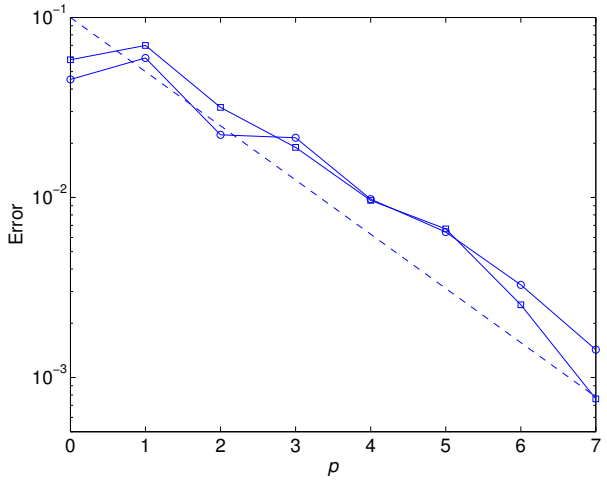

Fig. 35. The error $E_p^\ell = (\Delta t/T_0)\sum_{n\le\lfloor T_0/\Delta t\rfloor}|\tilde{X}_n - \bar{X}_n|$ as a function of p when $\ell = 1$ (circles) and $\ell = 2$ (squares). Also shown is the predicted estimated, 0.1×2^{-p} (dashed line)

	$p=0$	$p=1$	$p=2$	$p=3$	$p=4$	$p=5$	$p=6$	$p=7$
$\ell=1$	.058	.070	.032	.019	.0096	.0067	.0025	.00076
$\ell=2$	.045	.059	.022	.021	.0098	.0064	.0033	.0014

Table 2. The computed values for the error E_p^ℓ.

Other examples

We briefly mention a few other examples that have been analyzed. The parabolic homogenization problem has been analyzed in [AE03, EE02, MZ03]. The structure of the analysis is very similar to the examples discussed here. In particular, [MZ03] gives results that are similar to the ones discussed here for the elliptic homogenization problem. Error analysis and careful numerical studies for the hyperbolic homogenization problem were presented in [Che05, CES04].

Examples with discrete microscale models were considered in [EL04b]. The discrete models can be molecular dynamics or kinetic Monte Carlo methods. The macroscale model considered in [EL04b] was gas dynamics or general nonlinear conservation laws. It is proven in [EL04b] that the e(HMM) error consists of three parts: the relaxation error, the error due to the finite size of the simulation box, and the sampling error. Clearly as the system size increases, the finite size effect decreases but the relaxation error increases. Therefore this result gives some suggestions on how to choose the size of the microscale simulation. Unfortunately there are very few explicit results on the

dependence of these errors on the box size. All known results are proved for lattice models. We refer to [EL04b] for a discussion on this issue.

10 Limitations of HMM

As was discussed in [EE03a], there are problems for which HMM does not work well. One class of such problems are problems for which the time history of the detailed microstructural behavior has to be parametrized in order to determine the macroscale properties. One such example is the homogenization problem for the Carleman model, discussed in [EE03a]. Consider the Carlman equation with multiscale initial data:

$$\frac{\partial u}{\partial t} + \frac{\partial u}{\partial x} = v^2 - u^2 \tag{145}$$

$$\frac{\partial v}{\partial t} - \frac{\partial v}{\partial x} = u^2 - v^2$$

$$u(x,0) = a(x, x/\varepsilon)$$
$$v(x,0) = b(x, x/\varepsilon)$$

where $a(x,y), b(x,y)$ is assumed to be smooth and 1-periodic in y. The homogenized equation for this problem is given by [Tar81]:

$$\frac{\partial \tilde{u}}{\partial t} + \frac{\partial \tilde{u}}{\partial x} = \int_0^1 \tilde{v}(x,y,t)^2 dy - \tilde{u}^2 \tag{146}$$

$$\frac{\partial \tilde{v}}{\partial t} - \frac{\partial \tilde{v}}{\partial x} = \int_0^1 \tilde{u}(x,y,t)^2 dy - \tilde{v}^2 \tag{147}$$
$$\tilde{u}(x,y,0) = a(x,y)$$
$$\tilde{v}(x,y,0) = b(x,y)$$

Tartar proved [Tar81]

$$\lim_{\varepsilon \to 0} \left(\left| u(x,t) - \tilde{u}\left(x, \frac{x-t}{\varepsilon}, t\right) \right| + \left| v(x,t) - \tilde{v}\left(x, \frac{x+t}{\varepsilon}, t\right) \right| \right) = 0$$

Here the natural macroscale variables U are the weak limits of the full microscale solutions:

$$U(x,t) = \int_0^1 \tilde{u}(x,y,t) dy = \lim_{\delta \to 0} \left(\lim_{\varepsilon \to 0} \int K_\delta(x-z) u(z,t) dz \right)$$

$$V(x,t) = \int_0^1 \tilde{v}(x,y,t) dy = \lim_{\delta \to 0} \left(\lim_{\varepsilon \to 0} \int K_\delta(x-z) v(z,t) dz \right)$$

where K_δ is some kernel compactly supported in $(-\delta, \delta)$ with,

$$\int_{-\delta}^{\delta} K_\delta(x)dx = 1$$

However for this problem, there is no time scale separation between the dynamics of (U, V) and the remaining components of (u, v), such as higher order moments. In fact, to obtain information on (U, V), one has to keep track of the dynamics of the microstructure. Therefore a blind application of HMM will give wrong results.

As was shown in [Eng87], this particular problem can be effectively treated using a combination of the particle method and a proper sampling procedure for the microstructure.

A second example with a very similar feature is the transport equation with oscillatory velocity fields

$$\partial_t u + \partial_{x_1}\left(a\left(\frac{x_2}{\varepsilon}\right)u\right) = 0. \tag{148}$$

The homogenized equation for this problem is [Tar81]

$$\partial_t U + \bar{a}\partial_{x_1} U = \partial_{x_1}^2 \int_{-\alpha}^{\alpha} d\omega(\gamma) \int_0^t dsU(x_1 + \gamma(t-s), x_2, s) \tag{149}$$

and it shows dependence on the memory. Here ω is some kernel that depends on a, $\bar{a}$ is the average of a over its period. We refer to [EE02] for discussions of this example.

Both examples can be treated by a more general idea proposed in [EE03a]. This is the idea that one should view the microstructure as being living on a fiber bundle over the real space-time domain. For the example of Carleman equation, we can view y-space as being the fiber. When the microscale model is a kinetic equation, the fiber that represents the microstructure space is the momentum space (see Figure 5). Same can be said about the linear transport equation. One can then design numerical methods based on the idea of evolving the microstructure over the fiber. An application of this idea is presented in [YE04] for the transport equation.

Another limitation of HMM concerns with the a priori assumption on the constitutive relation, which is reflected in the constraints on the microscale solver. A crucial advantage of HMM is that it does not need the full knowledge of the macroscale model. But some knowledge about the macroscale model *is important*, as we now illustrate.

Consider the problem

$$\partial_t u + \nabla \cdot \left(b\left(\frac{x}{\varepsilon}\right)u\right) = \nabla \cdot \left(a\left(\frac{x}{\varepsilon}\right)\nabla u\right) \tag{150}$$

where b and a are smooth periodic functions with period 1. The homogenized equation for (150) is given by

$$\partial_t U + \nabla \cdot (\bar{b}U) = \nabla \cdot (A \nabla U) \tag{151}$$

where A is the homogenized coefficient matrix for the case when $b = 0$, $\bar{b}$ is the average of b over its period. Without knowing that the effective macroscale flux should depend on the derivative of the macroscale variable U, we might use HMM as in section 2.2, and impose as constraints over the microscale solver only that the average of u be the same as the local value of the macroscale variable U. In this case, the estimated flux will only contain the part that approximates $\bar{b}U$, not the part that approximates $A\nabla U$. This results in an $O(1)$ error for the macroscale quantities.

The failure in this case is due to the fact that in constructing the constrained microscale solver, we implicitly made the wrong constitutive assumption that the macroscale flux depends only on U, not the higher order derivatives of U. This is easily fixed by the methods described in section 2.2. But it shows that some knowledge about the macroscale model is crucial for designing the right HMM.

11 Conclusions and new directions

11.1 General procedures and main features of HMM

In summary, the main steps in developing an HMM style of multiscale method are as follows:

1. Identify the macroscale variables, and the macroscale structure of the problem, such as variational structure, conservation laws, diffusion processes, etc.

2. Express the microscale model in the form that is consistent with the identified macroscale structure. In our examples for fluids and solids, this step involves deriving the conservation laws from MD, and expressing the fluxes, such as stress, in atomistic variables. This is the basis for connecting the macroscale and microscale models.

3. Select the macroscale solver, and identify the data that need to be estimated from the microscale solver.

4. Design the constrained microscale solver that gives the needed data. Technically this is often the most difficult step, and is subject to continuous improvement. One should exploit as much as possible any special features that the problem has, in order to maximize efficiency. Also important for this step is the data processing techniques used in extracting the macroscale data from results of the microscale model.

HMM is a top-down framework: It is based on the macroscopic solver and uses the microscale model as a supplement. Its two-component procedure offers a number of interesting features, including:

1. The ability to make maximum use of our knowledge on all scales. For example, when choosing the macroscale solver, we may take advantage of

what is known at the macroscale, such as conservation form, variational structure, etc, as well as the nature of the physical process such as shock formation, phase transformation.

2. The ability to make maximum use of the special features of the problem. This is already shown above with the examples. very naturally within the framework of HMM. The time scale separation, for example, is made use of by the fact that satisfactory approximation for the needed data can be obtained by carrying out the microscale solver on relatively short time intervals.

We have seen that the framework of HMM provides useful guidance for systematically designing multiscale methods in a wide variety of applications. It also provides a natural setting for carrying out mathematical analysis of multiscale algorithms.

Despite its success, there are still many more interesting possibilities that have yet to be explored. We will end this review with a discussion of some of the directions for further work.

11.2 New application areas

The application areas that have been explored so far are a small subset of all the potential application areas for HMM. Some obvious possibilities include: coarse-grained procedure for studying rare events, bio-molecular dynamics, bio-membranes, bio-films, and epitaxial crystal growth.

In particular, type D problems should be explored.

In the areas that HMM has already been applied such as the ones discussed above, there is much room for further work to use these methods to solve more real-world problems. Examples include: crack propagation in solids, interaction of defects in solids, instabilities and hysteresis in microfluidics, elastic properties of strongly heterogeneous composite materials and more complex interface dynamics that involve non-trivial atomistic features.

Much of the work on HMM is done either for the situation when both the micro and macro models are continuum models, or when the micro model is molecular dynamics and the macro model is continuum mechanics. Extending HMM to situations when the micro model is either Monte Carlo, Brownian dynamics or quantum mechanics remains to be carried out and is promised to be a very fruitful direction of research.

11.3 Algorithm development

As part of the general multiscale methodology, the two most important aspects of algorithmic development are (1) adaptivity and (2) data processing.

Adaptivity is important for many applications, and HMM offers new possibilities for adaptive algorithm. The most obvious place where adaptivity enters is adaptive model refinement for type A problems. So far adaptive strategy is

not well understood. Our existing model refinement strategy is based on an estimate of the local variation of the numerical solutions. In contrast, adaptive mesh refinement for finite element methods are based on a systematic posteriori error estimates which is itself a highly non-trivial task of numerical analysis. It is desirable to develop such systematic adaptive strategies for adaptive model refinement.

There are other possibilities of adaptive algorithms for HMM. For example the size of the micro domain on which the micro model is solved to give the macro data can be adaptively chosen depending on the local microstructure. One can also decide adaptively whether new micro solutions should be obtained to give the needed macro data, or the previously obtained micro solution and/or macro data can be used in some way. In particular, if the unknown component of the macro model is of some specific functional form, then one can determine the parameters in the functional form "on the fly". Once this functional form is obtained to satisfactory accuracy, then it can be used to give directly the macro data in subsequent time intervals. In this way, the algorithm undergoes a learning process as the computation proceeds. An example of using this strategy, which was called "semi-empirical methods", was given in [EE03a] for the linear parabolic homogenization problem. There it is known that the averaged fluxes are linear functions of the macroscopic gradient. Therefore one only has to determine the coefficients of these linear relations using a few data points obtained from the HMM procedure. This procedure should be explored in more general situations.

A more ambitious adaptive procedure is to determine adaptively the correct macroscale variable and the form of the macroscale model from carefully designed microscopic experiments. This is an attractive possibility and there are obvious ideas to try, but so far there are little concrete results in this direction.

The second important aspect of algorithmic development is data processing. Indeed one key factor that directly influences the efficiency of the HMM procedure is the signal to noise ratio in the microscale simulation. Even though high order accurate kernels that satisfy the high order moment and regularity conditions discussed in section 9.2 have been developed [ET04], they seem to be most useful for data that have specific structure such as periodicity. Most data obtained from microscopic simulations are quite stochastic and lack specific structure. Therefore it is important to develop more advanced techniques for analyzing such data. The most obvious suggestion is to use wavelets. But even this has not been fully explored.

There are two main tasks for the data processing step. The first is to extract approximations to the needed macroscale data from the microscopic data. The second is to decide whether the extracted data is accurate enough and hence the microscopic simulation can be stopped. Both needs further work.

Another important component that needs to be further improved is the boundary conditions for the microscale systems. Take the example of

atomistic-continuum matching conditions, most existing work on boundary conditions are still somewhat unsatisfactory due to their complexity and the restriction of low (essentially 0) temperature. The more general boundary conditions, such as the thermostat boundary condition discussed in [LE05], require further analysis and validation.

11.4 Analytical issues

The most pressing analytical issue at the present time is the analysis of HMM for type A problems. The difficulty is associated with the fact that for type A problems, it often requires fundamental understanding about the properties of the defects in order to carry out some analysis, and currently there are very few examples for which this has been done.

There are still many issues remaining as far as type B problems are concerned. Estimating accurately $e(\text{HMM})$ often requires understanding quantitatively the rate of convergence of various systems in the thermodynamic limit, as well as the behavior of the relaxation times as a function of the microscopic system size. Again there are very few analytical results in this area, particular for systems described by molecular dynamics and quantum mechanics (see the discussion in [EL04b]). But even for homogenization problems, our understanding of these issues are quite unsatisfactory. Careful numerical studies can help to clarify these issues as well as suggest the right form of the analytical results (see for example [EL04b, Re04b]).

In conclusion, what has already been done on HMM, in terms of numerical algorithms, analysis, modeling and application, is only the tip of the iceberg. This limited experience has given us sufficient confidence that HMM does provide a very attractive framework for multiscale modeling. However, realizing the full potential of HMM is still an enormous task, as well as opportunity.

Acknowledgement: In writing this review, we have drawn material from the work of many of our collaborators, including Assyr Abdulle, Li-Tien Cheng, Ibrahim Fatkullin, Tiejun Li, Di Liu, Pingbing Ming, Richard Tsai, Xingye Yue and Pingwen Zhang. We are very grateful for their effort and their work that made this review possible. We are also grateful to Randy LeVeque and Wing Kam Liu for suggestions for improving an earlier draft, and to Shi Jin for providing a more complete list of references on kinetic schemes. In addition, we would to thank the office of ONR for supporting a large part of the work discussed here. The of work E is supported in part by ONR grant N00014-01-1-0674, DOE grant DE-FG02-03ER25587 and Natural Science Foundation of China through a Class B Award for Distinguished Young Scholars 10128102. The work of Engquist is supported in part by NSF grant DMS99-73341. The work of Xiantao Li is supported in part by ONR grant N00014-01-1-0674 and DOE grant DE-FG02-03ER25587. The work of Vanden-Eijnden is supported in part by NSF grants DMS02-09959 and DMS02-39625.

References

[Abd02] Abdulle, A.: Fourth Order Chebychev Methods with Recurrence Relations. SIAM J. Sci. Comput., **23**:6, 2041–2054 (2002)

[Ab04a] Abdulle, A.: On J.A.A-Priori Error Analysis of Fully Discrete Heterogeneous Multiscale FEM. Preprint (2004)

[Ab04b] Abdulle, A.: private communication (2004)

[AE03] Abdulle, A., E, W.: Finite Difference Heterogeneous Multi-Scale Method for Homogenization Problems. J. Comput. Phys., **191**, 18–39 (2003)

[AS04] Abdulle, A., Schwab, C.: Heterogeneous Multiscale FEM for Diffusion Problem on Rough Surface. SIAM MMS, **3**, 195–220 (2005)

[ABB99] Abraham, F.F., Broughton, J.Q., Bernstein N., Kaxiras, E.: Concurrent Coupling of Length Scales: Methodology and Application. Phys. Rev. B, **60**:4, 2391–2402 (1999)

[ABB98] Abraham, F.F., Broughton, J.Q., Bernstein, N., Kaxiras, E.: Spanning the Continuum to Quantum Length Scales in a Dynamic Simulation of Brittle Fracture. Europhys. Lett., **44**:6, 783–787 (1998)

[AS99] Adalsteinsson, D., Sethian, J.A.: The Fast Construction of Extension Velocities in Level Set Methods. J. Comput. Phys., **148**, 2–22 (1999)

[AS95] Adalsteinsson, D., Sethian, J.A.: A Fast Level Set Method for Propagating Interfaces. J. Comput. Phys., **118**:2, 269–277 (1995)

[AD76] Adelman, S.A., Doll, J.D.: Generalized Langevin Equation Approach for Atom/Solid Surface Scattering: General Formulation for Classical Scattering of Harmonic Solids. J. Chem. Phys., **64**:6, 2375–2388 (1976)

[AT87] Allen, M.P., Tildesley, D.J.: Computer Simulation of Liquids. Oxford University Press, New York (1987)

[Arn89] Arnold, V.I.: Mathematical Methods in Classical Mechanics. 2nd ed., Graduate Texts in Mathematics, **60**, Springer-Verlag (1989)

[Bab77] Babuska, I.: Solution of Interface by Homogenization, I, II, III. SIAM J. Math. Anal., **7**, 603–645 (1976); **8**, 923–937 (1977)

[Bab76] Babuska, I.: Homogenization and Its Applications, Mathematical and Computational Problems. In: Hubbard, B. (ed) Numerical Solutions of Partial Differential Equations-III, (SYNSPADE 1975, Maryland, May 1975), 89–116 Academic Press, New York (1976)

[BCO94] Babuska, I., Caloz, G., Osborn, J.: Special Finite Element Methods for a Class of Second Order Elliptic Problems with Rough Coefficients. SIAM J. Numer. Anal., **31**, 945–981 (1994)

[BBO03] Babuska, I., Banerjee, U., Osborn, J.: Survey of Meshless and Generalized Finite Element Methods. Acta Numerica, **12**, 1–125 (2003)

[BBO04] Babuska, I., Banerjee, U., Osborn, J.: Generalized Finite Element Methods – Main Ideas, Results and Perspective. International Journal of Computational Methods, **1**, 67–103 (2004)

[BCR93] Becquart, C.S., Clapp, P.C., Rifkin, J.A.: Molecular-dynamics simulations of tweed structure and the ω phase in Ni-Al. Phys. Rev. B, **48**, 6–13 (1993)

[BLP78] Bensoussan, A., Lions, J.L., Papanicolaou, G.C.: Asymptotic Analysis for Periodic Structures. North-Holland Pub. Co., Amsterdam (1978)

[BCA87] Bird, R.B., Curtiss, C.F., Armstrong, R.C., Hassager, O.: Dynamics of Polymeric Liquids. In: Kinetic Theory **2**, John Wiley, New York (1987)

[Bol94] Boley, D.L.: Krylov Space Methods on State-Space Control Models. Circ. Syst. Signal Proc., **13**:6, 733–758 (1994)

[Bou77] Bourgat, J.F.: Numerical Experiments of the Homogenization Method for Operators with Periodic Coefficients. Lecture Notes in Math., **707**, 330–356, Springer-Verlag (1977)

[BLP92] Bourgat, J.F., Le Tallec, P., Perthame, B., Qiu, Y.: Coupling Boltzmann and Euler Equations without Overlapping. In: Domain Decomposition Methods in Science and Engineering, Amer. Math. Soc., 377–398 (1992)

[BLT96] Bourgat, J.F., Le Tallec, P., Tidriri, M.: Coupling Boltzmann and Navier-Stokes Equations by Friction. J. Comput. Phys., **127**:2, 227–245 (1996)

[BPS86] Bramble, J.H., Pasciak, J.E., Schatz, A.H.: The Construction of Preconditioners for Elliptic Problems by Substructuring Methods. Math. Comp, **47**, 103–134, 1986.

[Bra02] Brandt, A.: Multiscale Scientific Computation: Review 2001. In: Barth, T.J., et. al. (eds) Multiscale and Multiresolution Methods: Theory and Applications, Yosemite Educational Symposium Conf. Proc. (2000) Lecture Notes in Comp. Sci. and Engrg., **20**, 3–96, Springer-Verlag (2002)

[Bra92] Brandt, A.: Multigrid Methods in Lattice Field Computations. Nucl. Phys. B (Proc. Suppl.), **26B**, 137–180 (1992)

[Bra77] Brandt, A.: Multi-Level Adaptive Solutions to Boundary Value Problems. Math. Comp., **31**:138, 333–390 (1977)

[Bra95] Brandt, A.: Multiscale Research in Molecular Dynamics. Gauss Center Report WI/GC-3 (1995)

[CKB00] Cai, W., de Koning, M., Bulatov, V.V., Yip, S.: Minimizing Boundary Reflections in Coupled-Domain Simulations. Phys. Rev. Lett., **85**:15, 3213–3216 (2000)

[CP85] Car, R., Parrinello, M.: Unified Approach for Molecular Dynamics and Density-Functional Theory. Phys. Rev. Lett., **55**:22, 2471–2474 (1985)

[CW76] Chakravorty, S., Wayman, C.M.: Thermoelastic Martensitic Transformation in Beta' Ni-Al Alloys. Metall. Trans. A, **7**:4, 555–582 (1976)

[CD98] Chen, S., Doolen, G.D.: Lattice Boltzmann Methods for Fluid Flows. Ann. Rev. Fluid Mech., **30**, 329–364 (1998)

[Che05] Chen, S.: Ph.D. Thesis, Brown University, expected in 2005.

[CES04] Chen, S., E, W., Shu, C.W.: The Heterogeneous Multi-Scale Method Based on Discontinuous Galerkin Method for Hyperbolic and Parabolic Problems. SIAM MMS, **3**:4, 871–894 (2004)

[CE04] Cheng, L.-T., E, W.: The Heterogeneous Multiscale Method for Interface Dynamics. In: Cheng, S.Y., et. al. (ed) Contemporary Mathematics: A Special Volume in Honour of Stan Osher to appear

[CLE05] N. Choly, N., Lu, G., E, W., Kaxiras, E.: Multiscale Simulations in Simple Metals: A Density-Functional Based Methodology. Phys. Rev. B, **71**, 094101 (2005)

[Cho67] Chorin, A.J.: A Numerical Method for Solving Incompressible Viscous Flow Problems. J. Comput. Phys., **2**, 12–26 (1967)

[Cho03] Chorin, A.J.: Conditional Expectations and Renormalization. SIAM J. Multiscale Modeling Sim., **1**, 105–118 (2003)

[Cho98] Chorin, A.J.: Vorticity and Turbulence. In: Applied Mathematical Sciences **103**, Springer-Verlag (1998)

[Cho89] Chorin, A.J.: Computational Fluid Mechanics: Selected Papers. Academic Press, New York (1989)

[Cho68] Chorin, A.J.: Numerical Solution of the Navier-Stokes Equations. Math. Comp., **22**, 745–762 (1968)

[CHK02] Chorin, A.J., Hald, O., Kupferman, R.: Optimal Prediction with Memory. Physica D, **166**:3-4, 239–257 (2002)

[CKK98] Chorin, A.J., Kast, A.P., Kupferman, R.: Optimal Prediction of Underresolved Dynamics. Proc. Natl. Acad. Sci. USA, **95**:8, 40944098 (1998)

[CRD01] Cormier, J., Rickman, J.M., Delph, T.J.: Stress calculation in atomistic simulations of perfect and imperfect solids. J. Appl. Phys., **89**, 99–104 (2001)

[CC95] Cui, J.Z., Cao, L.Q.: The Two-Scale Analysis Method for Woven Composite Materials. In: Zhong, Z.-H. (ed), Engineering Computation and Computer Simulation I, Hunan University Press, 203–212 (1995)

[CC02] Curtarolo, S., Ceder, G.: Dynamics of an Inhomogeneously Coarse Grained Multiscale System. Phys Rev Lett., **88**, 255504 (2002)

[CM03] Curtin, W.A., Miller, R.E.: Atomistic/Continuum Coupling in Computational Material Science. Modelling Simul. Mater. Sci. Eng., **11**, R33–R68 (2003)

[Daf00] Dafermos, C.M.: Hyperbolic Conservation Laws in Continuum Physics. Springer-Verlag, Berlin (2000)

[DR01] Denniston, C., Robbins, M.O.: Molecular and Continuum Boundary Conditions for a Miscible Binary Fluid. Phys. Rev. Lett., **87**:17, 178302 (2001)

[Des95] Deshpande, S.M.: Kinetic Flux Splitting Schemes. Computational Fluid Dynamics Review, John Wiley & Sons, Chechester (1995)

[DE86] Doi, M., Edwards, S.F.: The Theory of Polymer Dynamics. Oxford Science Publications (1986)

[Dur91] Durlofsky, L.J.: Numerical Calculation of Equivalent Grid Block Permeability Tensors for Heterogeneous Poros-Media. Water. Resour. Res., **27**, 699–708 (1991)

[Dus79] Dussan, E.B.: On the Spreading of Liquids on Solid Surfaces: Static and Dynamic Contact Lines. Ann. Rev. Fluid Mech., **11**, 371–400 (1979)

[E03] E, W.: Analysis of the Heterogeneous Multiscale Method for Ordinary Differential Equations. Comm. Math. Sci., **1**:3, 423–436 (2003)

[E92] E, W.: Homogenization of Linear and Nonlinear Transport Equations. Comm. Pure Appl. Math., **45**, 301–326 (1992)

[E04] E, W.: Multiscale Modeling: Challenges and Opportunities. Submitted to Proceedings of CSIAM (2004)

[EE02] E, W., Engquist, B.: The Heterogeneous Multi-Scale Method for Homogenization Problems. Submitted to SIAM J. Multiscale Modeling Sim. (2002)

[EE03a] E, W., Engquist, B.: The Heterogeneous Multi-Scale Methods. Comm. Math. Sci., **1**, 87–133 (2003)

[EE03b] E, W., Engquist, B.: Multiscale Modeling and Computation. Notices of the Amer. Math. Soc., **50**:9, 1062–1070 (2003)

[EEH03] E, W., Engquist, B., Huang, Z.: Heterogeneous Multiscale Method: a General Methodology for Multiscale Modeling. Phys. Rev. B, **67**:9, 092101 (2003)

[EH01] E, W., Huang, Z.: Matching Conditions in Atomistic-Continuum Modeling of Materials. Phys. Rev. Lett., **87**:13, 135501 (2001)

[EH02] E, W., Huang, Z.: A Dynamic Atomistic-Continuum Method for the Simulation of Crystalline Materials. J. Comput. Phys., **182**, 234–261 (2002)

[EL04a] E, W., Li, X.: Multiscale Modeling of Crystalline Solids. Handbook of Computational Material Science, to appear

[EL04b] E, W., Li, X.: Analysis of the Heterogeneous Multiscale Method for Gas Dynamics. To appear in Methods of Analysis and Applications (2005)

[EL04a] E, W., Li, X., Vanden-Eijnden, E.: Some Recent Progress in Multiscale Modeling. In: Attinger, S., Koumoutsakos, P. (eds) Multiscale Modeling and Simulation, Lecture Notes in Computational Science and Engineering, **39**, 3–22, Springer (2004)

[EL04b] E, W., Liu, D., Vanden-Eijnden, E.: Analysis of Multiscale Methods for Stochastic Differential Equations. Comm. Pure Appl. Math. in press.

[EMZ04] E, W., Ming, P.B., Zhang, P.W.: Analysis of the Heterogeneous Multiscale Method for Elliptic Homogenization Problems. J. Amer. Math. Soc., posted on September 16, 2004, to appear in print

[EV04] E, W., Vanden-Eijnden, E.: Metastability, Conformational Dynamics and Transition Pathways in Complex Systems. In: Attinger, S., Koumoutsakos, P. (eds) Multiscale Modeling and Simulation, Lecture Notes in Computational Science and Engineering, **39**, 35–68, Springer (2004)

[EY04] E, W., Yue, X.Y.: Heterogeneous Multiscale Method for Locally Self-Similar Problems. Comm. Math. Sci., **2**, 137–144 (2004)

[EHW00] Efendiev, Y.R., Hou, T., Wu, X.: Convergence of a Nonconforming Multiscale Finite Element Method. SIAM J. Numer. Anal., **37**:3, 888–910 (2000)

[Eng87] Engquist, B.: Computation of Oscillatory Solutions to Hyperbolic Differential Equations. Lecture Notes in Math., **1270**, 10–22, Springer-Verlag (1987)

[ER02] Engquist, B., Runborg, O.: Wavelet-Based Numerical Homogenization with Applications. In: Barth, T.J., et. al. (eds) Multiscale and Multiresolution Methods: Theory and Applications, Yosemite Educational Symposium Conf. Proc. (2000) Lecture Notes in Comp. Sci. and Engrg., **20**, 97–148, Springer-Verlag (2002)

[ET04] Engquist, B., Tsai, R.: Heterogeneous multiscale method for a class of stiff ODEs. Math. Comp., accepted for publication (2004)

[EA93] Ercolessi, F., Adams, J.B.: Interatomic potentials from first-principles calculations: the force-matching method. Europhys. Lett., **26**, 583 (1993)

[FV04] Fatkullin, I., Vanden-Eijnden, E.: A Computational Strategy for Multiscale Systems with Applications to Lorenz 96 Model. J. Comput. Phys., **200**:2, 605–638 (2004)

[FWF00] Flekky, E.G., Wagner, G., Feder, J.: Hybrid Model for Combined Particle and Continuum Dynamics. Europhys. Lett., **52**:3, 271–276 (2000)

[Fre85] Freidlin, M.I.: Functional Integration and Partial Differential Equations. In: Griffiths, P.A., et. al. (ed) Annals of Mathematics Studies, Princeton Univ. Press, Princeton, NJ (1985)

[FW98] Freidlin, M.I., Wentzell, A.D.: Random Perturbations of Dynamical Systems. 2nd ed., Springer-Verlag (1998)

[FS01] Frenkel, D., Smit, B.: Understanding Molecular Simulation: from Algorithms to Applications. 2nd ed., Academic Press (2001)

[GBC99] Garcia, A.L., Bell, J.B., Crutchfield, W.Y., Alder, B.J.: Adaptive Mesh and Algorithm Refinement Using Direct Simulation Monte Carlo. J. Comput. Phys., **154**, 134–155 (1999)

[GK03] Gear, C.W., Kevrekidis, I.G.: Projective Methods for Stiff Differential Equations: Problems with Gaps in Their Eigenvalue Spectrum. SIAM J. Sci. Comput., **24**:4, 1091–1106 (2003)

[GKT04] Gear, C.W., Kevrekidis, I.G., Theodoropoulos, C.: 'Coarse' Integration/Bifurcation Analysis Via Microscpic Simulators: Micro-Galerkin Methods. Submitted to Comp. Chem. Eng. (2004)

[GLK03] Gear, C.W., Li, J., Kevrekidis, I.G.: The Gap-Tooth Scheme for Particle Simulations. Phys. Lett. A, **316**, 190–195 (2003)

[GMM86] Glimm, J., McBryan, O., Menikoff, R., Sharp, D.H.: Front Tracking Applied to Rayleigh-Taylor Instability. SIAM J. Sci. Statist. Comput., **7**, 230–251 (1986)

[GR96] Godlewski, E., Raviart, P.A.: Numerical Approximation of Hyperbolic Systems of Conservation Laws. Springer-Verlag, New York (1996)

[GSE05] Guo, W., Schulze, T., E, W.: Simulation of Impurity Diffusion in a Strained Nanowire Using Off-lattice KMC. Submitted to Phys. Rev. B (2005)

[Had99] Hadjiconstantinou, N.G.: Hybrid Atomistic-Continuum Formulations and the Moving Contact-Line Problem. J. Comput. Phys., **154**:2, 245–265 (1999)

[HP97] Hadjiconstantinou, N.G., Patera, A.T.: Heterogeneous Atomistic-Continuum Representation for Dense Fluid Systems. Intl. J. Modern Phys. C, **8**:4, 967–976 (1997)

[HW91] Hairer, E., Wanner, G.: Solving Ordinary Differential Equations II, Stiff and Differential-Algebraic Problems. Springer-Verlag (1991)

[HPC96] Helmsen, J., Puckett, E., Colella, P., Dorr, M.: Two New Methods for Simulating Photolithography Development in 3D. In: SPIE 1996 Symposium Proc., Intl. Symposium on Microlithography, Santa Clara, CA, **2726**, 253–261 (1996)

[HW97] Hou, T.Y., Wu, X.-H.: A Multiscale Finite Element Method for Elliptic Problems in Composite Materials and Porous Media. J. Comput. Phys., **134**, 169–189 (1997)

[Hug96] Hughes, B.D.: Random Walks and Random Environments. In: Random Environments, **2**, Oxford University Press (1996)

[IK50] Irving, J.H., Kirkwood, J.G.: The Statistical Mechanical Theory of Transport Processes IV. J. Chem. Phys., **18**, 817–829 (1950)

[JLT03] Jenny, P., Lee, S.H., Tchelepi, H.A.: Multiscale Finite Volume Method for Elliptic Problems in Subsurface Flow Simulation. J. Comput. Phys., **187**, 47–67 (2003)

[KL04] Kadowaki, H., Liu, W.K.: Bridging Multiscale Method for Localization Problems. Computer Methods in Applied Mechanics and Engineering, **193**:30–32, 3267–3302 (2004)

[KWL05] Karpov, E.G., Wagner, G.J., Liu, W.K.: A Green's Function Approach to Deriving Non-Reflecting Boundary Conditions in Molecular Dynamics Simulations. International Journal for Numerical Methods in Engineering, to appear

[KYP04] Karpov, E.G., Yu, H., Park, H.S., Liu, W.K., Wang, J.: Multiscale Boundary Conditions in Crystalline Solids: Theory and Application to Nanoindentation. Submitted to Phys. Rev. B (2004)

[KMV03] Katsoulakis, M., Majda, A.J., Vlachos, D.G.: Coarse-grained stochastic processes for lattice systems. Proc. Natl. Acad. Sci. USA, **100**, 782–787 (2003)

[KGH03] Kevrekidis, I.G., Gear, C.W., Hyman, J.M., Kevrekidis, P.G., Runborg, O., Theodoropoulos, C.: Equation-Free, Coarse-Grained Multiscale Computation: Enabling Microscopic Simulators to Perform System-Level Analysis. Comm. Math. Sci., **1**:4, 715–762 (2003)

[KP92] Kloeden, P.E., Platen, E.: Numerical Solutions of Stochastic Differential Equations. From Applications of Mathematics, **23**, Springer-Verlag (1992)

[KO01] Knap, J., Ortiz, M.: An Analysis of the Quasicontinuum Method. J. Mech. Phys. Solids., **49**:9, 1899–1923 (2001)

[KB95] Koplik, J., Banavar, J.R.: Continuum Deductions from Molecular Hydrodynamics. Ann. Rev. Fluid Mech., **27**, 257–292 (1995)

[Kur73] Kurtz, T.G.: A Limit Theorem for Perturbed Operator Semigroups with Applications to Random Evolutions. J. Functional Analysis, **12**, 55–67 (1973)

[LL80a] Landau, L., Lifshitz, E.M.: Statistical Physics, Part 1. 3rd ed., Pergamon Press (1980)

[LL80b] Landau, L., Lifshitz, E.M.: Theory of Elasticity. Pergamon Press (1980)

[Leb00] Lebedev, V.I.: Explicit Difference Schemes for Solving Stiff Problems with a Complex or Separable Spectrum. (Russian. Russian summary) Zh. Vychisl. Mat. Mat. Fiz. **40**:12, 1801–1812 (2000); English translation in Comput. Math. Math. Phys. **40**:12, 1729–1740 (2000)

[LF76] Lebedev, V.I., Finogenov, S.I.: Explicit Methods of Second Order for the Solution of Stiff Systems of Ordinary Differential Equations. Zh. Vychisl. Mat. Mat Fiziki, **16**:4, 895–910 (1976)

[LE72] Lees, A.W., Edwards, S.F.: The Computer Study of Transport Processes Under Extreme Conditions. J. Phys. C, **5**:15, 1921–1929 (1972)

[LP98] Le Tallec, P., Perlat, J.P.: Coupling Kinetic Models with Navier-Stokes Equations. CFD Review, **2**, 833–855 (1998)

[LeV90] LeVeque, R.: Numerical Methods for Conservation Laws. Birkhauser (1990)

[LLY99] Li, J., Liao, D., Yip, S.: Nearly Exact Solution for Coupled Continuum/Md Fluid Simulation. J. Computer-Aided Material Design, **6**:2-3, 95–102 (1999)

[LVZ04] Li, T., Vanden-Eijnden, E., Zhang, P., E, W.: Stochastic Models of Polymeric Fluids at Small Deborah Number. J. Non-Newtonian Fluid Mech., **121**:2–3, 117–125 (2004)

[LE05] Li, X., E, W.: Multiscale Modeling of the Dynamics of Solids at Finite Temperature. J. Mech. Phys. Solids (2004), in press.

[LPV] Lions, P.L., Papanicolaou, G., Varadhan, S.R.S.: Homogenization of Hamilton-Jacobi Equations. Unpublished

[LZR91] Liu, W.K., Zhang, Y.F., Ramirez, M.R.: Multiple Scale Finite Element Methods. International Journal for Numerical Methods in Engineering, **32**, 969–990 (1991)

[LKZ04] Liu, W.K., Karpov, E.G., Zhang, S., Park, H.S.: An Introduction to Computational Nanomechanics and Materials. Computer Methods in Applied Mechanics and Engineering, **193**, 1529–1578 (2004)

[LK03] Lu, G., Kaxiras, E.: An Overview of Multiscale Simulation of Materials. Preprint (2003)

[MTV01] Majda, A.J., Timofeyev, I., Vanden-Eijnden, E.: A Mathematical Framework for Stochastic Climate Models. Comm. Pure Appl. Math., **54**:8, 891–974 (2001)

[MMK02] Markeev, A.G., Maroudas, D., Kevrekidis, I.G.: 'Coarse' Stability and Bifurcation Analysis Using Stochastic Simulators: Kinetic Monte Carlo Examples. J. Chem. Phys., **116**, 10083 (2002)

[MBS00] Matache, A.M., Babuska, I., Schwab, C.: Generalized p-FEM in Homogenization. Numer. Math., **86**:2, 319–375 (2000)

[MM02] Matache, A.M., Melenk, J.M.: Two-Scale Regularity for Homogenization Problems with Non-Smooth Fine Scale Geometry. Preprint (2002)

[MT04] Miller, R., Tadmor, E.B.: The Quasicontinuum Method: Overview, Applications and Current Directions. Preprint (2004)

[MTP98] Miller, R., Tadmor, E.B., Phillips, R., Ortiz, M.: Quasicontinuum Simulation of Fracture at the Atomic Scale. Modelling Simul. Mater. Sci. Eng., **6**:5, 607–638 (1998)

[Mil02] Milton, G.W.: The Theory of Composites. Cambridge University Press (2002)

[Min04] Ming, P.B.: Analysis of Multiscale Methods. In preparation

[MY03] Ming, P.B., Yue, X.Y.: Numerical Methods for Multiscale Elliptic Problems. Preprint (2003)

[MZ03] Ming, P.B., Zhang, P.W.: Analysis of the Heterogeneous Multiscale Method for Parabolic Homogenization Problems. Submitted to Math. Comp. (2003)

[MT77] Murat, F., Tartar, L.: H-Convergence. Cours Peccot (1977), reprinted in Topics in the Mathematical Modeling of Composite Materials. Cherkaev, A., Kohn, R. (eds) Birkhauser, Boston, 21–43 (1997)

[NT90] Nessyahu, H., Tadmor, E.B.: Nonoscillatory Central Differencing for Hyperbolic Conservation Laws. J. Comput. Phys., **87**, 408–463 (1990)

[NC04a] Nie, X., Chen, S., E, W., Robbins, M.O.: A Continuum and Molecular Dynamics Hybrid Method for Micro- and Nano-Fluid Flow. J. Fluid Mech., **500**, 55–64 (2004)

[NC04b] Nie, X., Chen, S., E, W., Robbins, M.O.: Hybrid Continuum-atomistic Simulation of Singular Corner Flow. Physics of Fluids, **16**, 3579 (2004)

[OT95] O'Connell, S.T., Thompson, P.A.: Molecular Dynamics-Continuum Hybrid Computations: a Tool for Studying Complex Fluid Flows. Phys. Rev. E, **52**:6, R5792–R5795 (1995)

[OV00] Oden, J.T., Vemaganti, K.S.: Estimation of Local Modeling Error and Goal-Oriented Adaptive Modeling of Heterogeneous Materials. I. Error Estimates and Adaptive Algorithms. J. Comput. Phys., **164**, 22–47 (2000)

[OS88] Osher, S., Sethian, J.A.: Fronts Propagating with Curvature-Dependent Speed: Algorithms Based on Hamilton-Jacobi Formulations. J. Comput. Phys., **79**, 12–49 (1988)

[Pap77] Papanicolaou, G.C.: Introduction to the Asymptotic Analysis of Stochastic Equations. In: Diprima, R.C. (ed) Modern modeling of continuum phenomena (Ninth Summer Sem. Appl. Math., Troy, N.Y., 1975), Lectures in Appl. Math., **16**, 109–147, Amer. Math. Soc., (1977)

[PV81] Papanicolaou, G.C., Varadhan, S.R.S.: Boundary Value Problems with Rapidly Oscillating Random Coefficients. In: Fritz, J., et.al (eds), Random Fields, **27**, 835–873, Amsterdam: North-Holland (1981)

[PKL04] Park, H.S., Karpov, E.G., Liu, W.K., Klein, P.A.: The Bridging Scale for Two-Dimensional Atomistic/Continuum Coupling. Accepted by Phil. Mag. A (2004)

[PY89] Parr, R.G., Yang, W.: Density Functional Theory of Atoms and Molecules. Oxford University Press (1989)
[Per91] Perthame, B.: Boltzmann-type Schemes for Gas Dynamics and Entropy Property. SIAM J. Numer. Anal., **27**, 1405–1421 (1991)
[Per92] Perthame, B.: Second Order Boltzmann-type Schemes for Compressible Euler Equations in One and Two Space Dimensions. SIAM J. Numer. Anal., **29**, 1–19 (1992)
[Pes77] Peskin, C.S.: Numerical Analysis of Blood Flow in the Heart. J. Comput. Phys., **25**:3, 220–252 (1977)
[PM93] Peskin, C.S., McQueen, D.M.: Computational Biofluid Dynamics. Contemp. Math., **141**, 161–186 (1993)
[Phi01] Phillips, R.: Crystals, Defects and Microstructures. Cambridge University Press (2001)
[PT04] Priezjev, N.V., Troian, S.M.: Molecular Origin and Dynamic Behavior of Slip in Sheared Polymer Films. Phys. Rev. Lett., **92**, 018302 (2004)
[Pul80] Pullin, D.I.: Direct Simulation Methods for Compressible Inviscid Ideal Gas Flow. J. Comput. Phys., **34**, 231–244 (1980)
[QWL03] Qian, D., Wagner, G.J., Liu, W.K.: A Multiscale Projection Method for the Analysis of Carbon Nanotubes. Computer Methods in Applied Mechanics and Engineering, **193**:17-20, 1603–1632 (2003)
[QW04] Qian, T.Z., Wang, X.P.: Slip Boundary Condition in Driven Cavity Flows. Submitted to SIAM MMS (2004)
[QW04] Qian, T.Z., Wang, X.P.: Sinusoidal Fluid-Solid Interactions: From Molecular Simulations to Hydrodynamic Modeling. Preprint (2004)
[QWS03] Qian, T.Z., Wang, X.P., Sheng, P.: Molecular Scale Contact Line Hydrodynamics of Immiscible Flows. Phys. Rev. E, **68**, 016306 (2003)
[Re04b] Ren, W.: Accessment of the Errors in Multiscale Methods of Complex Fluids. In preparation
[RE05a] Ren, W., E, W.: Heterogeneous Multiscale Method for the Modeling of Complex Fluids and Microfluidics. J. Comput. Phys., vol. 204, no. 1, pp. 1-26, 2005.
[RE05b] Ren, W., E, W.: Multiscale Modeling of Complex Fluids I: Polymer Melts in the Non-Entangled Regime, in preparation.
[RM01] Robbins, M.O., Mser, M.H.: Computer Simulations of Friction, Lubrication and Wear. In: Bhushan, B. (ed), Modern Tribology Handbook, CRC Press (2001)
[RB99] Rudd, R.E., Broughton, J.Q.: Atomistic Simulation of Mems Resonators Through the Coupling of Length Scales. J. Modeling and Simulation of Microsystems, **1**, 29–38 (1999)
[RB98] Rudd, R.E., Broughton, J.Q.: Coarse-Grained Molecular Dynamics and the Atomic Limit of Finite Elements. Phys. Rev. B, **58**:10, R5893–R5896 (1998)
[RTK02] Runborg, O., Theodoropoulos, C., Kevrekidis, I.G.: Effective Bifurcation Analysis: Time-Stepper Based Approach. Nonlinearity, **15**:2, 491–511 (2002)
[SKR04] Samaey, G., Kevrekidis, I.G., Roose, D.: The Gap-Tooth Scheme for Homogenization Problems. Submitted to SIAM MMS (2004)
[Sah95] Sahimi, M.: Flow and Transport in Porous Media and Fractured Rock. John Wiley (1995)

[SP74] Sanders, R.H., Prendergast, K.H.: On the Origin of the 3-Kiloparsec Arm. Astrophysics Journal, **188**, 489–500 (1974)

[SFM01] Succi, S., Filippova, O., Smith, G., Kaxiras, E.: Applying the Lattice Boltzmann Equation to Multiscale Fluid Problems. Computing in Science and Engineering, **3**, 26–37 (2001)

[SK03] Schmidt, H., Klein, R.: A Generalized Level-Set/In-Cell-Reconstruction Approach for Accelerating Turbulent Premixed Flames. Comb. Theory & Modelling, **7**, 243-267 (2003)

[SSE03] Schulze, T., Smereka, P., E, W.: Coupling Kinetic Monte-Carlo and Continuum Models with Application to Epitaxial Growth. J. Comput. Phys., **189**, 197–211 (2003)

[SM02a] Schwab, C., Matache, A.-M.: Generalized FEM for Homogenization Problems. In: Barth, T.J., et. al. (eds) Multiscale and Multiresolution Methods: Theory and Applications, Yosemite Educational Symposium Conf. Proc. (2000) Lecture Notes in Comp. Sci. and Engrg., **20**, 197–237, Springer-Verlag (2002)

[SM02b] Schwab, C., Matache, A.-M.: Two-Scale FEM for Homogenization Problems. In: Babuska, I., et. al. (eds) Mathematical Modelling and Numerical Simulation in Continuum Mechanics Conf. Proc., Yamaguchi, Japan (2000) Lecture Notes in Comp. Sci. and Engrg., Springer-Verlag (2002)

[SCO04] Serebrinsky, S., Carter, E.A., Ortiz, M.: A Quantum-Mechanically Informed Continuum Model of Hydrogen Embrittlement. J. Mech. Phys. Solids, **52**, 2403–2430 (2004)

[Set96] Sethian, J.A.: Fast Marching Level Set Methods for Three Dimensional Photolithography Development. In: SPIE 1996 Symposium Proc., Intl. Symposium on Microlithography, Santa Clara, CA, **2726**, 261–272 (1996)

[SA97] Sethian, J.A., Adalsteinsson, D.: An Overview of Level Set Methods for Etching, Deposition and Lithography Development. IEEE Trans. Semiconductor Mfg., **10**, 167–184 (1997)

[SMT98] Shenoy, V.B., Miller, R., Tadmor, E.B., Phillips, R., Ortiz, M.: Quasicontinuum Models of Interfacial Structure and Deformation. Phys. Rev. Lett., **80**:4, 742–745 (1998)

[SMT99] Shenoy, V.B., Miller, R., Tadmor, E.B., Rodney, D., Phillips, R., Ortiz, M.: An Adaptive Finite Element Approach to Atomic-Scale Mechanics — the Quasicontinuum Method. J. Mech. Phys. Solids, **47**:3, 611–642 (1999)

[SCM02] Shilkrot, L.E., Curtin, W.A., Miller, R.E.: A Coupled Atomistic/Continuum Model of Defects in Solids. J. Mech. Phys. Solids, **50**, 2085–2106 (2002)

[SMC04] Shilkrot, L.E., Miller, R.E., Curtin, W.A.: Multiscale Plasticity Modeling: Coupled Atomistics and Discrete Dislocation Mechanics. J. Mech. Phys. Solids, **52**, 755–787 (2004)

[SMS04] Shimokawa, T., Mortensen, J.J., Schiotz, J., Jacobson, K.W.: Matching Conditions in the Quasicontinuum Method: Removal of the Error Introduced at the Interface between the Coarse-Grained and Fully Atomistic Regions. Phys. Rev. B, **69**, 212104 (2004)

[STK00] Smith, G.S., Tadmor, E.B., Kaxiras, E.: Multiscale Simulation of Loading and Electrical Resistance in Silicon Nanoindentation. Phys. Rev. Lett., **84**:6, 1260–1263 (2000)

[Spa76] Spagnolo, S.: Convergence in Energy for Elliptic Operators. In: Hubbard, B. (ed) Numerical Solutions of Partial Differential Equations-III,

(SYNSPADE 1975, Maryland, May 1975), Academic Press, New York, 469–499 (1976)

[Spo91] Spohn, H.: Large Scale Dynamics of Interacting Particles. Springer-Verlag (1991)

[SE04] Sun, Y., Engquist, B.: Heterogeneous Multiscale Methods for Interface Tracking of Combustion Fronts. In preparation

[TOP96] Tadmor, E.B., Ortiz, M., Phillips, R.: Quasicontinuum Analysis of Defects in Crystals. Philos. Mag., **A73**, 1529–1563 (1996)

[Tar00] Tartar, L.: An Introduction to the Homogenization Method in Optimal Design. In: Cellina, A., Ornelas, A. (eds) Optimal Shape Design, Lectures given at the Joint C.I.M./C.I.M.E. Summer School, Troia, Portugal (1998) Lecture Notes in Math., **1740**, 47–156, Springer-Verlag (2000)

[Tar81] Tartar, L.: Solutions Oscillantes Des quations De Carleman. Goulaouic-Meyer-Schwartz Seminar, 1980–1981, Exp. No. XII, 15 pp., cole Polytech., Palaiseau (1981)

[TQK00] Theodoropoulos, C., Qian, Y.-H., Kevrekidis, I.G.: 'Coarse' Stability and Bifurcation Analysis Using Time-Steppers: a Reaction-Diffusion Example. Proc. Natl. Acad. Sci. USA, **97**:18, 9840–9843 (2000)

[TR89] Thompson, P.A., Robbins, M.O.: Simulations of Contact-Line Motion: Slip and the Dynamic Contact Angle. Phys. Rev. Lett., **63**:7, 766–769 (1989)

[TT97] Thompson, P.A., Troian, S.M.: A General Boundary Condition for Liquid Flow at Solid Surfaces. Nature, **389**, 360–362 (1997)

[TE00] Tornberg, A.-K., Engquist, B.: Interface Tracking in Two-Phase Flows. In: Multifield Problems, State of the Art, Springer-Verlag, 58–66 (2000)

[Tor02] Torquato, S.: Random Heterogeneous Materials: Microstructure and Macroscopic Properties. Springer-Verlag (2002)

[TCO03] Tsai, Y.-H., Cheng, L.-T., Osher, S., Zhao, H.K.: Fast Sweeping Algorithms for a Class of Hamilton-Jacobi Equations. SIAM J. Numer. Anal., **41**:2, 673–694 (2003)

[Tsi95] Tsitsiklis, J.N.: Efficient Algorithms for Globally Optimal Trajectories. IEEE Trans. Autom. Control, **40**:9, 1528–1538 (1995)

[Tuc02] Tuckerman, M.E.: TextitAb initio Molecular Dynamics: Basic Concepts, Current Trends and Novel Applications. J. Phys. Condens Matter, **14**, R1297–1355 (2002)

[Van03] Vanden-Eijnden, E.: Numerical Techniques for Multiscale Dynamical Systems with Stochastic Effects. Comm. Math. Sci., **1**:2, 385–391 (2003)

[VC87] Voter, A.F., Chen, S.F.: Accurate Interatomic Potentials for Ni, Al and Ni3Al. MRS Symposia Proceedings, **82**, 175–180 (1987)

[VMG02] Voter, A.F., Montalenti, F., Germann, T.C.: Extending the Time Scale in Atomistic Simulation of Materials. Ann. Rev. Mat. Res., **32**, 321–346 (2002)

[WL03] Wagner, G.J., Liu, W.K.: Coupling of Atomistic and Continuum Simulations Using a Bridging Scale Decomposition. J. Comput. Phys., **190**, 249–274 (2003)

[WL76] Warshel, A., Levitt, M.: Theoretical Studies of Enzymic Reactions. J. Mol. Biol., **103**, 227–249 (1976)

[WWA04] Werder, T., Walther, J.H., Asikainen, J., Koumoutsakos, P.: Continuum-Particle Hybrid Methods for Dense Fluids. In: Attinger, S., Koumout-

sakos, P. (eds) Multiscale Modeling and Simulation, Lecture Notes in Computational Science and Engineering, **39**, 35–68, Springer (2004)

[XB04] Xiao, S.P., Belytschko, T.: A Bridging Domain Method for Coupling Continua with Molecular Dynamics. Comput. Methods Appl. Mech. Engrg., **193**, 1645–1669 (2004)

[Xu96] Xu, J. Two-Grid Discretization Techniques for Linear and Nonlinear PDEs. SIAM J. Numer. Anal., **33**:5, 1759–1777 (1996)

[SP94] Xu, K., Prendergast, K.H.: Numerical Navier-Stokes Solutions from Gas Kinetic Theory. J. Comput. Phys., **114**, 9–17 (1994)

[Yau00] Yau, H.T.: Asymptotic Solutions to Dynamics of Many-Body Systems and Classical Continuum Equations. In: Current Development in Mathematics. International Press (2000)

[YE04] Yue, X.Y., E, W.: Numerical Methods for Multiscale Transport Equations and Application to Two Phase Porous Media Flow. Submitted to J. Comput. Phys. (2004)

[YE05] Yue, X.Y., E, W.: Multiscale Modeling of Strongly Heterogeneous Media: Effect of Boundary Conditions and Cell Size of the Microscale Problem. In preparation

[Yur86] Yurinskii, V.V. Averaging of Symmetric Diffusion in Random Media. Sibirsk. Mat. Zh., **23**:2, 176–188 (1982); English transl. in Siberian Math J., **27**, 603–613 (1986)

[Zho03] Zhou, M.: A new look at the atomic level virial stress: on continuum-molecular system equivalence. Proc. R. Soc. Lond. A, **459**, 2347–2392 (2003)